Development of 3D Printable, Hydrophilic, and Rapidly Curing Silicone-based Ink Formulations for Various Biomedical Applications

by

Hossein Golzar

A thesis

presented to the University of Waterloo

in fulfillment of the

thesis requirement for the degree of

Doctor of Philosophy

in

Chemistry (Nanotechnology)

Waterloo, Ontario, Canada, 2022

Examining Committee Membership

The following served on the Examining Committee for this thesis. The decision of the Examining Committee is by majority vote.

External Examiner	Mohsen Akbari Associate Professor Dep. of Mechanical Engineering University of Victoria
Supervisor	Shirley Tang Professor Dep. of Chemistry University of Waterloo
Internal Member	John Honek Professor Dep. of Chemistry University of Waterloo
Internal Member	Jean Duhamel Professor Dep. of Chemistry University of Waterloo
Internal-external Member	Jonathan Blay Professor School of Pharmacy University of Waterloo

Author's Declaration

I hereby declare that I am the sole author of this thesis. This is a true copy of the thesis, including any required final revisions, as accepted by my examiners. I understand that my thesis may be made electronically available to the public.

Abstract

3D printing is the use of additive manufacturing techniques to deposit materials layer-by-layer. Compared to alternative tissue fabrication methods such as casting, 3D printing is unique, because it uses CT and MRI scans to create the most accurate 3D tissue models. 3D printing of biomimetic structures, especially elastic tissue mimetics, is a relatively young research field and is experiencing exponential growth. Among the four most commonly used 3D printing methods (power-bed fusion, vat polymerization, material-jetting, and material-extrusion), 3D micro-extrusion (ME) is the most suitable method for printing macroscale (centimeter size) and arrayed acellular/cell-laden biomimetic structures with high-throughput due to its capability in multi-material printing and ease of operation. However, for 3D ME printing of precise and functional human-mimetic substitutes, there is a need to develop an appropriate 3D printable ink with tunable mechanical and rheological features. Among different polymers, silicone elastomers have been widely utilized in different biomedical applications due to their remarkable features such as flexibility, adaptability, and biocompatibility, but the slow curing speed, low viscosity, and hydrophobicity of the existing silicones are challenges that hinder silicone applications. In this thesis, we have made an attempt to address these issues by deploying a series of strategies to develop UV-curable and hydrophilic silicone-based inks that can be used to rapidly 3D print a precise articular cartilage (AC) substitute, as a proof of concept. To do so, hydrophilic and rapidly curing (under three seconds) inks, consisting of aminosilicone, cellulose nanocrystal (CNC), and methacrylate anhydride (MA), are developed for the printing of human articular cartilage (HAC) substitutes, with a biomimetic multizonal structure, for the first time. The developed inks are shown to possess a suitable shear-thinning property and tunable mechanical strengths for 3D ME printing. The ability to print high aspect ratio and hemispherical structures without any sacrificial

supporting materials is demonstrated. The desired mechanical stiffnesses of HAC layers can be readily achieved by printing with aminosilicone inks containing different CNC and MA concentrations. A multilayered HAC with a gradual increase of the compression modulus from 0.25 to 1.32 MPa for the superficial layer to the deep zone, respectively, is successfully printed. Further, the durability of the 3D-printed HAC against a high repetition rate of cyclic compressions (400 cycles) is evaluated. Additionally, a customized HAC was printed to cover human femoral condyles.

Lastly, we have tried to employ our developed ink for the fabrication of microfluidic devices (MFDs), where silicone elastomers are extensively used. MFDs have grabbed significant interest due to their unique features such as low-cost fabrication, miniaturization, simplicity, and reduced reagent consumption. Compared to conventional MFD fabrication methods, mainly soft lithography, 3D printing has the following advantages: easy geometry customization, multi-material printing, one-step printing, and better device integrity (i.e. no bonding, no leakage). Our results demonstrated that various integrated MFDs with different channel sizes could be readily 3D printed using our developed ink.

Taken all together, this thesis presents a new class of silicone-based ink, with high commercialization readiness levels, that can be used for not only the fabrication of personalized and biocompatible tissue-mimetic models but also 3D printing integrated MFDs in one-step for various biomedical applications.

Acknowledgment

I would like to express my deepest gratitude to my supervisor, Prof. Shirley Tang, for her caring, constant support, and guidance throughout my PhD studies. I learned how to think outside the box and push myself to become a better scientist.

I hereby acknowledge my committee members, Prof. John Honek, Prof. Jean Duhamel, and Prof. Jonathan Blay for their time, guidance, and valuable suggestions since my first seminar, comprehensive exam, committee meetings, and up to my PhD thesis defense. I would also like to thank my external examiner, Prof. Mohsen Akbari, for reading my thesis and attending my thesis defense. I would like to thank Chris Kleven for his constant help setting up tools around the lab, and Dr. Boxin Zhao and Dr. Michael K. C. Tam for providing access to the compression tester and rheometer, respectively.

I would like to thank my lab mates and friends for their friendship, assistance, and scientific discussions: Dr. Yun Wu, Dr. Irfani Ausri, Andrew Wenger, Kyle Chu, Dr. Sayan Ganguly, Li Yan Wong, and Pei Li. I would also like to thank my co-op and undergraduate students, who helped me with my project: Yuran and Brandon.

I would like to thank my lovely parents, sister, and brother for their love and unconditional support. I would also like to thank my brother- and sister-in-law, Arang and Mahsa, who endured this long process with me, offering me endless support and love.

Finally, and most importantly, my deepest gratitude goes to my wife, Dorsa Mohammadrezaei, who has stood by me through all my absences, my fits of pique, my travails, and every step of my PhD journey, pushing me through tough times and preventing from several wrong turns. I would not be where I am today here without her love, support, and encouragement.

Dedication

To my wife and my lovely family.

Table of Content

List of Figures

List of Tables

List of Abbreviations

2D	two-dimensional
3D	three-dimensional
3DP-PDMS	3D-printable poly (dimethylsiloxane)
ABS	acrylonitrile butadiene styrene
AC	articular cartilage
ALG-PAAm	alginate-polyacrylamide
AM	additive manufacturing
AUD	aliphatic urethane diacrylate
BC	bacterial cellulose
CA	contact angles
$CDCl_3$	deuterated chloroform
CIJ	continuous inkjet
CLIP	continuous liquid interface production
CNC	cellulose nanocrystal
CNTs	carbon nanotubes
COC	cyclic olefin copolymer
CS	chitosan

DIW	direct ink writing
DLP	digital projection lithography
DMEM	dulbecco's modified Eagle's medium
DOD	drop-on-demand
DOX	doxorubicin
DTP	3,3′-dithiobis (propionyl hydrazide)
EAA	epoxy aliphatic acrylate
ECM	extracellular matrix
FA	folic acid
FBS	fetal bovine serum
FDM	fused deposition modelling
FFF	fused filament fabrication
GelMA	methacrylated gelatin
HA	hydroxyapatite
HAC	human articular cartilage
^{1}H-NMR	proton nuclear magnetic resonance
HTV	high temperature vulcanized
IPA	isopropyl alcohol

iPSC	human-induced pluripotent stem cell
LAP	lithium phenyl-2,4,6-trimethylbenzoylphosphinate
MA	methacrylic anhydride
ME	microextrusion
MeCol	methacrylated collagen
MFDs	microfluidic devices
mIMCD3	mouse inner medullary collecting duct cell line
MTT	(3-(4,5-dimethylthiazol-2-yl)-2,5-diphenyltetrazolium bromide)
MWCNTs	multi-walled carbon nanotubes
nHA	nanohydroxyapatite
OA	osteoarthritis
PBS	phosphate buffered saline
PC	polycarbonate
PDMS	poly (dimethylsiloxane)
PEG	poly (ethylene glycol)
PEG-DA-258	low-molecular weight diacrylated PEG resin
PEPN	phenylacetylene
PET	poly (ethylene terephthalate)

PETG	polyethylene terephthalate glycol
PMMA	poly(methyl methacrylate)
PS	polystyrene
PVA	polyvinyl alcohol
SC	aminosilicone-CNC
SCM	aminosilicone-CNC-MA
SilDNs	silicone double networks
Si-NPs	silica nanoparticles
SLA	stereolithography
SLM	selective laser melting
SLS	selective laser sintering
SM	aminosilicone-methacrylate
SWCNTs	single-walled carbon nanotubes
T_g	glass transition temperature
T_m	melting temperature
TNBS	2,4,6-Trinitrobenzenesulfonic acid
TPEs	thermoplastic elastomers
TPO	2,4,6-Trimethylbenzoyl-diphenylphosphine oxide

TPP	two-photon/multiphoton polymerization
TPU	thermoplastic polyurethane

Chapter 1 Introduction

1.1 3D Printing

Three-dimensional (3D) printing is the method involved with interpreting a computerized model into an actual printed pattern. This interpretation process utilizes a 3D printer to fabricate complex functional 3D constructs layer-by-layer based on the data of the 3D computer model using various materials including polymers (natural or synthetic), ceramics, and metals.[1–3] 3D printing has its own advantages over conventional fabrication methods, which need dices, molds, or lithographic masks, including ease of operation, cost efficiency, and fast-paced manufacturing process.[1] Hence, 3D printing technology has attracted significant interest in medical and industrial applications during the last decade.[4] The most common 3D printing techniques for biomedical applications can be classified into four significant groups, including powder bed fusion, vat polymerization, material jetting, and material extrusions, each of which has its own merits and drawbacks (Figure 1.1).

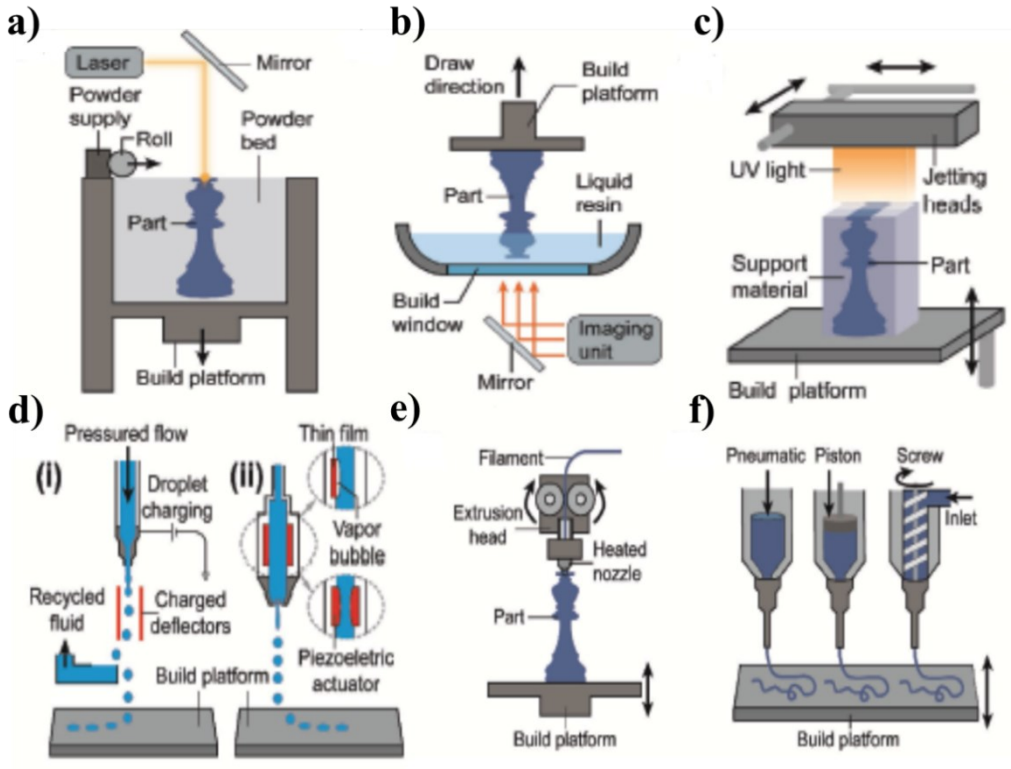

Figure 1.1 Schematic illustrations of various 3D printing methods. a) Power bed fusion, b) Vat photopolymerization, c) Inkjet printing, d) i) CIJ mode and ii) DOD mode of inkjet printing, e) FDM, and f) DIW printing. All these figures are reproduced with permission.[1,5]

1.1.1 Powder Bed Fusion

Powdered materials are sintered or melted using an electron or laser beam in the additive manufacturing procedure known as powder bed fusion. The laser is automatically pointed at particular locations in space indicated by a pre-rendered 3D model, binding the materials together to fabricate a solid structure. This 3D printing technique is also known as selective laser sintering (SLS) or selective laser melting (SLM) due to the differences in the phase state of the powder during the binding process.[6]

The SLS construction process (Figure 1.1a) consists of three steps: a) Powder deposition, in which by rolling or scraping, particles with diameters in the range of 10-100 μm are spread uniformly as a print layer in this stage, b) Powder solidification in which by scanning cross-sections cut from 3D models, the laser beam selectively fuses powders to create a bonded solid, and c) Lowering the platform in which the build platform is lowered by one layer of thickness in order to prepare for printing the following layer.[1] Until the printing is finished, these three procedures are repeated. SLS achieves approximately 100% material utilization because, unlike prior 3D printing methods that require extra support materials, the powders in non-fused regions may act as support materials that may be reused after printing.[7] The SLS's forming principle limits the materials that it may use to a few distinct kinds. In general, SLS powder should possess compatibility, aging stability, high flowability, and particularly good thermal characteristics.[8–10]

SLS cannot offer further compacting during component fabrication, in contrast to injection molding. Once a non-uniform powder layer is developed, bonded solid flaws are unavoidable. Additionally, as only some powders are sintered and fused to create the designed model, the remaining powders in non-fused regions may experience sustained heat stress that may induce deterioration, particularly for polymer materials.[1,3] Moreover, the difficulty in producing polymer elastomer powders is considered another significant issue hindering the application of SLS and SLM.[2] Today, relatively few soft polymer materials, such as polycarbonate (PC), thermoplastic elastomers (TPEs), and PCL, can be processed using SLS.[11] Although it is widely accepted that the biological and medical industries are the most active fields employing soft polymer materials for SLS, the SLS method's multi-material capacity is still inferior to other 3D printing technologies due to its restrictive material requirements.[12–14]

1.1.2 Vat Polymerization

Another additive manufacturing process is vat photopolymerization which can selectively cure liquid photopolymer in the vat through light-activated polymerization to create the designed structure. Stereolithography (SLA) was the first vat photopolymerization technique established in the early 1980s.[15] Based on the core principle of SLA, numerous other vat photopolymerization techniques have been created since then, such as continuous liquid interface production (CLIP),[16] digital projection lithography (DLP),[17] two-photon/multiphoton polymerization (TPP),[18] and computed axial. The vat photopolymerization printer is identical to that for SLS, as illustrated in Figure 1.1b, with the exception of the material state and light source. Depending on how the printer is set up, the light source's position and the build support plate's motion can be changed (the light source may be placed below or above the vat). A thin layer of patterned solid is created during printing by masking or the movement of the light source, which produces light to cure the liquid photopolymer. A new layer of liquid photopolymer flows into the print regions to print the next layer once the build support plate has moved by one layer thickness after printing the first layer. These steps are done one after the other until the required 3D model is complete. It is true that compared to other 3D printing methods, the vat photopolymerization can be considered the most accurate and fastest 3D printing method, but there is a significant trade-off between various parameters, including volume, high build speed, and resolution.[19] For instance, TPP may be utilized to create complex 3D structures within a few micrometers at the cost of limiting the building volume to only 1 cm^3, while CLIP can fabricate constructs with higher building volume (several hundred cm^3) with a much lower resolution, which is typically more than 100 μm. In comparison, while SLA/DLP resolution may reach several micrometers, their printing pace is substantially slower than CAL and CLIP.[19,20] Additionally, materials must meet the requirements

including excellent fluidity and photo curability to be considered a suitable candidate for vat photopolymerization.[1] When it comes to multi-material printing, vat photo-multi-material polymerization's capability is inferior, much like SLS's; however, the major restriction is composites rather than printing different materials. Indeed, vat photopolymerization has been facing several challenges in printing composite materials due to the effect of particle addition on the rheological features and transparency of the liquid solution. For example, the addition of particles may not only increase the liquid solution's viscosity which in turn can decrease the printability of the material but also lead to the printing of unstable and defective 3D structures because of the particle settlement. Moreover, particle addition can affect the printing efficiency and quality due to the light scattering features of the micro/nano-sized particles. [1,4,17]

1.1.3 Material Jetting

Material jetting or inkjet printing is an expensive additive manufacturing technique in which materials, in the form of droplets, are precisely deposited to fabricate the designed object.[21,22] As shown in Figure 1.1c, the conventional inkjet printing system consists of an X-Y-Z three-axis motion platform with an additional curing equipment, which can be a heating platform or UV light source, and multiple jetting heads. Low-viscosity liquids are expelled from the jetting nozzles and precisely deposited on the print stage, where they are subsequently cured into solids. Inkjet printers can generate droplets in two different modes; continuous inkjet (CIJ) and drop-on-demand (DOD) printing (Figure 1.1d). In each of these modes, droplets are formed by breaking the liquid into droplets by either electrically heating a needle or using a piezoelectric actuator to create a vapor bubble and pressure pulse, respectively.[22]

Due to the fast droplet formation speed (20–60 kHz), CIJ systems can often provide high printing speeds (>10 m s^{-1}).[22] However, DOD can only print at a slow pace (5-8 m s^{-1}) because of

the limitations imposed by acoustic frequencies (usually 1-20 kHz).[23] In terms of resolution, DOD has a higher resolution because the diameter of the droplets generated in CIJ is typically bigger than the nozzle diameter, while with DOD, the droplet diameter is approximately equal to the diameter of the nozzle.[23,24]

Although the high printing resolution and multi-material printing capability of inkjet printing make it an ideal 3D printing technique, it also has its weaknesses. The range of materials that can be utilized for inkjet printing is limited since the viscosity of the ink should be within the range of 3.5 and 12 mPa·s, hindering its application for 2D tissue engineering like cartilage construction.[25] In addition, when it comes to a jet complex solution like concentrated polymers or solution with large nanoparticles (usually particles with bigger than 100 nm diameter), clogging might cause a significant challenge which in turn limits the range of printed materials.[26,27]

1.1.4 Material Extrusion

Material extrusion, also known as extrusion printing, is a 3D printing technique in which the material is being extruded through a nozzle to create a continuous filament that is then used to fabricate the designed structure.[1] As can be seen in Figure 1.1e, similar to inkjet printing, a typical extrusion 3D printer consists of an X-Y-Z three-axis motion stage along with in situ curing device (optional) and several extrusion nozzles which provide the opportunity to have a multi-material printing. To fabricate a structure, the extruded filament is deposited at the desired location by moving either the printing stage or the nozzle head. Once a single layer is finished, the stage moves down, or the extrusion head moves up to make room for the next layer deposition.

Fused deposition modelling (FDM), also known as fused filament fabrication (FFF), was the first extrusion printing method to emerge (Figure 1.1e).[28] In this printing technique, the first thermoplastic filaments are heated within the nozzle during FDM to make them semi-molten.

These semi-molten filaments are then solidified by decreasing the temperature below their glass transition temperature. Microextrusion (ME) printing is built on the concept of FDM, in which a viscoelastic material is extruded through a nozzle using a piston, air pressure, or a screw (Figure 1.1f).[1,3] Once a layer is deposited, it may be hardened via various curing processes, such as thermal or photopolymerization.[29] Viscoelasticity plays a crucial role in ME printing since rheological features such as shear thinning property and proper recoverability are considered as factors that can guarantee good shape fidelity and continued filament deposition which are requisites for having a successful ME printing.[29,30]

Compared to other printing techniques, the range of the materials that can be utilized for ME printing is considerably wider since not only there are many polymers with the appropriate rheological qualities but also the majority of those unprintable polymers may be readily modified to become printable by incorporating rheological modifiers into a polymer matrix,[31–34] embedded printing[35–38] or two-step crosslinking.[39–41] ME printer's multi-material capability, which is enabled by several dispensers and composite inks, is further enhanced by this tolerance for material selection. Hence, ME printers can be used to create complex functional constructs using soft polymers with various viscosities such as silicone elastomers,[39–41] polyurethane,[42] and hydrogels.[43–46]

One of the main challenges hindering the broad application of soft materials for ME printing purposes is the structural deformation due to the gravity, particularly in cases wherein the curing phase is excluded from the printing process. There are several ways to solve this issue: a) In situ curing, by incorporating additional curing devices such as a UV lamp or heated chamber to cure the printed layer once they have been deposited;[47] b) Embedded printing, by using self-healing

gels as a support for the printed constructs;[36,37] c) Multi-material printing, by supporting softer material with the materials having a high Young's modulus to prevent the possible collapse.[48–50]

Generally, each printing method is suitable for printing different materials and has its own advantages and disadvantages. Vat photopolymerization and SLS both pattern and cure the 3D structures simultaneously, while in extrusion and inkjet printing, first, the material needs to be delivered to the designed spot using a nozzle or print head, followed by curing. This difference in pattering may lead to a significant gap in the multi-material printing capability. Indeed, multi nozzle-based printing can provide the chance of changing materials by simply altering the nozzles, while in vat polymerization and SLS, this would be a challenge or even impossible. This issue of changing materials during printing can become even worse due to the strict material requirements of SLS and vat polymerization. In fact, among various materials, including thermoset polymers, physical crosslink polymers, thermoplastic polymers, and photopolymers, only photopolymers and thermoplastic polymers can be respectively used for vat photopolymerization and SLS. However, almost all these materials can be printed using inkjet and extrusion-based printers. When it comes to resolution and printing speed, vat photopolymerization and SLS can beat the other printing methods.[1,4]

In this research, we used a ME 3D printer due to its features such as ease of operation, versatile polymerization methods, compatibility with different materials with various viscosities, and reasonable printing accuracy.[51–53] Among different ME 3D printers (pneumatic and mechanically driven), we used the pneumatic one, which provided us with better control over the printing process due to its mechanism in which forces are directly applied to pistons. All the printing parameters, including nozzle diameter, pressure, flow rate, filament width, and layer height, have been optimized to print 3D constructs precisely.

1.2 3D-Printable Biomaterials

The 3D-printable materials, known as inks, can be considered essential components that are mainly specific to the printing technique and dominate the performance and efficiency of the 3D-printed constructs.[54] In general, all the 3D-printable materials, including hydrogels, polymers, and bioinks, must meet specific requirements, including a) suitable viscosity to make them printable and structurally stable, b) proper shape fidelity, c) biocompatibility, d) tunable mechanical features, e) crosslink ability via UV irradiation, chemical, or physical crosslinking, f) biomimetic, and g) appropriate degradation rate.[55] Noteworthy is based on the application of the 3D-printed constructs and printing methods, each of these requirements might be modified. Therefore, a balance between all these requirements needs to be maintained to develop suitable printable biomaterials with striking features for various biomedical applications.[56,57]

To develop a hydrophilic and rapidly curing ME 3D-printable ink with tunable mechanical features, we have investigated several biomaterials, including ceramic-, polymer-based, hydrogels, and composites.

1.2.1 Ceramic-based Inks

The unique features of ceramic-based materials, such as high bioactivity, proper stiffness, and similarity to the natural human bone's mineral phase, make them an ideal candidate for dental surgeries and orthopedics applications. However, the hard processability of the ceramics hinders their application for direct printing methods.[58,59] For example, the high melting temperature of ceramic materials, above 2000 ºC, is far from the suitable range of FDM printers. SLA printers can also no longer be an option for 3D printing ceramic materials since they are not responsive to light.[59] The most attractive option to make them printable is to incorporate them as an additive, powder, into a composite system that allows the ceramic materials to be used as an ink for almost

all 3D printing methods. Among different ceramics, hydroxyapatite (HA), in its powder form, is frequently utilized for 3D printing purposes due to its widespread occurrence in mineralized human bone.[60,61] To achieve HA powder, the poly(acrylic acid) solution might be sprayed layer-by-layer to provide powder binding, and then the resulting structure would be sintered to become solid.[45]

1.2.2 Polymer-based Inks

Polymers have been extensively used for 3D printing applications due to their extraordinary features, including ease of operation, biocompatibility, low cost, proper degradation rate, and adjustable mechanical and rheological cues. Polymers can be utilized in different forms such as powders, filaments, solution, and solution/gels, making them ideal candidates for a variety of 3D printers, including SLS, FDM, SLA, and ME, respectively.[62,63] As mentioned previously, each of these 3D printing methods has its own printability criteria in terms of material parameters. For instance, suitable inks for ME printing should possess low viscosity to allow the deposition of filaments at low to moderate pressure along with proper shear-thinning property to facilitate the flow and avoid clogging. For SLS printers, to maintain a reasonable printing resolution, the diameter of the polymer beads should be within the range of 10-150 μm to let the particle flow through the bed. There are also other considerations; for example, the highest achievable melt temperature by the laser is approximately 200 ^{o}C.[64,65] Regarding SLA printing, polymers must be photocrosslinkable and undergo polymerization once they are exposed to UV radiation. The liquid bath's viscosity and density have to be sufficiently high to ensure the 3D-printed construct is strong enough to perform the desired function and that the remaining material in the bath can flow into the place once the stage descends after the completion of each layer. Numerous materials have been transformed into printable polymer bioinks for different 3D printing methods based on these design criteria.[21]

1.2.2.1 Thermoplastic Polymers

A thermoplastic polymer is a form of polymer that is easily moldable and pliable when heated above the glass transition temperature and solidifies upon cooling. This phenomenon can be rooted in the inherent intermolecular forces in thermoplastic polymers, which are the weak and reversible van der Waals forces. Therefore, thermoplastic polymers can easily soften above their glass transition temperature and show fluidic behaviours. It is worth noting that since there is no chemical bonding occurring during this process, the solidification may be completely reversible.[54]

Due to this unique characteristic, polymers may be recycled and remolded using a variety of processing methods, such as compression molding, injection molding, and calendaring. Thermoplastic polymers are therefore ideal for FFF.[66] Indeed, when such polymers are heated, their viscosity significantly decreases, making it easier to extrude through a nozzle. After being extruded, the filament cools and becomes considerably more viscous. The polymer keeps its form and solidifies quickly. Various commercial products have been created from filaments using 3D extrusion methods. Some polymers' extruded filaments, however, might readily undergo shrinkage, which in turn could affect the shape fidelity of the 3D printed constructs. Thus, to address the above-mentioned problems and broaden the application of these polymers, several studies have been conducted to develop new thermoplastic polymers with improved 3D printability.[66–69]

The main challenges hindering the broad application of the FFF method are poor interlayer adhesion and anisotropy.[70] Levenhagen and Dadmun attempted to solve these issues by incorporating low molecular weight additives into polylactide.[70,71] They reported that the presence of these additives resulted in more entanglement between neighboring printed layers, which can be caused due to higher diffusivity of the low molecular weight polymer over the filament

interface, leading to more robust interfaces. By adjusting the additive's molecular weight and its architecture, the adhesion and bonding of the printed layers can be tuned. Their results indicated that the improvement in the entanglement of neighboring layers and diffusion does not depend on the printing orientation since the moduli were the same even when the printing orientation was changed. They also improved their PLA-based ink by incorporating UV-curable methacrylate groups into its polymer matrix (Figure 1.2a).[72]

Another strategy to improve the 3D printability of thermoplastic polymers is chemically modifying such polymers with supramolecular interactions. For instance, the fast crystallization following extrusion and consequent poor adhesion between layers limit the application of poly (ethylene terephthalate) (PET) for 3D printing purposes. In a recent study, Wang and colleagues found that adding phenylacetylene (PEPN) groups with π–π interactions at the side chain could solve this issue (Figure 1.2b).[72] Indeed, since chain regularity is destroyed via pendant PEPN recrystallization is precluded upon cooling. Additionally, a smaller temperature gradient between melting temperature (T_m) and glass transition temperature (T_g) led filaments to rapidly solidify.[72]

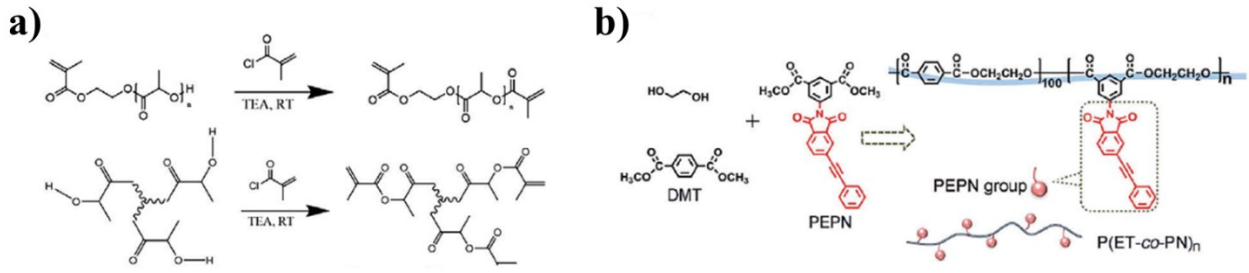

Figure 1.2 Various material design methods for 3D printing of thermoplastic polymers. a) Incorporation of the low-molecular-weight surface-segregating additives for improving adhesions between 3D printed layers. Reproduced with permission.[72] b) Incorporation of the π–π stacking networks into poly (ethylene terephthalate). Reproduced with permission.[73]

1.2.2.2 Thermoset Polymers

Thermoset polymers are crucial components used in many high-tech applications due to their robust thermomechanical characteristics and superior heat and chemical resistance. Thermal curing of thermoset polymers, unlike thermoplastic polymers, is irreversible due to the formation of chemical crosslinking. The majority of chemically crosslinked thermoset materials have a high T_g allowing them to resist high processing temperatures and are mechanically robust.[54]

It is difficult to construct 3D thermoset objects using extrusion techniques since they frequently cannot flow when pressure is applied. Shi et al.[74] showed how a thermosetting vitrimer epoxy ink might be readily extruded from the nozzle and maintain a high enough viscosity after being extruded by formulating the inks with a rheological modifier like nanoclay. However, with a high curing temperature, 3D-printed structures can still distort or collapse, undermining their shape fidelity. To address this issue, they increased the polymer viscosity via a chemical modification to prevent the 3D-printed construct from collapsing at the curing temperature. Subsequently, the 3D-printed constructs underwent a two-step curing process, including a precuring step at 60 ºC followed by another curing at 130 ºC for 20 and 6 hours, respectively. The remarkable printability of the developed epoxy-based system showed great potential for fabricating complex 3D constructs.[74]

Another promising strategy to make thermoset polymers more favorable for FFF 3D printers is the use of dynamic covalent chemistry.[75] Indeed, dynamic covalent chemistry provides a solution for reshaping and reprocessing the 3D printed thermoset polymers via a reversible crosslinking strategy. Reversible crosslinking has become possible with dynamic chemistry, which may improve the thermoset polymers' suitability for 3D printing. Yang et al.[76] developed a novel thermoset polymer that could be crosslinked via reversible furan-maleimide Diels–Alder

chemistry and investigated its 3D printability in terms of shape fidelity and printing resolution.[76] Due to the formation of thermally reversible bonds between bismaleimide groups and furan, the viscosity of their developed ink could be readily tuned by altering the temperature. Increasing the temperature during the polymer extrusion decreased the viscosity to 0.8 Pa s. The polymer was then subjected to a continuous cold air flow to raise its viscosity.[76]

1.2.2.3 Other Polymers

Silicone, known as polysiloxane, is a synthetic polymer extensively utilized in biomedical applications. Silicone mainly consists of a backbone of silicone-oxygen atoms along with organic substitutes attached to the silicon atoms.[77] This polymer possesses a variety of features, including macromolecular structural properties and inertness of the inorganic materials.[78,79] Silicone has a suitable bond strength because of the highly ionic Si-O bonds, which also contributes to its great chemical and thermal stability. Figure 1.3 depicts the production of a typical silicone form.[80]

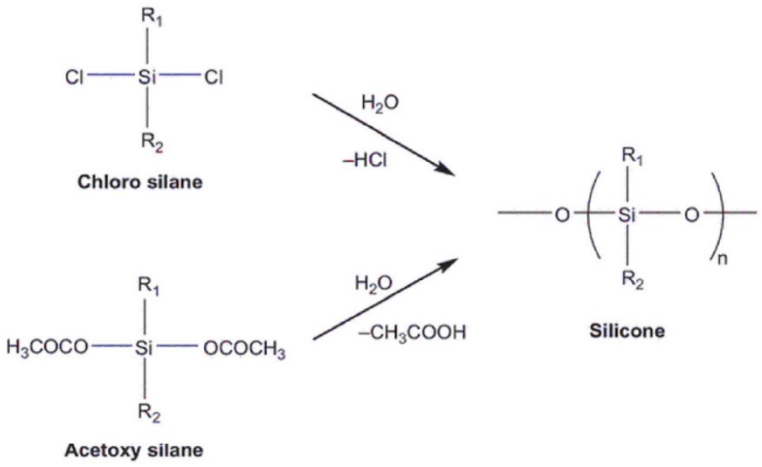

Figure 1.3 Schematic synthesis of silicone. Reproduced with permission.[80]

The unique physicochemical features of the silicones can be rooted in the presence of not only the flexible and long silicon atom bonds with oxygen and carbon but also the type and placement of the organic groups. The Si-O-Si bond angle is approximately 108º, which can make silicones highly flexible, resulting in low melting and glass transition temperatures.[81] Compared to the rotation energy of the C – C bonds, the lower rotation energy of the flexible and long Si-C and Si-O bonds may be of benefits to silicone's molecules by helping them to adopt the interfaces configuration with the lowest energy, leading to lower surface tension. Such a unique chemical structure allows the silicone to withstand high temperatures and enhances its oxidative resistance.[82] The strength of the silicone mainly attributes to its partial double bond and ionic properties. Silicones have backbone Si – O bonds with significant electronegativity differences between oxygen and silicon atoms.[82] The silicone's organic groups and their interactions with each other are other important factors affecting the surface features of the silicone. Overall, promising properties of silicones, including bioinertness, flexibility, biocompatibility, chemical, and thermal stability, make them a suitable candidate for various biomedical applications, particularly in fabricating tissue-mimetic substitutes.[37,83]

Silicone-based structures have been fabricated using traditional techniques such as lithography and molding for several years; however, such fabrication methods have their own limitations, like incapability for creating integrated and complex structures, time consuming and costly processing, which hinder their applications for biomedical purposes. Hence, during the last decade, researchers have been making an attempt to incorporate silicone-based inks into various 3D printing methods such as vat polymerization,[84,85] material extrusion,[86,87] embedding,[35] and material jetting,[88,89] which might revolutionize the industry of personalized substitutes and biomedical devices. The parameters of different 3D printing methods, including horizontal and vertical resolutions, printing

speeds, and curing mechanism of silicone utilized in recent studies, are summarized in Table 1.1.[84] Although not all variables were included in all articles, evaluating the existing data offers a better insight into the state of silicone-based inks' research and identifies areas for development.

Table 1.1 Comparison of 3D printing parameters of various silicone-based inks.

3D Printing Method	Authors/Company	Curing Mechanism	Lateral resolution (μm)	Vertical resolution (μm)	Printing Speed (mm/s)
Vat Polymerization	Wallin et al.[90]	UV/RTV	250-1000	N/A	N/A
	Bhattacharjee et al.[91]	UV	50-250	50	N/A
	Patel et al.[92]	UV	N/A	N/A	N/A
	Kim et al.[93]	UV	1000–2000	N/A	N/A
Material Extrusion	Zheng et al.[94]	UV	N/A	N/A	12.5
	Duoss et al.[95]	HTV	100–610	N/A	1–20
	Robinson et al.[96]	UV	N/A	N/A	4
	Liravi et al.[89]	UV/Moisture	250–300	100	5–10
	Lv et al.[97]	HTV	150	N/A	N/A
	Ozbolat et al.[86]	HTV	380–1800	N/A	0.5–5
	Hinton et al.[35]	HTV/Moisture	140–400	100	20
Embedding	O'Bryan et al.[37]	UV	30–700	N/A	2–10
	Fripp Design Ltd.	RTV	N/A	N/A	N/A
	Femmer et al.[98]	UV	100–400	N/A	N/A
Material Jetting	Wacker Chemie AG	UV	N/A	N/A	100-400
	McCoul et al.[26]	HTV/UV	200–400	2–4.5	50

Several silicone-based inks have been modified to make them suitable for SLA and DLP printing methods.[99,100] Wallin et al.[90] investigated the feasibility of using silicone double networks (SilDNs) for creating soft device architectures with micron resolution using an SLA printer (Figure 1.4a). They used condensation and photocurable thiol-ene reactions as their crosslinking methods providing the printed constructs with significant cohesive bonding along with high elongation and toughness, d$L/L_0 \sim 400\%$ and $U > 1$ MJ m^{-3}, respectively.[90] Bhattacharjee et al.[91] developed a 3D-printable polydimethylsiloxane (PDMS) (3DP-PDMS) resin using a desktop SLA printer. They successfully printed elastomeric 3D constructs that had similar characteristics to those of conventional thermally cured PDMS. They could also print a transparent microfluidic device with

a 500 μm channel width, which was biocompatible (Figure 1.4b). As can be seen in Figure 1.5b, they could print some complex and hollow structures without any sacrificial bath; it is worth noting that printing hollow structures is among one of the toughest 3D printing goals.[91]

As previously mentioned, SLA and DLP methods have their highlights and challenges. For example, it is true that these techniques are suitable for producing 3D constructs from a single ink with high resolution, but it may be challenging to modify them to create objects from numerous inks with various characteristics. Additionally, SLA and DLP printers are quite expensive, which has limited their widespread use. Compared to other printing methods, material extrusion attracts great interest for printing silicone-based inks due to its advantages, such as low cost and capability of extruding either one part silicone or two parts, which can be cured by moisture or thermal/UV hydrosilylation methods, respectively.[87,101,102] In 2013, Mannoor et al.[103] used the material extrusion technique to print a bionic ear using silicone, conductive polymer, and cell-laden hydrogel for the first time. They used the printed bionic ear as a substrate for culturing cells In vitro and In vivo, demonstrating the potential of 3D printing for fabricating personalized prosthetics.[103] Zheng et al. developed a sulfur-containing silicone elastomer for extrusion printing purposes by combining various low-viscosity silicone elastomers (Figure 1.4c). They used a combination of the base polymer, chain extender, thiol-ene chemistry, and crosslinker to produce a rapidly curing ink. Although their developed ink was capable of printing various structures like overhanging or tall ones, its low viscosity might cause a severe problem in controlling the ink flow for printing complex structures.[94] Additionally, based on their results and the material formulation, their developed ink might be hydrophobic. This hydrophobic nature may hinder the application of their developed ink for fabricating tissue-mimetic constructs, given that hydrophobic substrates can increase the chance of triggering body response.[104]

Overall, several factors need to be taken into account to develop a suitable 3D printable material for biomedical applications. Thanks to the unique chemical structure of the silicone, its biodurability and biocompatibility may be readily modified by changing the type and arrangement of its organic groups or performing post-serial extraction with organic solvents.[105] Besides biocompatibility, silicone-based ink needs to be further tuned, based on the desired 3D printing method, in terms of its: a) printability and rheological features; b) curing mechanism; c) hydrophobicity, and d) mechanical stability to be considered a proper 3D printable ink.[84,89]

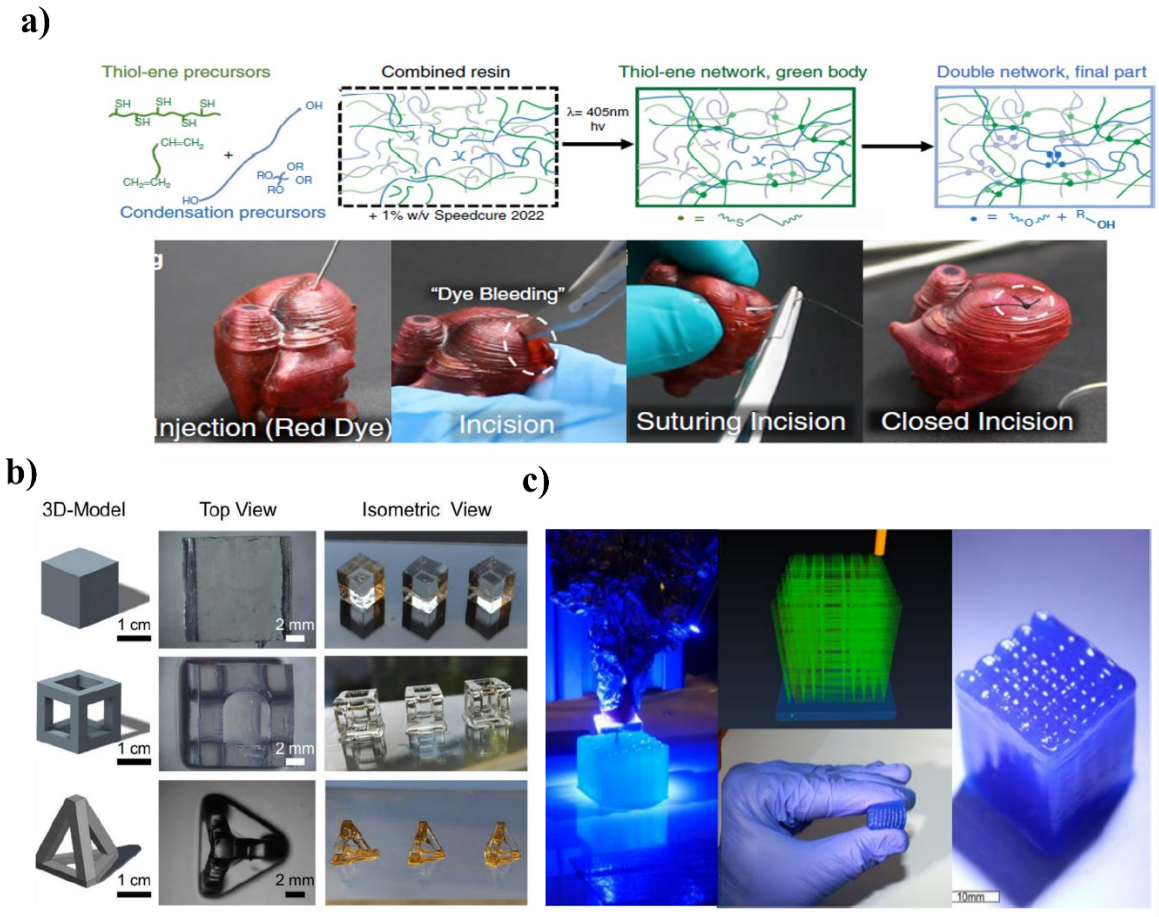

Figure 1.4 3D printing of various silicone-based materials. a) schematic illustration of the double network silicone developments via thiol-ene silicone (green species) and a condensation silicone (blue species). An example of a 3D-printed construct for the simulation of surgical skills.

Reproduced with permission.[90] b) Schematic illustration of the SLA printing of hollow constructs using a transparent silicone-based resin, reproduced with permission,[91] c) Schematic illustration of the extrusion printing of a low viscosity and UV-curable silicone-based ink. Reproduced with permission.[106]

a) Printability and rheological properties

One of the most crucial factors that can significantly affect the flow behavior of silicone elastomers is rheological properties. The rheological features of silicone elastomers should be tuned in terms of viscosity, loss and storage moduli, and so on, to make them suitable for various printing methods. One of the strategies to adjust the viscoelastic features of the silicones is to mix silicones of low and high molecular weight.[96] Robinson et al.[96] showed that by mixing a high molecular weight silicone with one of the low molecular weight in a 60:40 % ratio, the resulting ink demonstrated solid-like behavior at low shear stress, which in turn helps the ink to retain its shape fidelity after printing.[96] In another study done by Roh et al.,[107] a three-phase silicone ink, consisting of water, liquid silicone, and micro-particles of cured silicone, has been developed for extrusion-based printers. They developed an elastic ink with gel-like properties by covering the cured silicone micro-particles with liquid silicone to form capillary bridges. Although the developed ink can be used for printing in an aqueous solution or air, the printing resolution may be limited due to the existence of the silicone particles. Their developed ink also needed a post-curing step at a high temperature, 85 ^{o}C, to fully crosslink the silicone precursor existing between the silicone micro-particles which in turn hinders its application.[107]

b) Curing mechanism

High-temperature vulcanized (HTV) silicones are the most common type of silicone elastomers. These silicones must be partly cured between a few minutes to a few hours to allow previously deposited layers to withstand the stresses brought on by the weight of the top printed layers. This curing mechanism might not only slow down the printing process but also compromise the precision of the printed constructs. Additionally, curing the silicone after printing numerous layers may lead to the poor shape fidelity of the printed samples because of the previously deposited layers' weight.[84] Morrow et al.[108] reported other challenges, such as quick gelation time, high chance of structural deformation, and limited heat transmission range that significantly restrict the application of heat-curable silicones. Hence, UV-curable silicones, with their capability to be cured within the order of a few seconds, can be considered a potential alternative for heat-curable silicones in extrusion and jetting-based printing methods. Patel et al.[92] developed stretchable UV-curable elastomers by combining a difunctional crosslinker consisting of aliphatic urethane diacrylate (AUD) diluted with 33 wt% of isobornyl acrylate and an epoxy aliphatic acrylate (EAA) suitable for DLP-based printing. The elongation at the break of their developed ink was approximately five times bigger than that of commercially available silicone elastomer, and it can be stretched up to 1100%.

c) Hydrophobicity

Silicones' hydrophobicity frequently restricts its use when dealing with solutions containing biological materials.[109] Because of the hydrophobicity of the silicone's surface, the contact angle is 108^{o}, undesired proteins are non-specifically adsorbed to it, affecting analyte transport and lowering detection sensitivity and separation performance.[110] Silicone materials are also extensively used for fabricating microfluidic devices. This inherent hydrophobicity makes it challenging to flow aqueous solutions or combinations of aqueous and organic solutions through

the microfluidic channels, particularly when polar liquids are used.[111] Hence, several researchers have been attempting to make the silicone's surface hydrophilic and immune to protein adsorption. Their approaches have been mainly focused on employing different surface treatment methods like O_2 plasma, UV, or ozone, surface coating, silanization, and chemical vapor deposition.[112]

Even though these methods have been effective at increasing surface hydrophilicity to some extent, there are some concerns regarding their chemical stability, fabrication time, and the need to use special equipment, all of which limit wider application.[113] Furthermore, several of these techniques result in surface cracking, lower transparency, altered mechanical properties, increased roughness, and, more importantly, producing a temporary hydrophilic surface.[114,115] Indeed, as a result of the silicone chains' mobility, the surface gradually loses its initial hydrophilicity, defeating the purpose of the treatment.[116,117] Such issues fade the advantages of these silicone surface modifications and highlight the need to develop new methods for making hydrophilic silicones. Gökaltun et al.[118] reported a new surface modification method, surface segregating, to produce PDMS with a contact angle of 23.6º, which could retain its hydrophilicity for a longer time compared to other methods. To do so, they prepared a copolymer consisting of PDMS and poly (ethylene glycol) (PEG) segments (PDMS-PEG) and then incorporated it into PDMS. The PDMS-PEG segments spontaneously segregated to surfaces and faced an aqueous solution, which in turn improved hydrophilicity without needing post manufacturing steps.[118]

d) Mechanical stability

Numerous studies have been done on the mechanical characteristics of elastomers such as silicone.[119–122] The standard requirements for silicones used in biomedical applications not only include suitable tensile and tear strength, high elasticity, and adequate elongation at break, but they also need to have a proper hardness according to their application. For example, since prostheses

are frequently removed for sleep and affixed to the skin when awake, they must be robust and possess soft skin-like qualities. Hence, the surface qualities and mechanical properties of the currently available silicones need to be improved to make them appropriate for different biomedical applications, according to Aziz et al.[123]

Crosslinking density plays a significant role in tuning the flexibility and hardness of silicones. For example, Lv et al. demonstrated a new class of thermally curable silicones with tunable stiffness and hardness for extrusion-based 3D printing.[97] In their formulation, the crosslinking density has been controlled by using vinyl-terminated PDMS and dihydride chain extenders. Bhattacharjee et al.[91] also improved the elongation at break of the low viscosity silicones by mixing two different types of the silicone methacrylate macromers, PDMS macromers either with the side chains of methacryloxypropyl or terminated with methacryloxypropyl. The polymeric network was created via the side chains after photocuring, increasing elongation at break.

In general, there is still a need to develop a silicone-based ink with all the above-mentioned features, such as hydrophilicity, UV-curability, and suitable mechanical and rheological characteristics. Indeed, the improvement of silicone-based inks in the above-mentioned criteria may be of benefits to the fabrication of not only personalized and biocompatible tissue-mimetic substitutes but also biomedical devices.

1.2.3 Hydrogel Inks

3D cross-linked polymer networks known as hydrogels are capable of absorbing and retaining a high volume of water (up to 90% of their capacity).[124,125] 3D network of the hydrogel is interconnected via various interactions, including electrostatic, hydrophobic, van der Waals, hydrogen bonds, or a mixture of these interactions.[126] Hydrogels can mimic the natural 3D

extracellular matrix (ECM) microenvironments due to their outstanding features, such as biocompatibility, adjustable degradation rate, and mechanical cues.[127,128] In addition, hydrogels can be readily turned into biomimetic scaffolds by incorporating various bioactive molecules such as growth factors, fatty acids, and nucleic acids.[128] Some hydrogels also have shear-thinning and thixotropic features making them an ideal candidate for bioprinting purposes.[129]

Various fabrication techniques and tunable features of the hydrogel-based materials lead them to be utilized for multiple biomedical applications such as regenerative medicine and tissue engineering.[130–132]

When biological components and cells are incorporated into 3D-printable hydrogels, they are referred to as bionks.[131] The most suitable 3D printing technologies for printing bioinks and hydrogels are inkjet, light-assisted, and extrusion-based printing.[133,134] Ideal hydrogel inks for bioprinting must generally meet specific requirements, including a) rapid gelation, b) proper mechanical features, c) suitable shape fidelity, and d) flow under modest pressure.[135] Hence, the most straightforward method to develop an ideal hydrogel for bioprinting is to utilize a polymer solution that can be gelled after deposition using external stimuli such as temperature, ionic concentration, light, and pH.[55] In recent years, a diverse library of hydrogels with various gelation methods, rheological features, and biological cues have been investigated to meet the above-mentioned requirements.

Synthetic or natural proteins, including fibrin, gelatin, collagen, polysaccharides, such as chitosan, agarose, and alginate, and self-assembling peptides are considered the typical precursors for creating common hydrogels.[61,133,136] The hydrogels' printability can be extensively tuned by modifying the rheological features, particularly thixotropic and shear-thinning properties. Indeed, the printing parameters such as extrusion pressure, speed, and structural fidelity mainly attribute

to the rheological features of the hydrogels.[45] A bioink with shear-thinning behavior is a non-Newtonian material that loses its viscosity by increasing the shear rate. This phenomenon can reduce the applied shear stress on embedded cells which in turn can help cells withstand and survive during the bioprinting process.[137] In general, natural polymer-based bioinks, such as fibrin or collagen, possess low viscosity and weak mechanical cues, which hinder their application in tissue engineering, while synthetic polymer-based bioinks not only have better mechanical cues but they are also more viscous, to some extent. Hence, one of the most efficient approaches for developing hydrogel bioinks is to mix synthetic and natural polymers to prepare a shear-thinning bioink with similar bioactive cues to that of the natural ECM.[55]

The gelation process of the hydrogels can influence not only the cell viability but also the resolution of the printing as well. Among different gelation methods, ionic, thermal, and photo/chemical crosslinking are the most common techniques (Figure 1.5).[137]

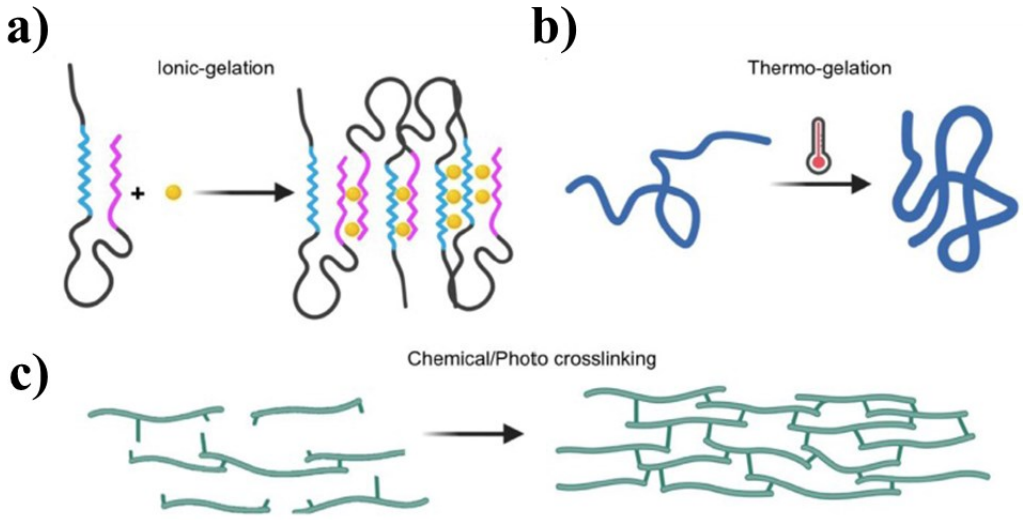

Figure 1.5 Different gelation processes of hydrogels. a) Ionic gelation, b) Thermo gelation, and c) Chemical and photo-crosslinking. Reproduced with permission.[55]

Regarding ionic gelation, the existence of electrically charged components enhances spontaneous physical gelation. When electrically charged hydrogels, known as polyelectrolytes, mix with multivalent anions/cations, the presence of the net charge on the backbone of polyelectrolytes results in forming complexes.[138]

For instance, Freeman et al.[138] investigated the impact of various ionic cross-linkers, such as $CaSO_4$, $CaCl_2$, and $CaCO_3$, and their concentration on the width of the printed alginate filaments. They found that regardless of the type of the crosslinker, the amount of the crosslinker is proportional to the molecular weight of the alginate. Indeed, compared to high molecular weight alginate, low molecular weight alginate needs about twice more crosslinker to create a printable ink. Their results also show that using $CaSO_4$ resulted in stiffer scaffolds. Although the existence of reversible interactions leads to constant viscosity during the ionic gelation process, the printed structures possess weak mechanical cues due to the presence of non-covalent interactions. Hence, there is a need to have a post-printing crosslinking step to enhance the mechanical stability of the printed constructs.[138]

In thermal gelation, high temperature leads to the formation of high molecular weight complexes, gel network, via the aggregation of unfolded building blocks. Disulphide bridges and hydrophobic collapses are considered the leading players in this process. Although thermal gelation is straightforward and well suited to biological systems, the resulting gel constructs are often thermos-reversible due to the presence of dynamic non-covalent interactions.[55]

The photo/chemical crosslinking method provides the most durable and mechanically tunable hydrogels. In this gelation method, the bioink's viscosity is not affected during the printing process since the polymerization occurs after the bioink has been extruded, in which the generated free radicals for crosslinking may affect cell viability to some extent.[139] Several conventional chemical

crosslinking methods are available, including condensation reaction, Michael addition, and thiol-ene reactions, which have been widely utilized to produce various hydrogels for various biomedical purposes.[55] It is true that the application of the chemical crosslinking method can provide a chance of producing hydrogels with adjustable degradation rate and mechanical properties, but it has its own drawbacks, such as low gelation speed and possible cytotoxicity of the crosslinkers as well.[55]

To address these issues, W.J. Zhang et al.[140] demonstrated a double crosslinking method of UV crosslinking and click reaction by incorporating methacrylate anhydride and 3,3′-dithiobis(propionyl hydrazide) (DTP), respectively, into the hyaluronic acid-based hydrogel.[140] Their crosslinking strategy not only shortens the gelation time to a few seconds under UV irradiation but also provides the opportunity to fabricate a biocompatible cell-laden construct with adjustable stiffness.[140] In another study done by Pereira et al.[141], a methacrylate modified pectin bioink was crosslinked through ionic gelation by using calcium ions and UV irradiation which could provide better control over rheological properties allowing them to adjust the storage modulus within the range of 259-3552 Pa.[141]

1.2.4 Composite Inks

Single-phase inks have been extensively utilized for diverse bioprinting and conventional printing applications. However, their applications have been hampered by a restricted selection of materials, poor printability, and inadequate mechanical strength.[142] Recent attempts have been made to develop functional 3D printable inks that are applicable to a wider variety of applications in response to the growing demand for printed materials with specified properties. Composite inks provide a greater degree of adaptability to meet the intended objectives. The fibrous nature of

various human biological tissues, ranging from soft to hard tissues, supports the application of composite inks in the area of tissue engineering.[143]

Composites are made up of two or more materials in different stages and have considerably different characteristics.[144] Therefore, a single-phase combination of nonfibrous precursors or monomer solution of fibrin or collagen is not considered a composite ink, while it may be a multicomponent ink.[145] If these components are combined with a base ink, such as polymer, hydrogel, or ceramic, to generate a multiphase substance, we may have a composite ink. Composite inks, compared to single-phase inks, must possess a wider variety of characteristics. For instance, Matrigel is a commercial hydrogel composite that is rich in laminin and collagen, but it has poor shape fidelity.[146,147] To address this issue, Fan et al.[148] incorporated agarose into the Matrigel matrix and developed a composite ink, which not only has proper rheological features for bioprinting but can also provide a suitable microenvironment for cellular activity.[148] Four-dimensional (4D) printing is made possible incorporating of controlled shape-altering properties into composite inks.[149] By using composite inks, more mechanical, electrical, and physicochemical tunability may be attained.[150,151]

In fact, composite inks each component's benefits to produce printed objects with enhanced qualities by mixing at least one kind of insoluble additive into a single-phase matrix.[144] Different additives, such as nanoparticles, nanotubes, and fibers, can be incorporated into the base inks to develop composites with not only desirable mechanical and rheological features but also suitable biocompatibility.[152] The inclusion of nanoclays, for instance, may enhance the printability of acrylamide and agarose inks by increasing their thixotropy.[153] Nanotubes may be included in composite hydrogel networks to offer more focal adhesion sites and to enhance cell adherence and migration inside bioprinted scaffolds.[154]

1.3 Additive Components

1.3.1 Collagen

The most prevalent protein in the body is collagen which has over 30 different types. A three-stranded structure of collagens is made of one alpha-2 and two alpha-1 polypeptide chains.[155,156] Proline, glycine, and hydroxyproline are among the most repeatable amino acids existing in collagen's structures.[156] Compared to other fibrous proteins, collagen fibrils possess a higher stiffness, approximately 2 GPa; however, these fibrils might be degraded at temperatures above 40 ^{o}C which in turn can erode their mechanical stability.[157] Collagen has been widely used for different tissue engineering applications because of its suitable features such as biocompatibility and biofunctionality, which are mainly rooted in the presence of diverse cell-adhesion ligands in the collagen's structure.[158] Sue et al.[159] combined collagen and chitosan to develop tunable hybrid bioinks that could be printed using a low-temperature 3D printing method. The addition of the chitosan led to the formation of hydrogen bonds with collagen that could significantly improve the collagen's printability. Moreover, they visualized cell proliferation and migration of the bone mesenchymal stem cells by using live/dead assay, which showed stem cells not only on the surface but also at the bottom of the scaffolds (Figure1.6a).[159]

1.3.2 Carbon Nanotubes

Carbon nanotubes (CNTs), hollow tubes of graphite sheet with 1-100 nm diameter, were first discovered by Iijima in 1991. There are two types of CNTs, single-walled (SW) and multi-walled (MW) CNTs, based on the number of concentric tubes. The diameter of the SWCNTs and MWCNTs are approximately 1-2 nm and 5-100 nm, respectively.[160] Based on CNTs dimension, MWCNTs are more favorable for tissue-engineering applications because their dimensions are similar to those of ECM's fibrous protein, whereas SWCNTs are more suitable for drug delivery

applications due to their higher chance of penetration into the cell membrane.[161,162] CNTs have been extensively used for various biomedical applications such as tissue engineering, biosensing, and drug delivery because of their suitable mechanical, chemical, and electrical features. However, the hydrophobicity of the pristine CNTs limits their application to some extent. To solve this issue, many researchers have tried to functionalize CNTs with various moieties, particularly hydrophilic groups, to enhance their dispersibility and biocompatibility. Thanks to the large surface area and the presence of sp^2 carbons on the CNTs' sidewall, CNTs have become an ideal candidate for surface functionalization purposes, either chemically or physically.[161] Izadifar et al.[163] developed a hybrid cardiac patch by incorporating carboxyl functionalized CNTs into alginate and methacrylated collagen (MeCol). They reported that the incorporation of the CNTs could remarkably increase the electrical conductivity of MeCol and develop an interconnected nanofibrous network. Compared to pure alginate, this interconnected network could facilitate cell attachment resulting in higher cell proliferation (Figure 1.6b).[163] In another study by Li et al.[164], a magnetic carrier consisting of CNTs and HA has been fabricated to act as a targeted drug delivery system. CNTs have been functionalized and loaded by oxygen-containing functional groups and the anticancer drug doxorubicin (DOX), respectively. They also significantly increased the loading efficiency of the CNT/HA carrier by grafting chitosan (CS) and folic acid (FA) into it through a condensation reaction.[164]

1.3.3 Cellulose

Nanocelluloses can be derived from a variety of cellulosic sources, such as algae, bacteria, and wood. The nanocellulose obtained from cellulose fibers may be classified depending on the parameters such as sources, treatment methods, and dimensions. Nanocellulose is classified into three types: bacterial cellulose (BC), cellulose nanocrystal (CNC), and cellulose nanofiber

(CNF).[165,166] Among various types of nanocellulose, CNC has grabbed great interest because of its remarkable features such as large-scale productivity, high mechanical strength, renewability, large surface area, low density, and biocompatibility.[167] CNC has a needle-shaped structure with an average diameter and length of 10 and 100 nm, respectively, which can be mechanically or chemically extracted from cellulose.[168]

Besides the above-mentioned remarkable properties of CNC, it can also induce shear-thinning property making it an ideal candidate for developing 3D printable inks. This shear-thinning property is rooted in the capability of CNC particles in self-assembling into chiral nematic liquid crystalline domains.[169] Kam et al.[170] developed acrylic acid-based hydrogels using CNC and a water-compatible photoinitiator, 2,4,6-trimethylbenzoyl-diphenylphosphine oxide (TPO). Their developed ink possesses a suitable shear-thinning property that photopolymerized in about 5 seconds, providing them with an opportunity to 3D print high-aspect ratio structures (Figure 1.6c).[170]

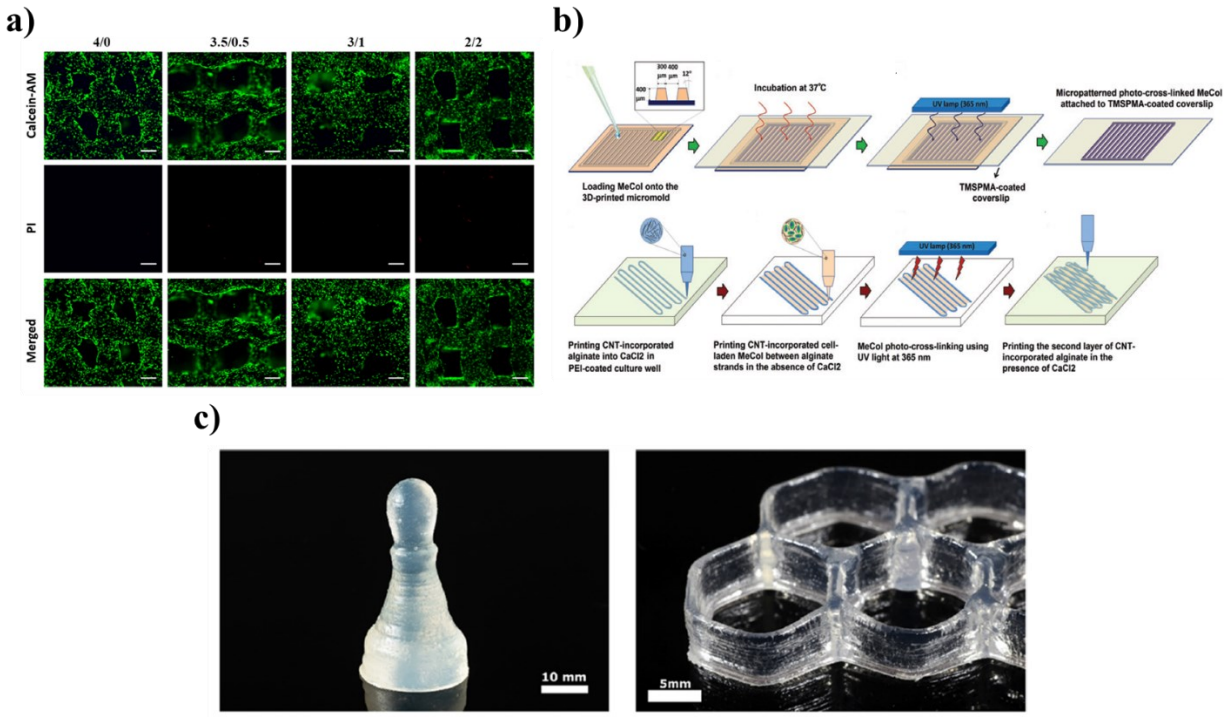

Figure 1.6 Examples of the application of additive materials for 3D printing purposes. a) proliferation and migration of the bone mesenchymal stem cells on the scaffold surface, 3D printed from collagen and chitosan. (Scale bar: 500 μm). Reproduced with permission.[159] b) schematic illustration of hybrid implant bioprinting a methacrylated collagen-CNT-based material. Reproduced with permission.[163] c) chess pawn and honeycomb structures 3D printed using a rapidly-curing CNC-based ink. Reproduced with permission.[170]

1.4 3D Printing in Biomedical Applications

Using formative (molds) or subtractive (machining) methods in conventional manufacturing, involving several phases and expensive infrastructure, limits the capacity to quickly incorporate changes to the final product. When it comes to the fabrication of complex geometries, the inefficiencies of such fabrication techniques may become more visible.[171] However, during the past forty years, 3D printing, or AM, has become a reliable method for quickly and affordably

constructing geometrically challenging items. The fundamental idea of 3D printing dates back to the 1980s and entails layering the deposition of material in three dimensions while being directed by a computer-generated model.[172] This fabrication method enables the development of incredibly complex designs that would be exceedingly challenging or impossible to construct using standard manufacturing procedures, leading to a surge in its usage by numerous sectors.[171] Nowadays, 3D printers have been extensively utilized to fabricate scaffolds that can be used for surgical planning,[173] therapeutic delivery,[174] tissue engineering,[175] and implant design.[176] Bioprinting, a novel but rapidly expanding use of AM, allows for the spatially specified seeding of cells in 3D space.[177] This makes it possible to create in vitro models of diseases and drugs as well as to biofabricate implantable tissues, including cartilage, skin, and bone.[178] Grix et al.[179] fabricated 3D liver lobule models with hollow channels using stereolithography. Their cell-laden ink and 3D model, consisting of methacrylated gelatin (GelMA), PEG, and hepatic stellate cells, showed a higher amount of hepatocyte-related gene expression in comparison with conventional 2D monolayer cell culturing methods. Stereolithography also provided them with the opportunity to embed channels within the model leading to the formation of a vascular network.[179] The prostheses and implants field is constantly evolving to not only make such tissue substitutes more compatible and favorable for the human body but also create precise and accurate 3D tissue-mimetic constructs with biomechanical properties similar to human ones.[180] Designing prostheses and tissue substitutes is a multidisciplinary subject that connects engineering, molecular biology, material science, and chemistry. 3D printing can provide the opportunity to bridge the gap between engineering and biology by fabricating biocompatible 3D constructs (based on the radiological images) that can precisely mimic the complex human tissue's structure and perfectly fit into the damaged tissues.[181] Eggbeer et al.[182] used an acrylate-based material to print a nasal prosthesis

with an inkjet-based printer, for the first time. Their printed nasal prosthesis was covered by a thin silicone layer and the tests demonstrated that the nasal prosthesis additively built has an equivalent level of aesthetic quality to one made similarly using the traditional molding method. Although the overall fabrication time of the artificial nasal was dramatically reduced due to the employment of 3D printing, the mechanical features of the printed construct failed to live up to the expectations. This study highlighted the importance of material selection for AM applications.[182]

Despite the rapid progress in using 3D printers for various biomedical applications, selecting suitable 3D printable biomaterials still needs to be considered the foremost challenge limiting the 3D printing development. As mentioned, a suitable biomaterial must satisfy all the required criteria for fabricating a functional 3D construct, including shape fidelity, biocompatibility, printability, tissue-mimetic functionality, and structural resolution, based on the selected 3D printing method. For instance, the biocompatible inks must mimic the functional and biomechanical characteristics of the selected organ or tissue in terms of mechanical stability, biodegradation rate, and cell interactions. Several strategies, such as mixing synthetic and natural polymers or using ECM-based hydrogel, have been used to meet this requirement.[183,184] Additionally, regarding ME 3D printable inks, viscosity is another factor that needs to be taken into account. Indeed, the selected ink needs to be readily extruded through the nozzle and solidified quickly after printing. Inducing the shear-thinning property by incorporating nanofillers into the polymer matrix can be a proper solution to meet this need.

In this project, we attempted to develop a hydrophilic and rapidly curing silicone-based ink with tunable mechanical features for ME 3D printing applications and investigated its capability in fabricating tissue-mimetic models and biomedical devices by choosing articular cartilage (AC) and microfluidic devices (MFDs), respectively, as models.

1.4.1 Cartilage

Cartilage is a flexible connective tissue readily seen throughout the body in external ears, spine, nose, and synovial joints. This aneural and avascular tissue has three different types, known as hyaline, fibrous, and elastic, all of which possess a low cell density (chondrocytes). Chondrocytes are responsible for producing and secreting the main components of the cartilage ECM.[185,186] The ECM of cartilage has a distinct variety of proteoglycans interwoven within a highly hydrated collagen fibrillar architecture to carry out the biomechanical duties of structural strength and deformation resistance. This matrix is produced and assembled by chondrocytes with the help of many other non-collagenous proteins, proteoglycans, and glycoproteins. Each of the three cartilage forms has a different distribution and types of proteoglycans and collagens, leading to variations in structure and biomechanical capabilities. For instance, fibrous cartilage possesses a dense population of type I collagen, providing significant tensile strength, and it is typically present in menisci, bone/ligament-tendon interfaces, and intervertebral discs.[187,188] Type VI collagen is present in the pericellular network of this cartilage, whereas type II collagen and proteoglycans are present in very small amounts throughout the ECM. Proteoglycans, type II collagen, and elastin fibers comprise the majority of the elastic cartilage's ECM. The tissue's yellowish hue is also caused by the elastin fibers.[189]

Among various cartilage types, we chose hyaline cartilage, known as articular cartilage (AC), as a model to assess the capability of our developed ink in fabricating tissue-like substitutes since AC is the most prevalent type of cartilage throughout the human body.[189]

1.4.1.1 Articular Cartilage (AC)

AC is glassy-like cartilage with high strength and low friction, located in the trachea, growth plates, bronchi, ribs, nose, and covering the bone's surfaces in synovial. This cartilage is mainly

responsible for lubrication, with a coefficient of friction on the order of 0.001-0.01, and superior mechanical support to diminish wear and relieve stress.[190–192] Unfortunately, articular cartilage lesions have a limited intrinsic capacity for regeneration due to their acellular and avascular nature, which results in osteoarthritis (OA) and skeletal disorder disabilities.[193] Degeneration of the articular cartilage has not only earned the moniker "undead cancer" but also the second-highest incidence of disability after heart disease. Hence, restoring patients' damaged cartilage as soon as possible is crucial to enhance their quality of life. To do so, the physicochemical features and architecture of the native AC tissue need to be well understood.[194] Indeed, adult AC is divided into two spatially distinct regions: the osseous region, which includes the subchondral bone zone, and the cartilaginous region, which includes the surface zone, the middle zone, the deep zone, and the calcified zone.[195] These zones, as depicted in Figure 1.7, exhibit various biochemical compositions, chondrocyte morphologies, and physiological traits.[196]

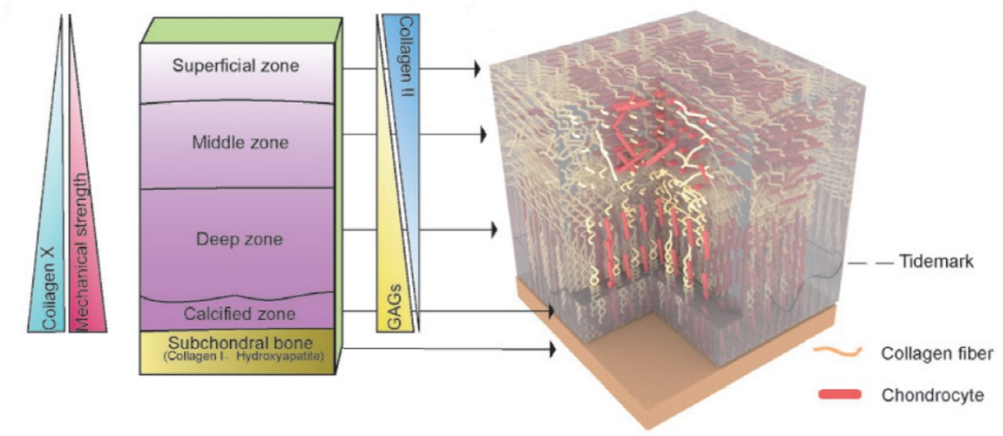

Figure 1.7 Schematic illustration of AC with its zonal structure. Reproduced with permission.[197]

The majority of current treatment procedures fall into two broad categories: nonsurgical (pharmaceutical) and surgical approaches, including bone marrow stimulation techniques (like microfracture and autologous chondrocyte implantation) and arthroscopic debridement.[198,199]

Although these therapies have made considerable progress, they fail to achieve the ideal regeneration of the original AC structure due to their limitations.[189]

Tissue engineering methods may offer fresh hope to AC regeneration, as current therapeutic therapy approaches do not provide long-term solutions.[193] Scaffolds, biomechanical and biochemical stimuli, and cells are all utilized in the fundamental tissue engineering method.[200] A range of artificial or organic materials have been researched recently as scaffolds for AC regeneration.[201] These methods are regarded as completely developed due to the excellent capacity of scaffold-based techniques to include numerous biological stimuli and the excellent initial mechanical characteristics of such scaffolds.[202] Arjamndi et al.[203] developed a hydrogel for cartilage replacement by introducing silica nanoparticles (Si-NPs) into an interpenetrating polymer network of alginate-polyacrylamide (ALG-PAAm). They found that using the Si-NPs leads to the formation of interfacial interaction between these nanoparticles and the polymer network, leading to the ultra-low coefficient of friction, suitable strength properties, and adjustable viscoelastic behaviours.[203] Nakamura et al.[204] used the scaffold-free Kenzan technique and human-induced pluripotent stem cell (iPSC)-derived neural crest cells for fabricating the articular cartilage. The fabricated 3D constructs, with 6 cm^2 in size, have maturated for three weeks to reach a mechanical strength similar to that of native cartilage (0.88 MPa). Despite the progress made through these studies, employing homogeneous scaffolds to repair AC cannot live up to the expectations due to the heterogeneous structure of AC, consisting of layers with various functional and metabolic characteristics.[205] Hence, researchers have been tried to develop scaffolds based on the multilayered structure, content, and biochemical needs of AC tissue.[206]

In an attempt to replicate the zonal mechanical characteristics of the AC, Zhu et al.[207] combined chitosan, collagen, and polycaprolactone to fabricate a porous and four-layered scaffold using a

low-temperature deposition processing method. They successfully created an AC-like construct with a suitable swelling index gradient and gradient increase of compressive modulus and stress from the top to the bottom layer. Their fabricated scaffold demonstrated a significant potential for use in AC regeneration.[207] In another study, Liu et al.[208] used GelMA and nanohydroxyapatite (nHA) to create a multi-layered osteochondral construct. They fabricated a simple cubic scaffold with three different layers, including cartilage, interfacial, and subchondral, with 15% GelMA, 20% GelMA, and 3% nHA, 30%GelMA and 3% nHA, respectively. Within three months after being transplanted into a rabbit knee with an osteochondral lesion, the construct demonstrated a suitable regeneration.[208]

It is true that, during the last decade, several cell-based therapies have been used to improve AC repair and regeneration, respectively, but most of these approaches not only possess a high failure rate but also are suitable only for the treatment of minor defects and, in particular, among young adults. Hence, we attempted to develop a series of hydrophilic and UV-curable silicone-based inks of different stiffnesses, with which to precisely 3D print a multilayered AC substitute from the CT images that may be of more benefit to all age groups.

1.4.2 Microfluidic Devices (MFDs)

Deciphering several biological phenomena has significantly benefited from the use of MFDs.[209] There are several microfluidic designs that may be utilized to in-vitro mimic the function of human organs.[210,211] These organs-on-chips can be used for drug screening and disease modeling.[212] Additionally, the research on cancer metastasis, tumor development, and their interactions with other cells have all been thoroughly conducted using MFDs. These "Tumor-on-chips" have demonstrated their effectiveness in applications for drug testing.[213] However, most of these MFDs are still only useful in laboratories for research purposes. Such MFDs are currently made using

soft lithography and PDMS. High-resolution photolithography is used to create the masters for soft lithography, which has been found efficient in reproducing characteristics from the micro to the nanoscale.[214,215] However, the use of PDMS MFDs in a clinical context is hampered by the fact that soft lithography necessitates a cleanroom facility for prototypes manufacturing, time-consuming manufacturing stages, and extensive prior knowledge.[215]

3D printing has emerged as a viable option for addressing the 'fabrication barrier' related to the MFDs by providing quick, low-cost, one-step, and completely 3D manufacturing of MFDs.[216,217] 3D printing is a "one-step" manufacturing process since it creates MFDs with just one machine, in contrast to soft lithography. Moreover, 3D printing can easily create complex 3D structures, such as overhanging structures, whereas soft lithography is restricted to planar 2-dimensional complexity. The unmatched manufacturing capabilities of 3D printing have increased its appeal in microfluidics.[217]

Among various 3D printing methods described in previous sections, extrusion-based, SLA, and inkjet 3D printing are widely utilized to construct MFDs using four core production techniques: direct printing, mold-based, modular, and hybrid manufacturing techniques.

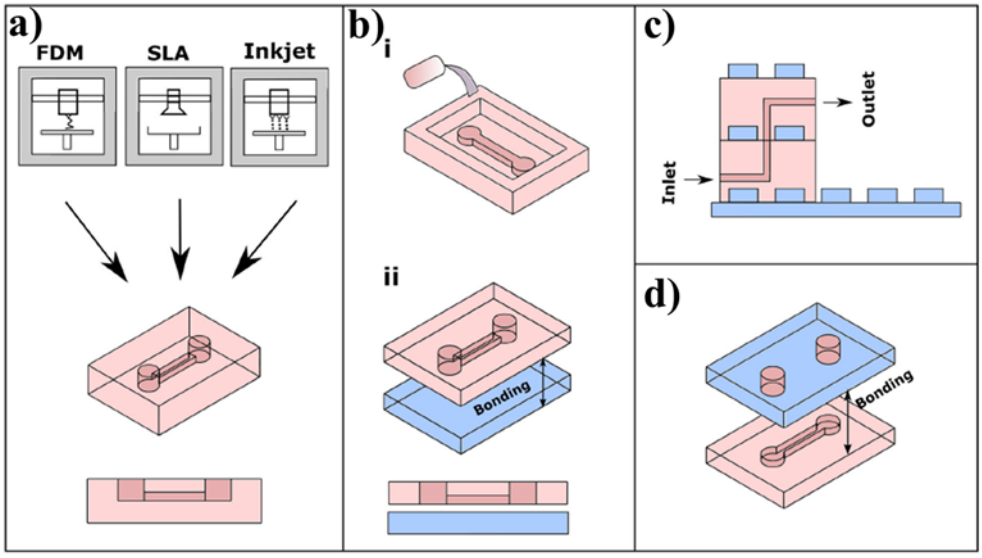

Figure 1.8 Schematic illustration of conventional MFDs fabrication methods. a) direct printing approach, b) Non-sacrificial mold-based approach: (i) replica molding process, (ii) sealing of channel with PDMS or glass slide, (c) modular approach, d) hybrid approach. Reproduced with permission.[218]

1.4.2.1 Direct Printing Method

The direct printing technique, known as the quickest MFDs fabrication method, has been extensively employed to create MFDs.[219] The direct printing method is a "one-step" manufacturing technique that can print various MFDs without bonding or assembly (Fig. 1.8a). The printed MFDs could, however, go through some post-processing procedures to enhance optical transparency, biocompatibility, and surface roughness. Nelson et al.[219] used FDM technique to create transparent and flexible MFDs, made of Thermoplastic polyurethane (TPU), with channel diameters within the range of 50 to 400 µm. They showed that the printed MFDs were not only compatible with most of the organic solvents, except chloroform and acetone, but also biocompatible and optically transparent when mouse inner medullary collecting duct (mIMCD3) cells were cultured on them. They also found that the polymer sagging

occurring during the deposition of the bridging layer to close the channels may affect the channel visibility. To address this issue, they changed the geometry of the channels to diamond, triangular, and ellipsoid shapes.[219] Salentijn et al.[220] investigated the various polymers in terms of their solvent compatibility, biocompatibility, and autofluorescence for FDM 3D printing purposes to show their potential for fabricating MFDs. They also found that fluid leakage can be prevented by depositing four walls with 20% infill density.[220] A unique technique was created by Ching et al.[221] that involved 3D printing the microchannels' pattern on flat poly(methyl methacrylate) (PMMA) substrates. After printing the pattern, another PMMA substrate was placed and fixed on top of it, using spacers and mechanical fasteners to seal the printed channels. Thanks to this patterning method, they could create various MFDs, including Y-mixer, droplet generator, and fluidic valves with dimensions as small as 32 and 30 μm in width and height, respectively.[221]

SLA technique is another option for direct 3D printing of MFDs with high resolution. Kuo et al.[222] used a low-molecular weight diacrylated PEG resin (PEG-DA-258) to 3D print MFDs with submillimeter resolution (channel width of 27 μm). They also demonstrated the successful fabrication of various MFDs, including passive/active micro-mixer, 3D-fluid routers, and high-aspect ratio microchannels. In another study by Gong et al.,[223] fabricated microchannels with even lower dimensions (18 × 20 μm) by utilizing PEG-DA-258 containing resin and a custom-made DLP printer.[223]

1.4.2.2 Mold-based Method

Sacrificial molds and non-sacrificial molds are both used in the mold-based technique. The mold-based technique is considered an indirect 3D printing method for creating MFDs. A soft lithography mold is often 3D printed, and replicas are molded from thermally curable or photocurable materials. The final stage calls for gluing replica molded objects with either glass

slides or PDMS using a plasma treatment technique, assuming the molds are not sacrificed. On the other hand, with sacrificial molds, the final step is dissolving sacrificial elements to remove the mold. While non-sacrificial molds can be utilized repeatedly, sacrificial molds may only be utilized once. In contrast to soft lithography, which needs numerous steps for the master fabrication, the 3D printed mold-based technique significantly decreases the time for producing the devices. Figure 1.8b depicts the replica molding and bonding process using a non-sacrificial mold.[218]

FDM can be used to create both sacrifice-based and non-sacrificial molds by using various materials such as acrylonitrile butadiene styrene (ABS), poly(vinyl alcohol) (PVA), and PLA.[224–226] Saggiomo et al.[227] used sacrificial molds of ABS and PDMS replica molding to construct a different variety of MFDs such as Hilbert cube and spiral channels. Additionally, they have demonstrated the feasibility of incorporating different electronic components during the molding of PDMS replicas by integrating UV LED light, copper wire, and Arduino microcontroller for other purposes such as fluorescence detection, NMR spectroscopy, and RGB color sensing, respectively.[227] Shankles et al.[224] employed 3D-printed ABS molds to create droplet and gradient generators with built-in custom software. The computer application provides a list of parameterized microfluidic characteristics and includes a slicer program generating G codes. They included cleaning the surface of ABS using acetone as part of the manufacturing process, significantly reducing the molds' surface roughness.[224]

SLA has been utilized extensively to create non-sacrificial molds for PDMS MFDs due to its fewer and simpler manufacturing stages compared to soft lithography. The efficiency of the printed molds can be significantly improved by employing a suitable post-processing technique to keep PDMS from sticking to the surface of the mold and remove catalysts and uncured resin remaining

on the surface of the mold.[216] Chan et al.[216] reported that by heating the printed molds to 130 °C, the remaining uncured resin might undergo silanization, which would prevent PDMS from sticking to the surface of the mold. By adopting suitable post-processing processes and maximizing peeling direction, they have shown how to manufacture replicas of intricate overhanging structures.[216]

For the creation of sacrificial molds, 3D printing has proven effective using materials including sugar, wax, agarose, and pluronic.[228,229] For instance, Wu et al.[228] came up with an innovative omnidirectional 3D printing technique to print fugitive organic ink inside a matrix of thermally or photochemically curable resin, serving as the physical support of the ink. To do so, they printed 3D microvascular networks using pluronic F127, an organic ink that might liquefy at temperatures below 4 °C.[228] Brossard et al.[230] employed an inkjet printer to create a sacrificial mold for MFDs fabrication. They used a hexanediol ink which could be immediately frozen when in contact with a chilled substrate (5 °C). After printing the sacrificial mold, PDMS was used to cast the sacrificial mold, which was later heated until it evaporated. With the help of this technique, the channel width may be reduced to 50 μm.[230]

1.4.2.3 Modular Method

The modular MFD$_S$ are similar to Lego® models in which discrete microfluidic units, like Y-shaped, T-junction, chambers, and fluidic valves, may be put together to create completely functional MFDs (Fig. 1.8c).[231,232] The modular technique, in contrast to the traditional manufacturing method, has the benefit of quickly changing the microfluidic chips by combining single components in various arrangements without constructing a new device. Now that 3D printing has made manufacturing more accessible, it is feasible to create microfluidic modules combined with connections to make assembly quick and simple.[232]

Bhargava et al.[232] created a collection of stereolithographically produced standardized parts and connections. They demonstrated the quick reconfigurability of these systems by building and connecting various modules, including mixer, fluidic junction, and straight channel, to mix liquids with tunable mixing ratio and produce microdroplets.[232]

In order to circumvent channel obstruction caused by trapped resin, Ching et al. recently developed a complex 3D microchannels network, discretized into several subunits (up to 36 branching points).[233]

1.4.2.4 Hybrid method

To address the drawbacks of the direct printing method, such as gas impermeability and limited optical transparency, the hybrid method uses the advantages of PDMS and hard polymers to fabricate a single MFD. Polymers, for instance, can reduce non-specific protein absorption and water evaporation, which are problems with all-PDMS devices.[234] The incorporation of flexible materials like PDMS in hybrid devices enables them to provide the manipulation of fluid flow via the use of mechanical stimulation and microvalves, which cannot be accomplished with all-polymer MFDs. As can be seen in Figure 1.8d, a hybrid MFD is built using a 3D-printed microchannel device, sealed by using a transparent layer including outlets and inlets.

SLA and FDM 3D printing methods have been utilized extensively in the development of hybrid devices. Due to the roughness of the printed layer for bridging the channels, microchannels created with the FDM method are commonly found to be opaque when characterized by an optical microscope. To improve the transparency of the 3D printed channels, transparent substances like PDMS and PMMA can be used to replace the bridging layer and seal the microchannels. For instance, Mehta et al.[235] bond hard top polymers like cyclic olefin copolymer (COC), poly(ethylene terephthalate glycol) (PETG), and polystyrene (PS) to a soft polymer such as polyurethane, via

plasma treatment, to create a hard−soft hybrid MFD.[235] Solvent binding is another approach to binding 3D-printed polymers with PMMA. In this technique, 3D printed substrate and PMMA were immersed in ethanol prior to exposure to UV radiation.[236] The UV irradiation resulted in dissolving the PMMA, which also produced acrylate monomers that finally led the two polymers to be bounded. Using this technique, Duong et al.[237] were able to create a hybrid serpentine channel, a mixer, and a double emulsion generator (Figure 1.9).

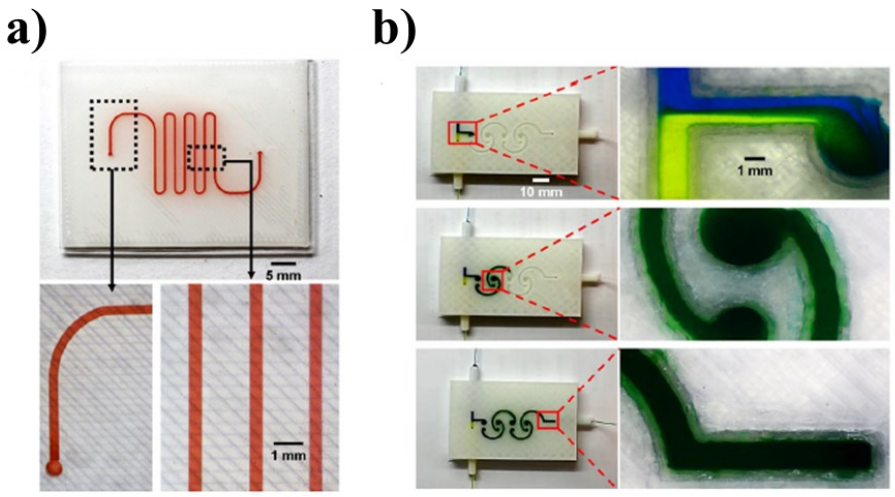

Figure 1.9 Example of 3D printed MFDs via the hybrid method. a) serpentine microchannel. b) mixing at different locations in the hybrid 3D printed mixing device. Reproduced with permission.[237]

Channel obstruction from retained uncured resin, limited optical transparency, and low gas permeability are all problems associated with MFDs manufactured using the SLA 3D printer. Since the SLA microchannels are reachable from the top and are not incorporated within the device, the hybrid technique enables the cleaning process to be comparatively quicker and more dependable.[218] Carrell et al.[238] bounded SLA printed construct with a glass slide utilizing an

interlayer of resin or PDMS. APTES or silicone spray are alternative approaches to seal SLA-manufactured open-faced microchannels.[238]

Overall, although 3D printing possesses a significant potential for the fabrication of MFDs, a few issues, including printing resolution, biocompatibility, low gas permeability, wettability, bounding, and low optical transparency, limit the widespread application of 3D printing in this field. Therefore, in this research, we aim to use our developed hydrophilic and soft silicone-based ink to fabricate various MFDs, such as T-junction and Y-channel, with multiple layers using an ME 3D printer, for the first time, to address some of the above-mentioned issues.

1.5 Motivation and Scope of the Thesis

As discussed in the introduction, it is essential to develop a 3D printable ink formulation that can be readily tuned in terms of mechanical and rheological characteristics to fabricate not only 3D tissue models with mechanical and biochemical features similar to that of human but also various biomedical devices such as MFDs. Among different polymers, silicone elastomers have been extensively utilized in biomedical applications because of their remarkable features such as flexibility, adaptability, and biocompatibility, but the slow curing speed, low viscosity, and hydrophobicity of existing silicone materials are challenges that hinder many applications. Specifically,

- Existing silicone materials are optimized for soft lithography or molding, which makes it extremely challenging to fabricate 3D structures with non-standard shapes and structural heterogeneity, such as the geometric structures of tissue/organs with variable mechanical stiffness.

- Using soft lithography requires the molding and bonding of multiple pieces to fabricate 3D structures with inner cavities, embedded micro-channels, and concaved surfaces, which is laborious and often leads to misalignment and leakage.
- Existing silicone materials are typically hydrophobic, and post-fabrication surface treatments are required for biological applications.

3D printing is the use of AM methods to deposit materials layer-by-layer. 3D printing of biomimetic constructs, especially elastic tissue mimetics, is a relatively young research field experiencing exponential growth. Besides biomimetic substitutes, MFDs have also grabbed significant interest because of their unique features, such as low-cost fabrication, miniaturization, simplicity, and reduced reagent consumption. Compared to conventional MFD fabrication methods, mainly soft lithography, 3D printing has the following advantages: easy geometry customization, multi-material printing, one-step printing, and better device integrity (i.e., no bonding, no leakage). Among various 3D printing methods, ME is the most suitable one for not only printing macroscale (centimeter size) and arrayed acellular/cell-laden biomimetic substitutes but also fabricating various integrated MFDs with different shapes and channel sizes. However, for 3D ME printing, the printability of an ink material is dictated by its rheological features. Hence, the developed ink needs to possess a shear-thinning property to be able to extrude through the printer nozzle.

Our main objectives are:

- Achieving one-step printing of hydrophilic customized/personalized tissue/organ mimetic elastic structures with complex geometries and heterogeneity

- Enabling 3D ME printing of silicone elastomer as an alternative to soft lithography via optimizing the rheological properties of a low viscous silicone elastomer for ME 3D printing
- Optimizing ME 3D printer operating factors, including the printing speed, needle size, pneumatic pressure, and layer height.
- Mechanical characterization of 3D-printed silicone structures fabricated via ME 3D printing.
- 3D-printing the HAC with its zonal structure and various MFDs as a proof-of-concept.

This thesis includes four chapters. A comprehensive overview of various 3D printing methods and their suitable biomaterials is reviewed in Chapter 1. The related literature on the state-of-the-art research on the various biomedical applications of 3D printers is also provided, along with a list of significant challenges. In addition, recent advances in HAC and MFDs fabrication are thoroughly reviewed. Chapter 2 presents the development of a hydrophilic and rapidly curing (under three seconds) inks, consisting of aminosilicone, CNC, and methacrylate anhydride (MA), for the 3D printing of HAC substitutes, with a biomimetic multizonal structure. Our results showed a new class of silicone-based inks that can be utilized for not only the fabrication of personalized and biocompatible tissue-mimetic substitutes but also in-situ surgical applications. The following article has been drafted according to this chapter:

- **Golzar, H.,** Wu, Y., Ganguly, S., & Tang, X. S., Development of a Hydrophilic and Rapidly Curing Silicone-based Ink with Tunable Mechanical Characteristics for the 3D Printing of Articular Cartilage Substitutes. *Addit. Manuf.,* (submitted Jan. 2023)

To provide a proof-of-principle demonstration of additional significant applications of our novel silicone-based ink, chapter 3 demonstrates the capability of our developed ink in fabricating

various MFDs, such as T-junction and Y-channel. Our results highlight the advantages of 3D printing of MFDs including easy geometry customization, one-step printing, and better device integrity (i.e., no bonding, no leakage). In chapter 4, conclusions and recommendations for future work are outlined.

Chapter 2 Development of a Hydrophilic and Rapidly Curing Silicone-based Ink with Tunable Mechanical Characteristics for the 3D Printing of Articular Cartilage Substitutes

2.1 Introduction

Among different human tissues, articular cartilage (AC) attracts significant interest due to its unique feature in providing bone ends in diarthrodial joints with an efficient lubricating system.[239] Owing to the AC's gradient layer structure, consisting of a superficial smooth layer, a transitional zone, a deep dense zone, this viscoelastic tissue can bear high-load and cyclic compressions. Poor self-regeneration of the AC due to its avascular and aneural nature is a significant concern for the aging/athletic population.[240–243] During the last decade, several surgical methods and cell-based therapies have been used to replace damaged AC with an artificial molded AC or improve AC repair and regeneration, respectively.[244] However, most of these approaches have failed to live up to expectations due to the unique mechanical features and complicated multi-layered 3D structure of AC, in which the stiffness gradually increases from the surface to the deep zone.[245–247]

Thanks to advances in additive manufacturing, 3D printing provides the opportunity to produce a complex structure layer by layer to precisely mimic the AC structure. Among different 3D printing methods, ME 3D printing has grabbed more attention due to its ease of operation and capability of using multiple inks with different viscosities; however, developing ink formulations to replicate human AC with matching mechanical features is still considered as a major challenge.[248,249]

Silicone elastomers have been widely utilized in different biomedical applications because of their remarkable features such as flexibility, adaptability, and biocompatibility, but the slow curing speed, low viscosity, and hydrophobicity of the existing silicones are challenges that hinder

silicone-based applications.[250,251] To address these issues, we have deployed a series of strategies to develop UV-curable and hydrophilic silicone-based inks that can be used to rapidly 3D print a precise AC substitute. Of all silicone elastomers, aminosilicone has been chosen as a main precursor because of its amino functional groups that offer extra substrate affinity and provide a more cell-favorable environment due to their hydrophilic nature.[252]

Moreover, aminosilicone should possess proper rheological feature and mechanical strength to be considered as a potential candidate for ME 3D printing purposes.[253,254] Hence, the low-viscosity of the aminosilicone still remains a challenge that needs to be resolved. Although there are several nano-sized rheology modifiers, including polymers and particles, that can be added to unprintable materials to tune their rheological properties, interestingly, few reports have described modifying silicone elastomers by adding these nano-sized rheology modifiers, and almost all of them used hydrophobic modifiers. For instance, hydrophobic nanosilica have been incorporated into silicone elastomer to induce suitable shear-thinning property along with a super stretchability feature.[255] Zheng et al. combined multiple chemically modified silicone elastomers to develop a UV-curable ink that had a low viscosity.[94]

In this chapter, we introduced CNC into the polymer matrix as a hydrophilic nano-sized rheology modifier due to its abundant hydroxyl groups to not only induce shear-thinning property but also improve the mechanical strength of aminosilicone.[256–258] Finally, to transcend the conventional casting process that has been widely used to fabricate silicone implants, MA and a photoinitiator, lithium phenyl-2,4,6-trimethylbenzoylphosphinate (LAP) were incorporated into the polymer matrix, allowing the ink to rapidly cure as it extrudes through the ME 3D printer nozzle. Simultaneously incorporating the CNC and MA noticeably enhanced the mechanical strength of the 3D-printed AC model.

By combining the aforementioned strategies, we have demonstrated that we can develop a series of hydrophilic and UV-curable silicone-based inks of different stiffnesses, with which to 3D print a multilayered AC substitute that is the first of its kind. Besides characterizing the developed inks in terms of their chemical and rheological features, the 3D printed AC substitutes have been mechanically tested to investigate their load bearing capability against cyclic compression (up to 400 cycles). Lastly, the biocompatibility of the 3D printed substitutes has been evaluated for possible AC replacement applications.

2.2 Materials and Methods

2.2.1 Materials

Methacrylic anhydride (MA), deuterated chloroform ($CDCl_3$), lithium phenyl-2, 4, 6,-trimethylbenzoyphosphinate (LAP) were purchased from Sigma Aldrich. Aminosilicone (Silamine D2 EDA, with viscosity and amine value of 6000 cpc and 170, respectively) was purchased from Siltech Corporation. Dulbecco's modified Eagle's medium (DMEM), TNBS (2,4,6-Trinitrobenzenesulfonic acid), trypan blue stain (0.4%), phosphate buffered saline (PBS) and fetal bovine serum (FBS) were purchased from VWR. Live/dead viability/cytotoxicity kit, penicillin/streptomycin, and MTT (3-(4,5-dimethylthiazol-2-yl)-2,5-diphenyltetrazolium bromide) assay were purchased from Thermo Fisher. Cellulose nanocrystal (CNC, with lengths and diameters of 200–400 nm and of 10–20 nm, respectively) was provided by Professor Michael K. C. Tam from the Department of Chemical Engineering at the University of Waterloo. All the aqueous solutions were prepared by using Milli-Q water (18.2 MΩ cm–1).

2.2.2 Synthesis of Aminosilicone-CNC-MA (SCM) Hybrid Ink

SCM hybrid inks were prepared by dispersing different concentrations of CNC, ranging from 1 to 7 wt%, in 2 mL of Milli-Q water, followed by mixing with aminosilicone (3 g), referred to as SC1 to SC7 (Aminosilicone-CNC with 1 to 7 wt%). Then, various amounts of MA, ranging from 1 to 7 wt%, were added to the mixture to prepare SCM hybrid inks with different concentrations of CNC and MA, referred to as SC(1-7 wt%)M(1-7 wt%). The resulting mixture was stirred at 80 ºC in the dark for 3 h with a closed cap to perform nucleophilic acyl substitution to the pendant amine functionalities in the silicone elastomer. To remove water and excess MA, the mixture was then stirred for 2 h at 160 ºC without the cap, followed by adding LAP (0.5 wt%) and stirring for another 1 h at 90 ºC. The aminosilicone and hybrid inks were dissolved in $CDCl_3$ to obtain a concentration of 50 mg mL^{-1} and analyzed using proton nuclear magnetic resonance (^{1}H-NMR).

2.2.3 Rheological Tests

A Bohlin-CS Rheometer was used to investigate the viscoelastic features of the hybrid inks. A cone-plate geometry with a 4º angle and 40 mm diameter at room temperature was used for this purpose. The steady shear rate sweep (10^{-1} to 10^3 s^{-1}) was measured to characterize the materials' behavior. Storage (elastic) modulus, loss (viscous) modulus, and complex shear modulus, denoted by G′, G″, and G*, respectively, are considered important parameters in investigating the rheology characteristics of a material. Indeed, the storage and loss modulus represent the elastic behaviour and the liquid-like characteristic of a material, respectively, which can be obtained via preforming an oscillatory test. G*, G′, and G″ can be obtained through the following equations:

$$\sigma_{(t)} = G^* \gamma_{(t)} \qquad \text{Equation 2.1}$$

$$G^* = G' + iG'' \qquad \text{Equation 2.2}$$

Where γ and σ are the shear rate and shear stress which vary with time, respectively. Hence, the angular frequency sweep was examined to measure G′ and G″ within the frequency ranges from 0.1 to 10 Hz in a linear strain region of 0.1%. Shear recovery experiments were performed at the high and low step strains of 500% and 0.1%, respectively, at 1 Hz frequency, each step lasting 5 min. All rheological examinations were repeated at least three times ($n \geq 3$).

2.2.4 ζ-potential Analysis

The ζ-potential measurement was conducted using a Zeta-Sizer (Malvern, Nano ZS90) at 25 °C. The samples were dispersed in different buffers and sonicated in a bath sonicator for 10 min prior to measurements. All measurements were repeated at least three times ($n \geq 3$).

2.2.5 TNBS assay

The degree of substitution of the hybrid inks was calculated as the difference between the free primary amines existing in aminosilicone prior and after the grafting of methacryloyl group, according to the G-Biosciences method.[259] In brief, 100 μg.mL^{-1} and 0.01 w/v% solution of unknowns (aminosilicone and hybrid inks) and TNBS were prepared in 0.1 M $NaHCO_3$, respectively. Then, 250 μL of TNBS solution was mixed and incubated with 500 μL of unknown solution for 2 h at 37 ºC. Afterwards, 125 and 250 μL of HCl and SDS (10 w/v%), respectively, were added to the mixture to terminate the reaction. The absorbance of the pure aminosilicone and unknowns were measured at 335 nm. The degree of substitution was calculated as follows:

$$DOS\ \% = \left(1 - \frac{A_m}{A_0}\right) \times 100 \qquad \text{Equation 2.3}$$

Where A_0 and A_m represent the absorbance of the pure aminosilicone and unknown.

2.2.6 Swelling Tests

SCM hybrid inks were printed and cured in a rectangular shape with a dimension of 2 × 4 cm^2. The printed structures were soaked in PBS buffer for 7 days (168 h) at room temperature. At each time point, samples were removed from the PBS buffer, dried with Kimwipes, and their length and width were measured as L_f and W_f, respectively. The relative length and width were calculated, as follows:

$$Relative\ length = \frac{L_f - L_0}{L_0} \quad \text{Equation 2.4}$$

$$Relative\ width = \frac{W_f - W_0}{W_0} \quad \text{Equation 2.5}$$

2.2.7 Hydrophilicity Tests

Water contact angles (CA) of the cured SCM hybrid inks were measured at room temperature. To do so, SCM hybrid inks were casted in a circular PDMS mold and UV crosslinked for 10 min at room temperature. Then, the CA were determined within 3 s after dispensing a 5 µL water drop onto the surface of the cured samples.

2.2.8 Mechanical Tests

To investigate the mechanical features of the SCM hybrid inks, normal and cyclic compression tests were performed by using a Universal Test Machine. The cylindrical specimens were printed with 5 mm height and 7 mm diameter and placed between two plates that can measure the applied force to compress the samples. The normal and cyclic compression tests were conducted at a speed of 2 and 0.5 mm s^{-1}, respectively. Compression moduli were determined from the slopes of loading stress vs strain curves, at the initial 10% strain ($n \geq 3$), where the stress and strain are defined as follows:

$$\sigma = \frac{P}{A_0}$$ Equation 2.6

$$\varepsilon = \frac{L_0 - L}{L_0}$$ Equation 2.7

Where σ, ε, P, L_0, and L are stress, strain, force loaded on the sample, original length, and final length of sample in the axis of compression, respectively. A_0 is the original cross-sectional area perpendicular to the axis of compression.

2.2.9 3D Printer and Printing Procedure

A BioBot Basic printer (Advanced Solution, USA) was used to print the structures. SCM hybrid inks were loaded into 10 mL pneumatic syringes and centrifuged for 10 min at 3250 G to remove the bubbles. 3D structures were designed by using SolidWorks and printed with a moving speed of 1.5 mm/s and various extrusion pressure from 60 psi to 68 psi, based on the nozzle diameter (from 108 to 337 μm). Hollow cylinder and dome structures were printed with an inner diameter of 20 mm and height of 19 and 10 mm, respectively. A goose neck UV light setup was used for in situ crosslinking.

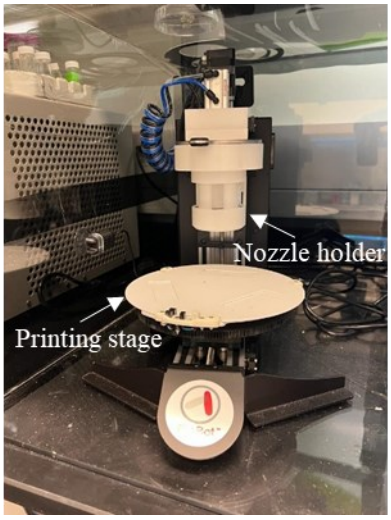

Figure 2.1 Photograph of multi-nozzle ME 3D printer

A scaled-down femur bone with 4.5 cm height was printed using a DLP printer (ANYCUBIC Photon Mono 4K, China). The printed femur was then washed with ethanol 70% (v/v) for 2 min. Additionally, a multilayered HAC with a thickness of 3 mm was designed to cover the femoral condyles. Deep, transitional, and superficial layers were printed using SC5M5, SC3M5, and SC3M3 inks, respectively. The extrusion pressure varied from 60 to 68 psi with the printing speed of 1 $mm.s^{-1}$. Finally, printed customized HAC was placed on top of the femur head confirming the successful printing strategy.

2.2.10 In Vitro Biocompatibility Assay

NIH/3T3 cells were cultured in Dulbecco's modified Eagle's medium (DMEM), supplemented with FBS (10% (v/v)) and penicillin/streptomycin (1% (v/v), at 37 °C and 5% CO_2. The cytotoxicity of the SCM hybrid inks were investigated by using an MTT assay. Rectangular constructs were printed by using SCM hybrid inks and washed with PBS for a few days to remove the excess of unreacted materials. NIH/3T3 cells were cultured in 24-well plates at a density of 2×10^4 cells per well and incubated for 24 hr prior to the addition of a printed construct to each well. Subsequently, the MTT assay was performed on days 1, 3, and 5, based on the manufacturer's protocol. Cells were additionally stained using a live/dead assay kit on days 1, 3, and 5 in accordance with the manufacturer's instructions for evaluating the cell viability via fluorescence imaging (Zeiss LSM 700 confocal microscope, Germany).

2.3 Results and Discussion

To prepare 3D printable, hydrophilic and UV-curable silicone-based ink with tunable mechanical properties, we developed different inks based on a composite comprised of aminosilicone, CNC and MA. A suitable ink for ME 3D printing should possess a shear-

thinning property that allows it to be extruded through a pressurized nozzle easily and retain its original shape after printing.[260–262] Aminosilicone does not possess such a rheological feature, making it difficult to use for ME 3D printing applications. Currently, the incorporation of nano-sized rheology modifiers into unprintable materials is considered an efficient way to resolve this issue.[263–265]

Among different nano-sized rheology modifiers, CNC has grabbed great interest due to its favorable features such as renewability, high mechanical strength, and low cytotoxicity.[266–268] Hence, we have evaluated the effects of incorporating different amounts of CNC particles in the aminosilicone matrix and the rheological properties of our aminosilicone-CNC (SC) inks (Figure 2.2). As can be seen in Figure 2.2a, although the addition of 1 wt% CNC in aminosilicone did not induce significant shear-thinning, increasing the CNC concentration (from 1 to 7 wt%) greatly enhanced both the static viscosity and the shear-thinning property. This result may be attributed to the interactions among the CNC particles themselves, as well as between the CNC particles and the polymer matrix.[269,270] Based on ζ-potential measurement results (Figure 2.2b), CNC particles repel each other due to the their highly negative surface charge, resulting in good dispersion in the polymer matrix, while aminosilicone wraps around the CNC particles through electrostatic attraction because of its positively charged amine groups.[271] Thus, once a shear stress is applied, the entangled CNC and aminosilicone network re-aligns and the ink's viscosity decreases.[271] Although, there is no significant difference between the viscosities of SC5 and SC7, CNC aggregation was observed in SC7. Hence, aminosilicone with 3 and 5 wt% CNC were chosen for further crosslinking using MA.

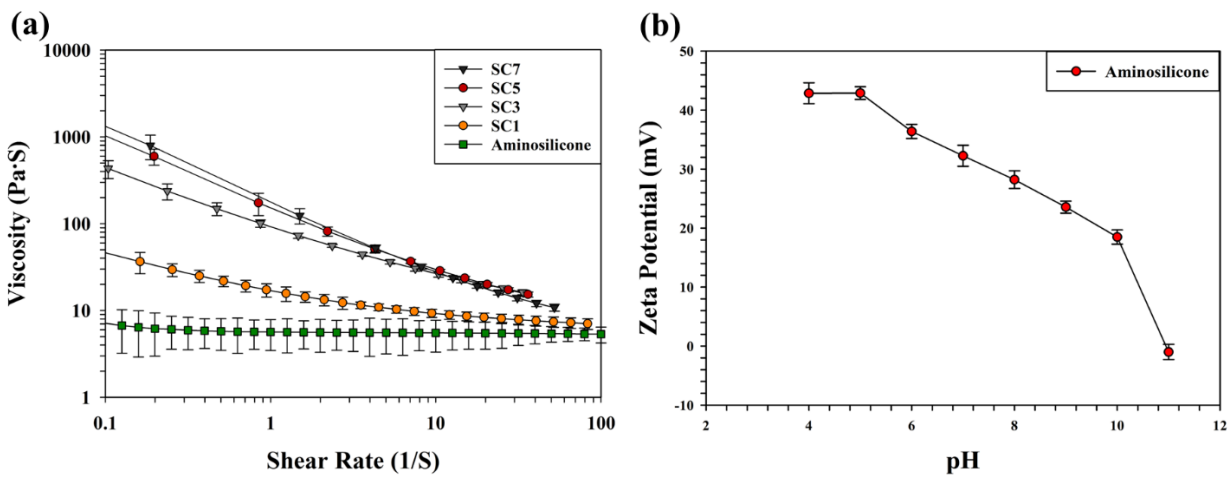

Figure 2.2 Rheological characterization of SC inks. a) Flow curves of SC1, SC3, SC5, and SC7. b) ζ-potential of pure aminosilicone at different pH. Error bars represent ± SD, n ≥ 3.

The incorporation of MA into the SC matrix elevated the viscosity over the entire shear rate range (0.1-1000 s^{-1}), but had no significant effect on shear-thinning (Figure 2.3a). To gain a better understanding of the correlation between viscosity (η) and shear rate (γ), power-law equation has been used to fit the flow curves (Table 2.1),

$$\eta = K\gamma^{(n-1)} \quad (1)$$

where K and n represent the consistency index and flow index, respectively. The flow index (n) is widely used to define the flow behavior of a fluid, where $n > 1$, $n = 1$, and $n < 1$ represent shear-thickening, Newtonian, and shear-thinning flow respectively.[272] The derived n and K values for the aminosilicone-CNC-MA (SCM) inks are tabulated in Table 2.1. All the developed inks showed n values of less than 1, confirming the shear-thinning property induced by CNC incorporation.[273] The consistency index also significantly increased (i.e., by 1 order of magnitude) by increasing the MA concentration, demonstrating higher viscosities at a constant shear rate. This increase might be attributed to the formation of intermolecular hydrogen bonding between the carbonyl group of the grafted MA with either CNC or the secondary amine group of the aminosilicone,

leading to a tighter and denser network.[274] These changes can efficiently improve the printability of the aminosilicone-based inks by decreasing flow resistance at high shear rates during extrusion.

Table 2.1 Summary of power-law parameters of SCM hybrid inks.

Sample	n	K
SC3M3	0.56 ± 0.05	144 ± 24
SC3M5	0.57 ± 0.08	752 ± 28
SC5M3	0.59 ± 0.06	387 ± 31
SC5M5	0.59 ± 0.09	1328 ± 45
Aminosilicone	0.96 ± 0.12	6 ± 2

Note that we picked 3 and 5 wt% of MA to prepare our inks because 1 and 7 wt% of MA failed to cure under UV exposure due to the lack of crosslinking sites and developed a highly viscous solution with aggregated CNC particles, respectively. Overall, all of the aminosilicone-CNC-MA (SCM) inks not only possessed a noticeably higher static viscosity compared to pure aminosilicone but also showed a proper shear-thinning property as well; for instance, the SC3M3 (aminosilicone with 3 wt% CNC and 3 wt% MA) ink and pure aminosilicone showed a viscosity close to 700 and 7 Pa·s under static conditions (shear rate ~ 0 s^{-1})and 5 and 3 Pa·s at the shear rate of 1000 s^{-1} , respectively (i.e., 2 orders of magnitude lower for SC3M3). Furthermore, frequency sweep profiles indicated that the elastic modulus G′ of all aminosilicone-based compositions was higher than their loss modulus G″ at low frequencies, indicating a solid-like structure, while G″ overrode G′ at frequencies above 1 Hz (Figure 2.3b).[275] Additionally, the results showed that increasing the CNC and MA concentration resulted in the formation of a stronger network since the elastic modulus dramatically increased from 200 to 3000 Pa at 0.1 Hz for SC3M3 and SC5M5, respectively.[276]

To investigate the self-healing behavior of the developed inks, step-strain experiments were performed (Figure 2.3c and 2.3d). When the strain was switched between high and low (0.1 and

500%), all inks showed an inversion of elastic and viscous moduli under the high strain followed by quick recovery of the elastic modulus at low strain. SC3M3 was separately shown in Figure 2.3c as an example to highlight the self-healing behavior of the developed inks. The self-healing efficiencies of all inks have been evaluated by performing three cycles of cyclic strain testing with 300-seconds intervals between tests (Figure 2.3d). The results indicated nearly 100% recovery. This self-healing feature may be rooted in the reversible and quick re-establishment of the electrostatic interactions between positively charged free primary amino groups that existed on the aminosilicone chain and the negatively charged CNC.[277] Overall, the shear-thinning property and fast recovery of the developed aminosilicone-based inks make them suitable for ME printing.

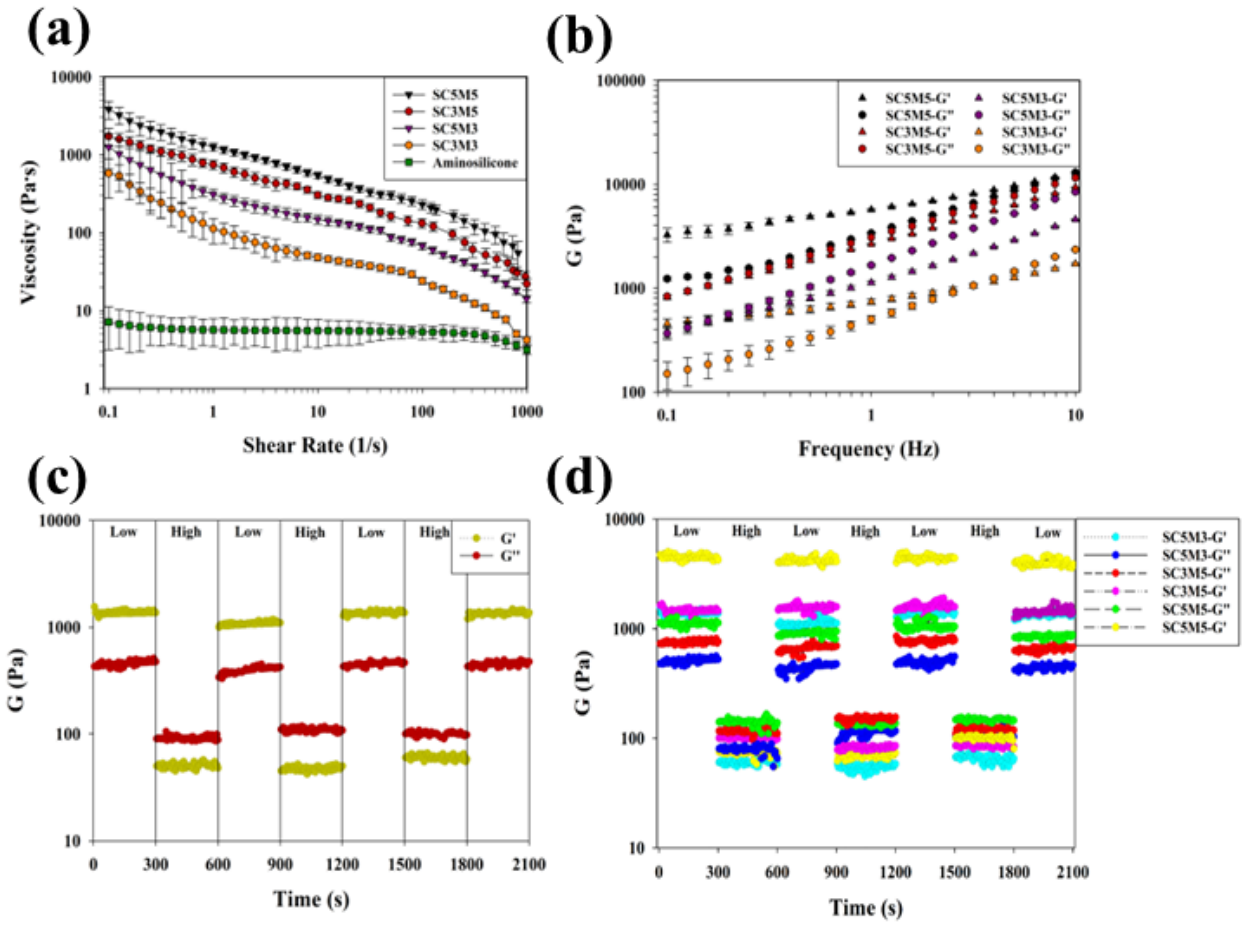

Figure 2.3 Rheological characterization of SCM hybrid inks. a) Flow curves of aminosilicone, SC3M3, SC3M5, SC5M3, and SC5M5. b) Elastic (G′) and viscous (G″) moduli of SC3M3, SC3M5, SC5M3, and SC5M5 as a function of oscillatory frequency. Step-strain measurements of c) SC3M3, and d) SC3M5, SC5M3, and SC5M5 over three cycles at 25 ◦C, demonstrating shear-recovery of the SCM hybrid inks. Error bars represent ± SD, n ≥ 3.

The methacryloyl group was grafted to the side chain of aminosilicone through an addition mechanism depicted in Figure 2.4. As can be seen in this figure, this mechanism starts with an attack of the primary amine groups of aminosilicone on MA's carbonyl groups resulting in the formation of a tetrahedral intermediate. The second step of the mechanism is the elimination of the leaving group, containing the second carbonyl group of the MA. This elimination occurs by

collapsing the tetrahedral intermediate leading to the reformation of the C=O carbonyl bond and a new acyl compound.[270]

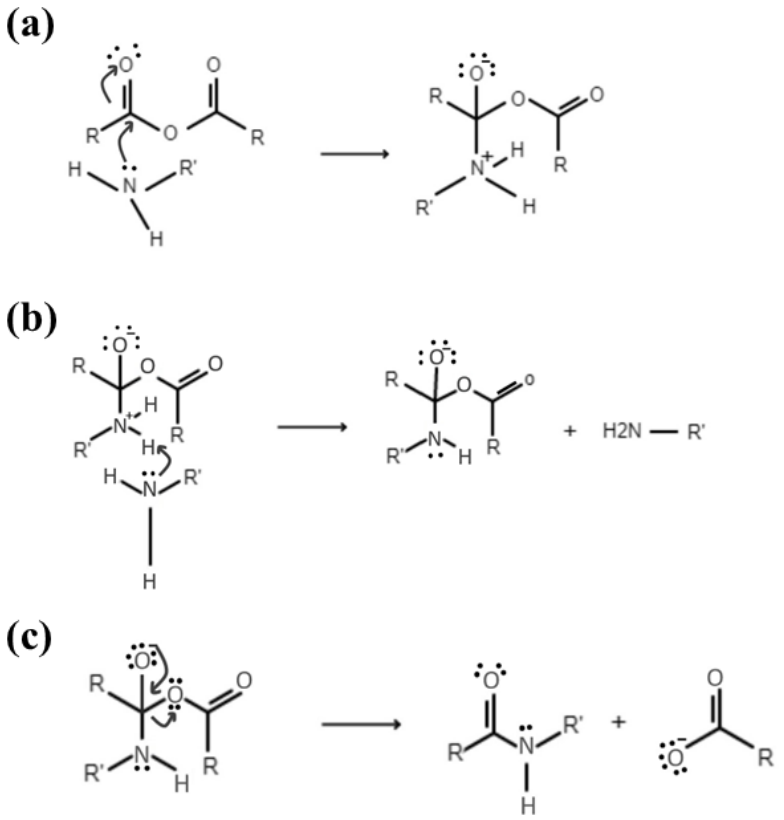

Figure 2.4 Mechanism of the reaction between amine and anhydride. a) nucleophilic attack, b) proton transfer, c) leaving group removal.

The successful grafting of the methacryloyl group to the aminosilicone chain was confirmed via ^{1}H-NMR spectroscopy and a TNBS assay (Figure 2.5). As can be seen in Figure 2.5b, there are four distinctive peaks at 1.9, 2.7, 5.3, and 5.8 ppm in the SCM H-NMR spectra, which correspond to the methyl protons of the methacrylamide grafts (1), the methylene protons of the unreacted aminoethylaminopropyl (2), the acrylic protons of the methacrylamide grafts (3).[275,278,279] The decreased signal in peak (2) and the emergence of peaks (1 and 3) in the spectrum of SC3M3 indicate the successful grafting of the methacryloyl groups.[278,280]

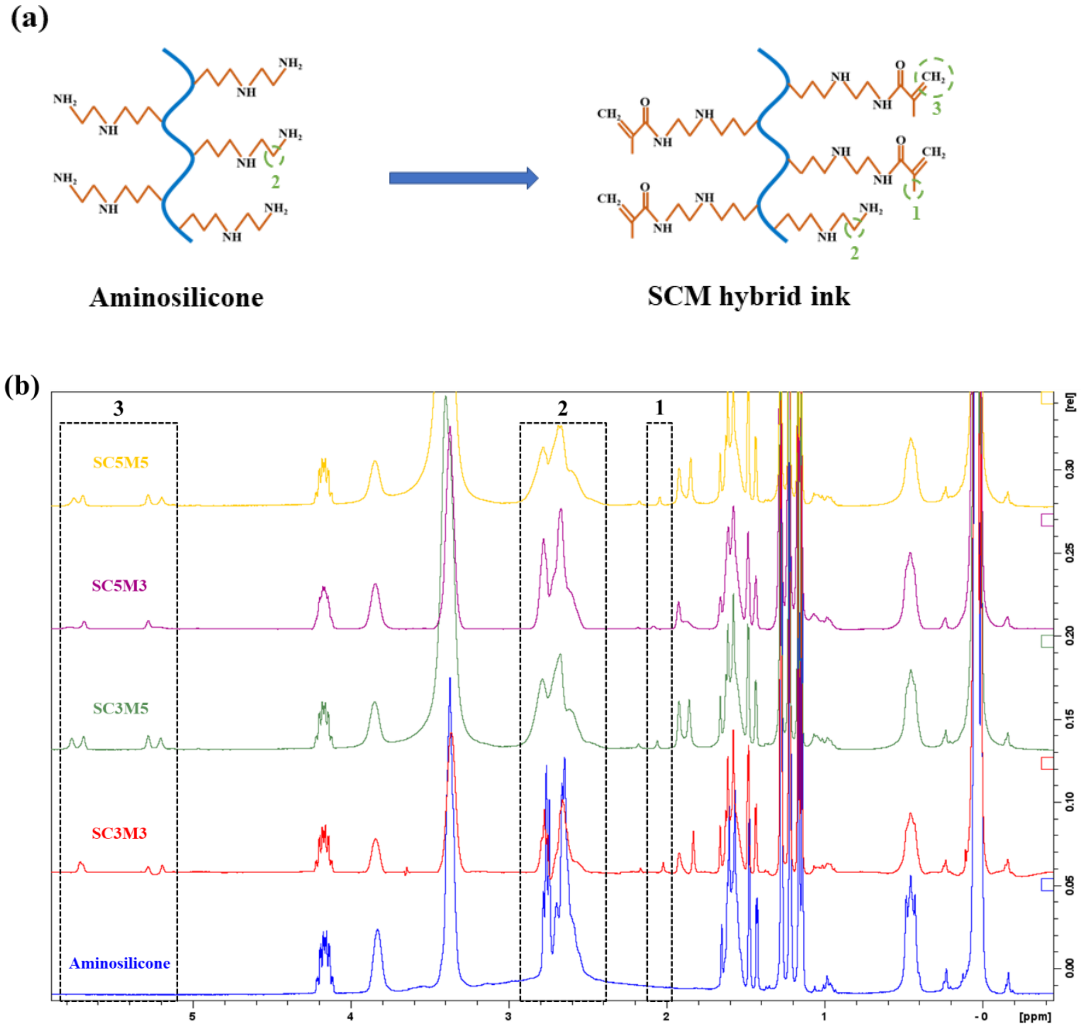

Figure 2.5 Structural characterization of SCM hybrid inks. (a) Schematic illustration of grafting MA to aminosilicone, b) H-NMR spectra of pure aminosilicone, SC3M3, SC3M5, SC5M3, and SC5M5 hybrid inks.

In addition, a TNBS (2,4,6-trinitrobenzene sulfonic acid) assay was performed to quantify the degree of substitution of the developed inks as well as the amount of free primary amines. TNBS is a highly sensitive and rapid means of quantifying the free primary amines.[281] As shown in Table 2.2, increasing CNC and MA concentrations led to a higher degree of substitution, from 14% to 45% for SC3M3 and SC5M5, respectively.[282] It is noteworthy to mention that the amount of the

free primary amines in pure aminosilicone is approximately 2.23 mmol, based on the calibration curve for TNBS assay with glycine standards. The TNBS results were in good agreement with the analysis of the ^{1}H-NMR spectra.

Table 2.2 Degree of the substitution of the SCM hybrid inks.

Sample	ABS @335 nm	Degree of Substitution (%)
SC3M3	0.44 ± 0.02	14 ± 4.1
SC3M5	0.33 ± 0.03	36 ± 3.9
SC5M3	0.36 ± 0.03	30 ± 4.2
SC5M5	0.28 ± 0.01	45 ± 2.2

The printability of the SCM inks was evaluated in terms of extrudability, accuracy, homogeneity, resolution and shape fidelity.[283] Several factors may affect extrudability, such as the printing parameters, ink viscosity, and shear-thinning properties.[284] A rheological study is considered an indirect method of investigating extrudability.[284] As mentioned in the previous section (Table 2.1), all developed inks had a flow index 'n' below 1, confirming their shear-thinning behavior.

Printing accuracy is a parameter known to show the similarity between the printed structure and the designed one.[283] Printing accuracy can be investigated along with homogeneity and resolution. To evaluate these parameters, a zig-zag pattern was designed, and the width of the printed filaments, with/without UV-exposure, was measured (Figure 2.6a and Table 2.3). As can be seen, although the width of the printed filaments differed slightly from the designed ones, the printed patterns were uniform and precisely mimicked the designed structure. When a viscoelastic ink extrudes through a nozzle, the diameter of the extruded fiber is greater than the nozzle diameter

by a factor of 'α', a phenomenon referred to as die-swelling.[285,286] Many parameters, such as the nozzle diameter, material characteristics, and applied shear stress, can affect the 'α' factor.[286] The results show that there are no significant differences between the 'α' factor of the SCM inks. Of additional interest, the incorporation of a gooseneck UV light inside the 3D printer chamber significantly reduces filament spread and improves accuracy; for instance, the 'α' factor of SC3M3 decreased from 1.68 to 1.41 after UV exposure.

The horizontal resolution is a crucial factor in printing complex structures.[283] Indeed, a higher resolution can provide the opportunity to create more-accurate structures. Hence, different nozzles with various inner diameters have been tested to determine the best-achievable resolution for the developed inks. As shown in Figure 2.6a and Table 2.3, the SC3M3, SC5M3, SC3M5, and SC5M5 inks can be uniformly extruded from 32, 30, 25, and 23 G nozzles, respectively, by applying the pressure of 63 to 68 psi. To the best of our knowledge, our developed inks, SC3M3 and SC3M5, with their horizontal resolution of 152 and 229 μm, respectively, exhibit the higher resolution of all the extrudable silicone-based inks developed so far since the highest resolution for silicone-based inks reported in the literature is 260 μm (25G nozzle).[94,255]

Table 2.3 Summary of printing parameters of SCM hybrid inks. Error bars represent ± SD, n ≥ 3.

Sample	Needle (G)	Lateral speed (mm/s)	Pressure (psi)	Designed filament size (µm)	Actual filament size W/UV (µm)	Actual filament size WO/UV (µm)	α-Factor (W/UV-WO/UV)
SC3M3	32	1	68	108	152 ± 5.2	181 ± 6.1	1.41 - 1.68
SC3M5	25	1	65	260	380 ± 6.8	454 ± 5.6	1.46 - 1.75
SC5M3	30	1	63	159	229 ± 4.4	274 ± 6.6	1.44 - 1.72
SC5M5	23	1	65	337	498 ± 3.1	594 ± 2.2	1.47 - 1.76

Shape fidelity, another parameter that needs to be evaluated to confirm the capability of an ink to retain its original shape after deposition, can be examined with several tests, including filament collapse and height maintenance (Figure 2.6b).[287] To assess shape fidelity, the deflection area of the printed filament across gaps at various distances, including 1, 2, 4, 8, and 16 mm, was examined. As can be seen in Figure 2.6b, increasing the concentration of CNC and MA led to minimum deflection of the printed filaments. Interestingly, almost all the SCM inks were able to bridge the gap between pillars, even up to 16 mm, by generating a straight filament. Note that among different ink formulations, the collapsed area of the SC3M3 was a bit higher, at a 16 mm distance value, which might be related to its lower crosslink density.

Moreover, to demonstrate our inks' rapid-curing and shape-retaining capabilities, we printed a high aspect ratio cylindrical structure by using SC3M3 hybrid ink, the weakest one compared to the other inks (Figure 2.6c). As shown in Figure 2.6c, the printed part had a height of 18.2 mm and a diameter of 20 mm without any cavities or voids. The cylinder wall thickness is approximately 1 mm and highly uniform throughout its height. Therefore, the aspect ratio of the

printed cylinder was a remarkable 18:1 (height:thickness). Note that our inks have the capability of printing even taller structures; however, the maximum height possible with our 3D printer is 19 mm. Additionally, all structures were printed under in-situ UV exposure. This experiment confirms that the fast-paced curing feature of the developed inks--approximately 2-3 seconds--can support the creation of high aspect ratio structures through layer-by-layer printing with no cavities or voids between the layers.

Besides tall structures, hemispherical or dome structures are considered among the most challenging shapes for ME printing.[94] The fast-paced curing feature of our inks offers the opportunity to print such structures without using sacrificial supports. As can be seen in Figure 2.6c, we used SC3M3 hybrid ink, as an example, to print a hollow domed structure with a 20 mm diameter, 10 mm height, and uniform consistency. This example confirms that creating overhanging constructs with a gradual curvature shape need no longer be considered a challenge for ME printers.

In addition, to assess the capability of our ink in fabricating human-like structures, we printed the femur head's AC using SC3M3 hybrid ink. As shown in Figure 2.6c, the printed AC precisely covers the femur head without any defect.

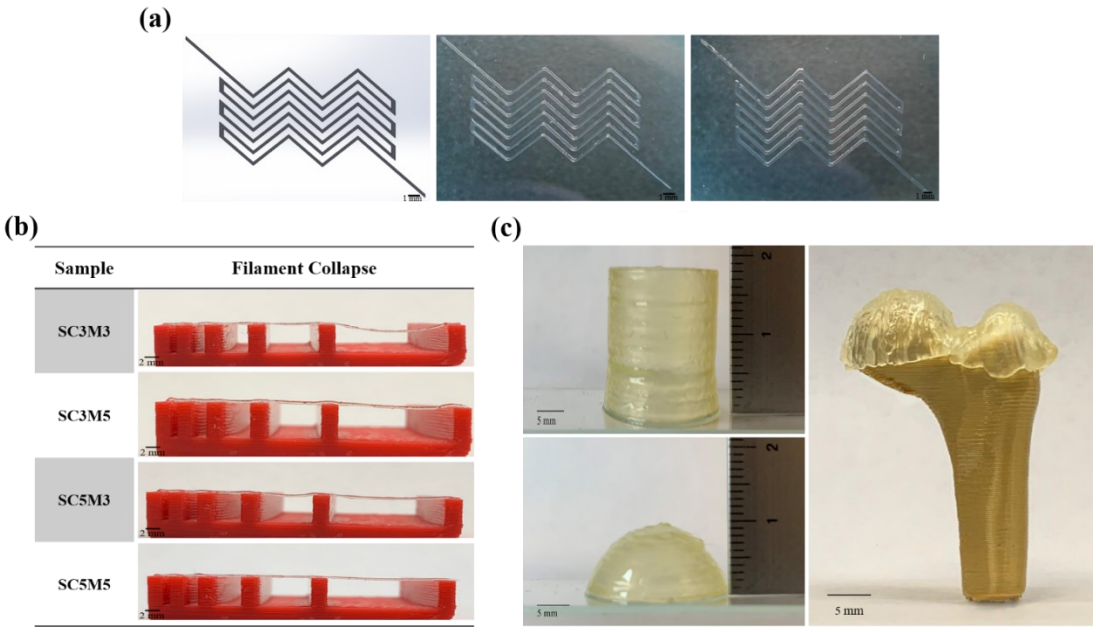

Figure 2.6 Printability of SCM hybrid inks. a) 3D printing zig-zag pattern; left panel: schematic design; middle panel: with UV-exposure; right panel: without UV-exposure. b) Filament collapse test of different SCM hybrid inks. b) 3D printing of high-aspect ratio, overhanging, and HAC structures using S3CM3 ink.

Indeed, free radical polymerization, involving three different types of reactions: initiation, propagation, and termination, is responsible for providing our developed inks with such a remarkable crosslinking feature (Figure 2.7). As can be seen in Figure 2.7, during the initiation reaction, UV irradiation of LAP generates the radicals for polymerization. After initiation, many monomers add to the propagating chain. The propagation reaction is eventually terminated by encountering two propagating chains that undergo disproportionation or coupling.[288] Overall, all our inks possess excellent printability characteristics in terms of extrudability, accuracy, homogeneity, resolution, and shape fidelity.

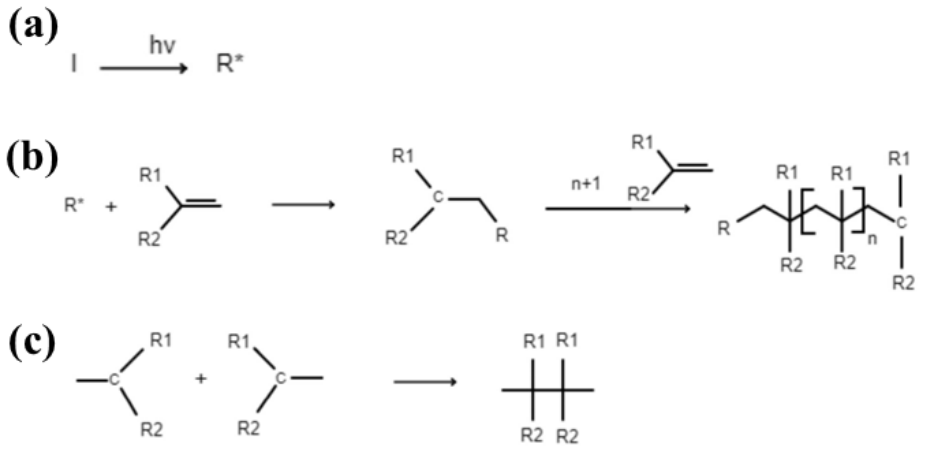

Figure 2.7 Mechanism of free radical polymerization. a) Initiation, b) propagation, c) termination.

The swelling feature of the developed inks is an important factor for their tissue engineering applications since they can significantly affect the mechanical features of the printed constructs over time.[289] The swelling feature of our 3D-printed constructs was examined in PBS, as shown in Figure 2.8a. All the developed inks showed a quick swelling during the first 24 h and reached equilibrium within 48 h. Increasing the CNC and MA concentrations has an inverse effect on the degree of swelling; that is to say, when the CNC concentration is increased, the degree of swelling also increases, whereas raising the MA concentration leads to less swelling. For instance, during the first 24 h, the relative length of the SC3M3 expanded by 12%, while that of SC3M5 expanded by only 6%. A similar trend was observed for SC5M3 and SC5M5. Indeed, two factors may affect the water retention of the printed constructs here; first, crosslinking density, and second, incorporation of the hydrophilic groups into the polymer matrix.[290–292] By increasing the MA concentration, more amine groups were replaced by hydrophobic methacryloyl groups, resulting in higher crosslinking density and a more-tangled polymer network. This phenomenon, in turn strengthens the hydrophobic nature of the aminosilicone and limits the matrix network expansion, thereby decreasing the water retention of the printed constructs.[290] On

the other hand, the addition of the CNC, which possesses abundant hydrophilic groups such as hydroxyl, improves the water absorbance of the polymer network. Therefore, the swelling ratio of our inks was tunable by altering their compositions.

One of the main challenges hindering the application of surgically substitutable silicones is that the body often triggers an immune response against them, called the foreign body response, which isolates the substitutes.[293] The immune response around the substitutes can be controlled by modifying the material's surface properties, such as hydrophilicity.[294,295] Indeed, hydrophilic surfaces are more favorable for cell growth and adherence since they can provide cells with a suitable substrate for attachment via adhesive proteins such as vitronectin.[296,297] Hence, the wettability of our printed structures and aminosilicone-methacrylate (SM) gels was evaluated by measuring a contact angle (CA) (Figure 2.8b). As can be seen in Figure 2.8b, the CA values of all our printed structures are below 90^{o}, confirming their hydrophilic surfaces. Although the incorporation of the CNC can improve the hydrophilic feature of the printed structures, adding MA slightly increased the CA values, probably due to the hydrophobic nature of the methacryloyl groups. So far, almost all of the studies on silicone-based substitutes have used surface modification methods such as O_2 plasma to make the silicone surface more hydrophilic; however, the induced hydrophilicity does not last long.[298] Therefore, for long-term applications, we believe that inducing anti-immune features such as hydrophilicity by modifying the nature of the substitutable silicone-based materials may be of more benefits than surface modification methods. The results are in good agreement with those of the swelling ratio test.

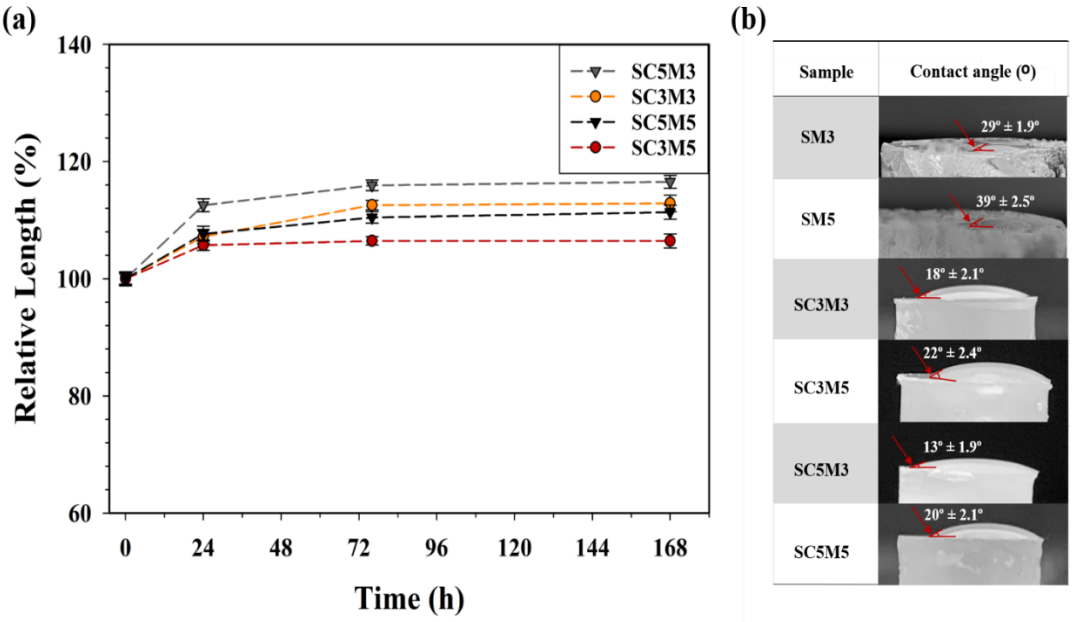

Figure 2.8 Swelling and hydrophilic properties of SCM hybrid inks. a) Swelling kinetics of SC3M3, SC3M5, SC5M3, and SC5M5 hybrid ink up to 168 hr incubation in PBS. b) Wettability evaluation of SM3, SM5, SC3M3, SC3M5, SC5M3, and SC5M5 hybrid inks by measuring contact angle. Error bars represent ± SD, n ≥ 3.

The constructs printed with our inks were investigated in terms of mechanical strength at different time points (immediately, after 1 week and 2 weeks), and their compression stress/strain curves are depicted in Figure 2.9. Increasing the concentration of MA and CNC can significantly improve the mechanical strength; for instance, the compression moduli for SC3M3, SC3M5, SC5M3, and SC5M5 are 0.25, 0.96, 0.38, 1.32 MPa, respectively, demonstrating approximately 1.5-, 3.84- and 5.28-fold increases in the compression modulus by raising CNC, MA, and CNC-MA concentration from 3 to 5%, respectively. This improvement can be related to the presence of CNC particles and the macromolecular chain entanglements within the polymer network. Indeed, once compression stress is applied on the printed structure, the polymer network transfers the stress through polymer chains to CNC particles. This mechanism hinders the crack propagation

phenomenon at high deformation.[299] Besides the polymer-CNC entanglement effect, the energy of the applied compression stress can be dissipated by forming reversible hydrogen bonds between CNC particles and aminosilicone chains as well.[299] CNC particles can also affect energy dissipation by aligning themselves in the direction of applied stress. In fact, this CNC-particle movement results in further energy dissipation and higher stress-cracking resistance.[300] Moreover, the alignment of CNCs along the axis of deformation might stiffen the material further, enhancing the modulus and resulting in a steeper increase in stress as a function of strain, which can be used to explain the non-linear stress-strain curve in Figure 2.9.[300] Therefore, the effect of interfacial noncovalent bonding, such as hydrogen bonding, polymer-chain covalent crosslinking, and the entangle-disentangle mechanism within the polymer network significantly improves the stiffness of the printed structures. Note that increasing the MA concentration leads to a higher crosslinked polymer network, which in turn results in lower elasticity and ultimate strain. For instance, the ultimate strain for SC3M3 is approximately 60%, which is 20% more than that of SC3M5.

To print human-like articular cartilage (HAC), we need to have a combination of elasticity and stiffness that precisely mimics the zonal structure of AC.[301] AC contains different zones--superficial, transitional, and deep--respectively making up to 10-20%, 40-60%, and 30% of the AC's thickness. Each zone plays a different role; the superficial zone, which comes into direct contact with synovial fluid, provides most of the tensile features of AC.[245] Therefore, it needs to be more elastic to be able to resist the minor shear, compressive, and stress forces that constantly affect AC during humans' daily activities.[301] The second zone is transitional, and acts as a bridge between the superficial and deep zones. It is considered a borderline for resisting major compressional forces, meaning that it needs to be stiffer than the superficial zone. The deep layer contains bigger collagen fibrils, allowing it to bear the greatest compression forces.[245,301] One more

layer, a calcified layer that anchors AC to the calcified bone, is beyond the scope of this research. Our goal is to print the viscoelastic part of AC, so our three-zone HAC design precisely mimics AC's zonal structure. Since the compression modulus of AC varies from 0.24 to 1 MPa, we picked SC3M3, SC3M5, and SC5M5 inks for printing each layer.[301] We used SC3M3 to print the superficial zone since it provides higher elasticity and ultimate strain compared to other inks, due to its lower crosslinking degree. In addition, SC3M5 and SC5M5 were used to print the middle and deep zones, respectively, because they can bear high loads by providing the HAC with sufficient stiffness. As shown in Figure 2.9, the compression stress/strain curve of the printed HAC at lower strain behaves more like SC3M3, while at higher strain, it moves closer to the SC3M5 and SC5M5 curves. The results also show that the ultimate strain of the HAC slightly improved compared to that of SC3M5 and SC5M5. More importantly, the stress-strain curve of the printed HAC is similar to that of a natural human one (subset image in Figure 2.9a).[302] Additionally, all the printed constructs showed a time-dependent mechanical behavior (Figure 2.9). As can be seen in Figure 2.9, the compression moduli showed a gradual increase over time.

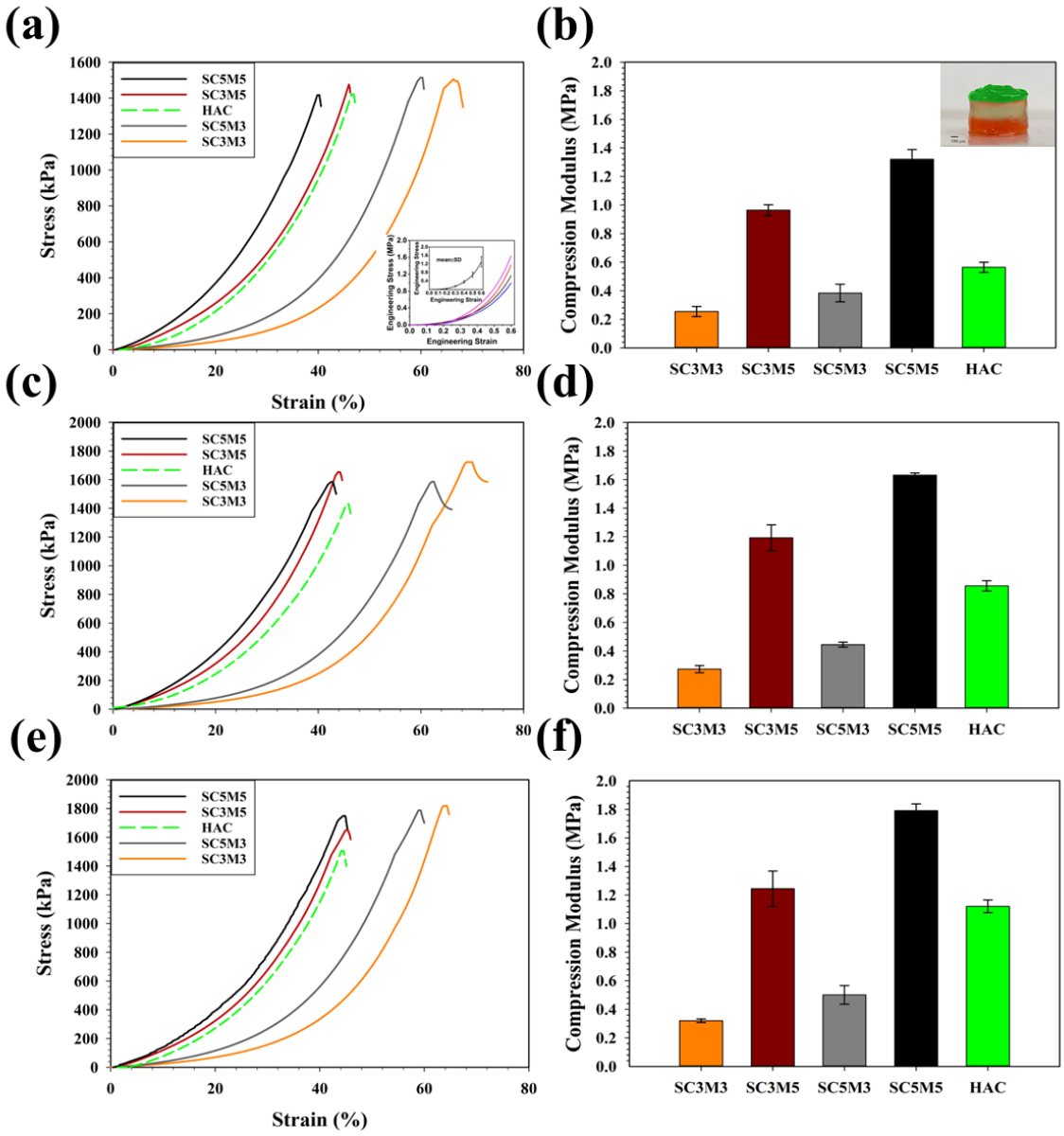

Figure 2.9 Mechanical characterization of SCM hybrid inks. Compression stress-strain curves and compression moduli, a, b) Immediately, c, d) 1 week, e, f) 2 weeks after 3D printing. Inset images: a) Stress–strain curves of natural human cartilage. Reproduced with permission.[302] b) Representative photograph of 3D printed HAC. Error bars represent ± SD, n ≥ 3.

To investigate the effect of repeated compressive cyclic loading on the mechanical stability of the printed HAC, cyclic unconfined compression tests were performed at different time points

(immediately, after 1 week, and 2 weeks) (Figure 2.10). Since the diurnal and post-activity strains on AC are usually in the range of 0 to 10% and 5 to 15%, respectively, the printed HAC was compressed up to 10% strain at a rate of 0.05 mm s^{-1}, and then released back to its original height at the same rate for 20 cycles.[303] For instance, as can be seen in Figure 2.10a, in which cyclic compression tests were performed immediately after printing, the printed HAC showed a nonlinear stress-strain curve in which not only the stress decreased between subsequent loading cycles, particularly during the initial and fifth cycles, and became negligible after 5–10 cycles but also the hysteresis area decreased when the cycling number was increased from 1 to 5. This softening and hysteresis may be explained by the Mullins effect and the presence of CNC in the polymer matrix.[304,305] Indeed, when stress is applied to the polymer chains, they compress, and CNC particles try to dissipate the crack energy by sacrificing their hydrogen bonds with the polymer chains.[299] Once the compression stress is removed, the polymer chains tend to rapidly regain their original shapes, but the CNC particles can not move at the same pace.[300] This phenomenon may result in interfacial friction between CNC particles and polymer chains, which in turn dissipates some energy.[300] In addition, after the fifth cycle, the stress-strain curves overlap to a large extent, and the compression moduli are likely to remain constant up to the twentieth cycle, meaning that the printed HAC becomes softer than its original structure.

To get a better insight into how multizonal structure printing affected the mechanical behaviors of the developed inks, cyclic tests were conducted on the printed structure using SC3M3 (Figure 2.10b, 2.10d, and 2.10f). As shown in Figure 2.10b (immediately after printing the samples), although the stress-strain curve of SC3M3 is similar to that of HAC in terms of hysteresis, the maximum stress of HAC at 10% strain dramatically increased compared to that of SC3M3, resulting in a higher compression modulus. This increase confirms the efficiency

of our multizonal structure printing. A similar trend occurs for other time points as well (Figure 2.10c, 2.10d, 2.10e, and 2.10f).

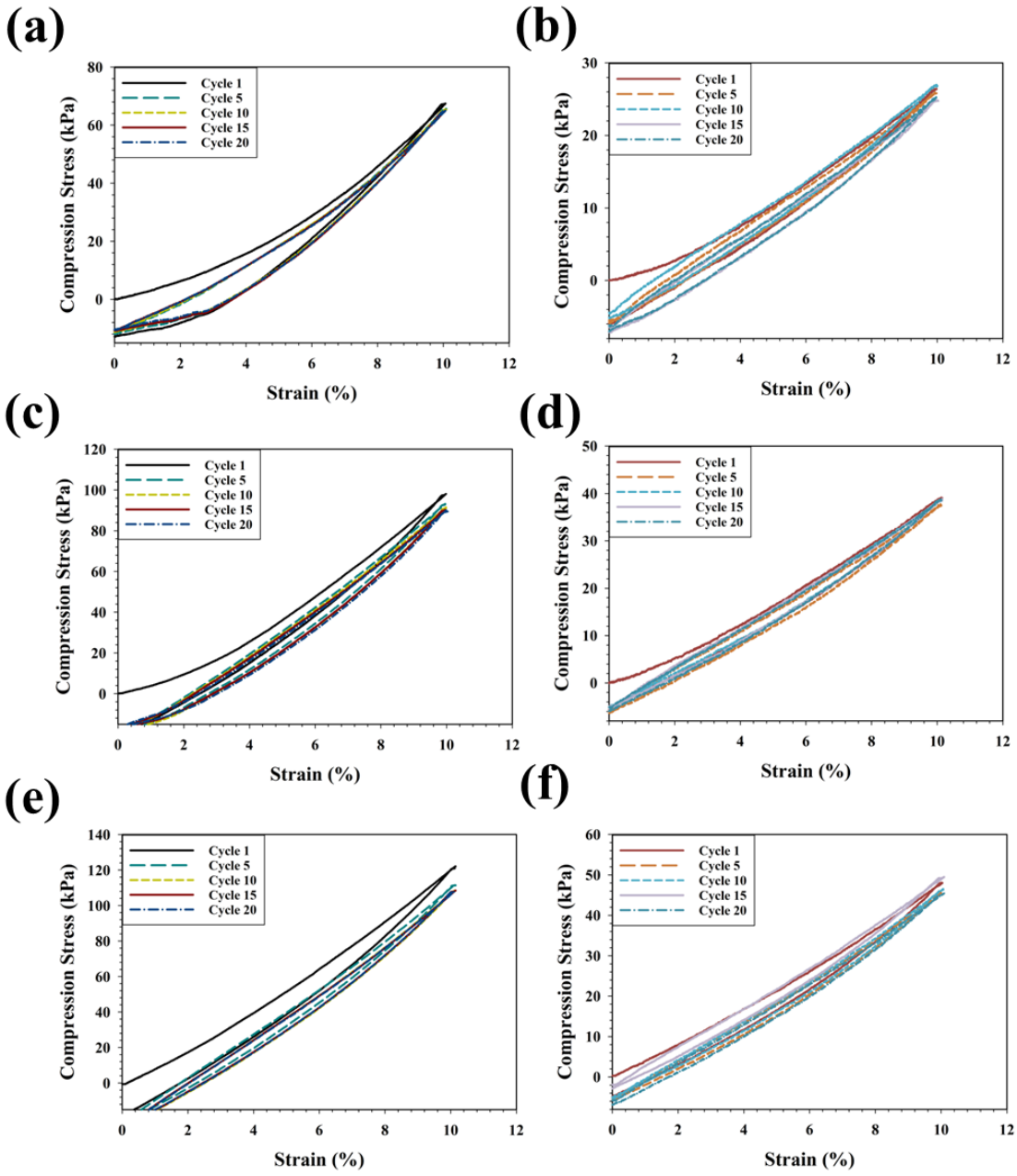

Figure 2.10 Cyclic compression tests of SCM hybrid inks at different time points. Cyclic compression stress–strain curves under a continuous 20-cycles compression test of 3D printed

HAC and SC3M3 cylinders; a, b) Immediately, c, d) 1 week, e, f) 2 weeks, after 3D printing, respectively.

To evaluate and compare the capability of the printed HAC and SC3M3 to withstand many repetitions of compression loads, cyclic tests were performed up to 400 cycles, with 40 min recovery time between every 100 cycles. (Figure 2.11). As displayed in Figure 2.11a, the maximum stress decreases from about 82.2 to 71.3 kPa within the first 200 cycles; however, the maximum stress reaches a plateau at 70 kPa during the remaining cycles, confirming that the softening effect on HAC is reversible to some extent. Figure 2.11a also illustrates that the differences between the highest and lowest maximum stresses of the printed HAC are much lower compared to those of SC3M3, which is in good agreement with the other mechanical test results. To examine the effect of time on the recovery features of the HAC and SC3M3, cyclic tests were performed at different time points (Figure 2.11b and 2.11c). The results show that all the printed structures become stiffer over time. In summary, by comparing the mechanical behaviors of the printed HAC with the human one (inset image of Figure 2.9a), we can confirm that our multi-material printing strategy works well, and the printed HAC structure can successfully mimic the multizonal structure of the human AC.[306]

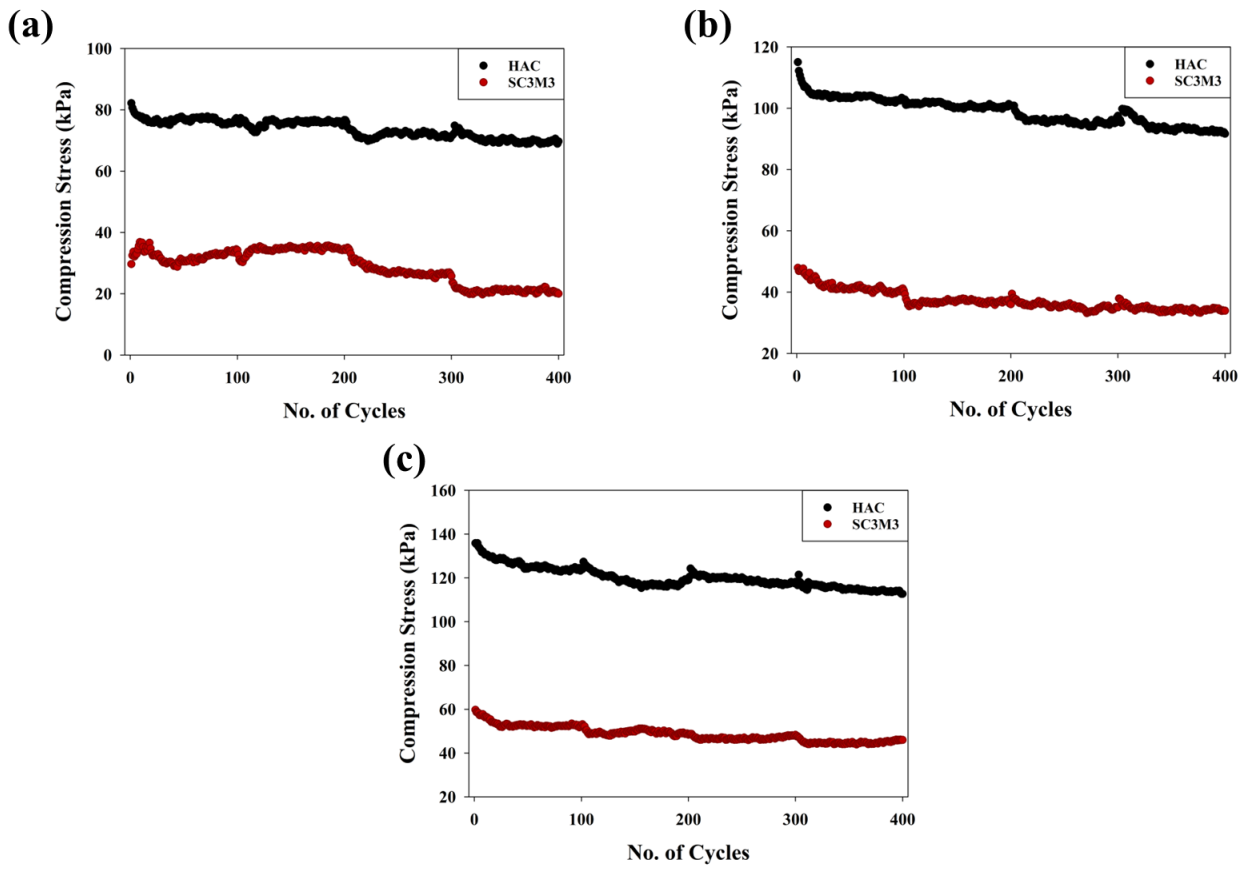

Figure 2.11 Cyclic compression tests of SCM hybrid inks at different time points. Compression stress for 3D printed HAC and SC3M3 cylinder at 10% strain over 400 cycles; a) Immediately, b) 1 week, c) 2 weeks after 3D printing. The gel was relaxed every 100 cycles for 40 min.

Eventually, to depict the capability of our developed inks in fabricating a multilayered AC substitute, a customized HAC was designed and printed to cover the femoral condyles (Figure 2.12). To do so, based on a CT image, a scaled-down femur was printed using a DLP printer (ANYCUBIC Photon Mono 4K, China). Then, a HAC substitute was designed by using SolidWorks. As can be seen in Figure 2.12, to show the multilayered structure of the printed HAC, both lateral and medial femoral condyles were completely covered by the first layer; however, the second and third layers just covered the exterior part of the femoral head. Our printed customized

HAC clearly shows the potential application of the developed inks in fabricating personalized tissue mimetic models.

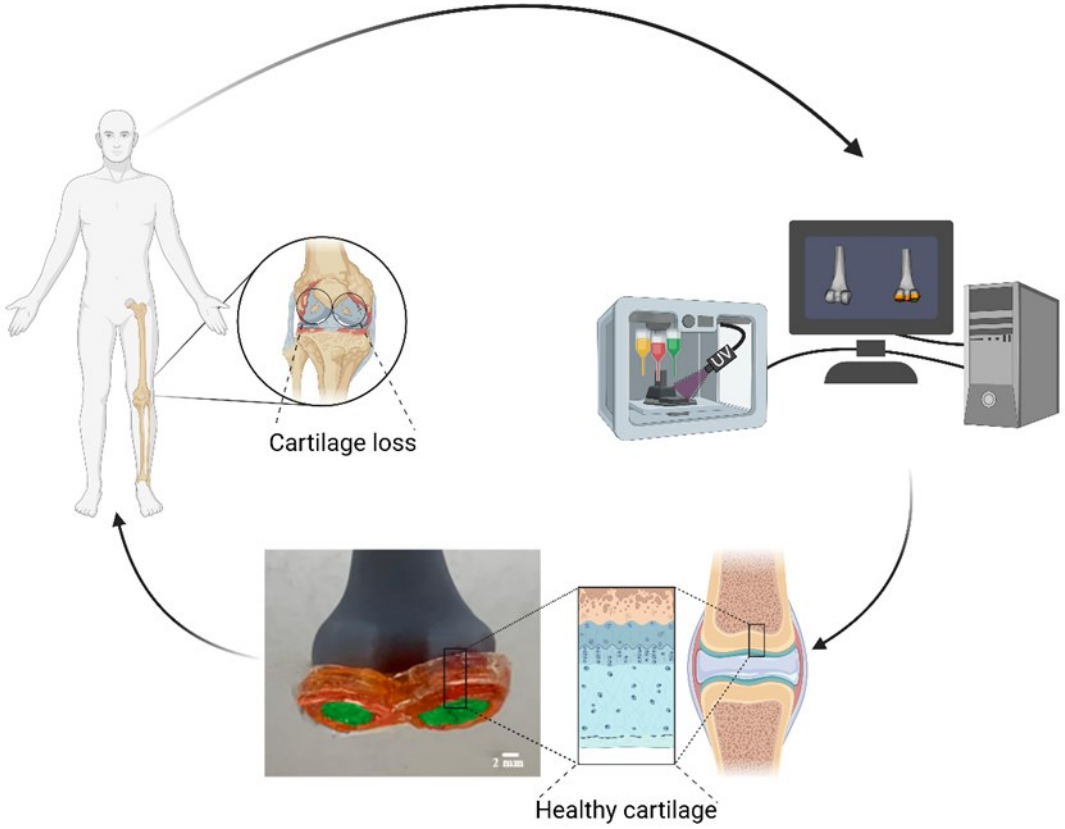

Figure 2.12 Schematic illustration of printing customized HAC. Created with BioRender.com

To evaluate the cytocompatibility of the developed inks, MTT and live/dead assays were performed on days 1, 3, and 5 (Figure 2.13). The results showed high cell viability (above 90 %) for the cells incubated with 3D printed constructs, using various inks, over 5 days of culture. Cells' viability was visualized using Live/dead assay, which is in good agreement with the MTT assay. Taken all together, our inks were found to have little to no toxic effects against fibroblast cells, confirming their biocompatibility.

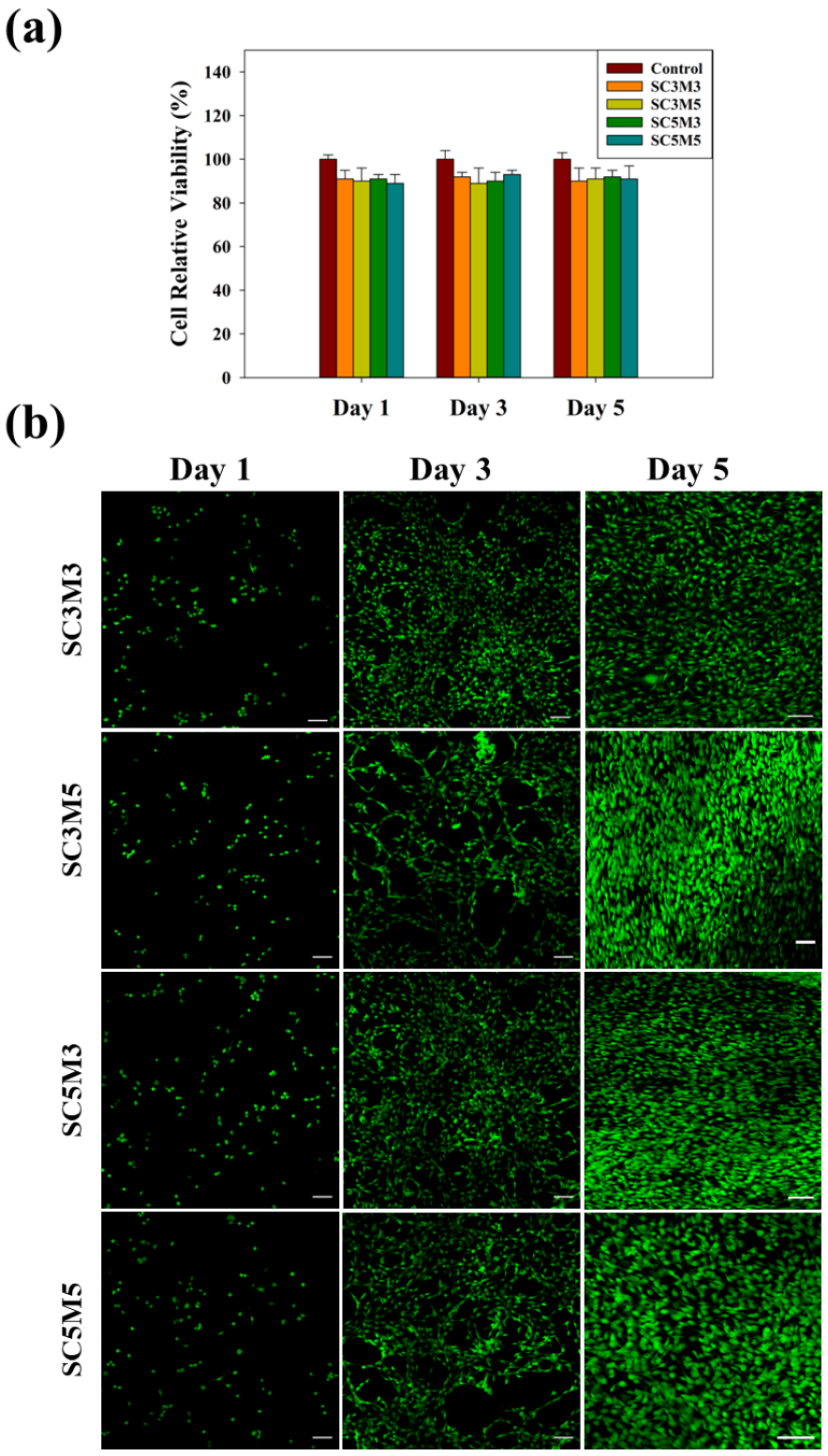

Figure 2.13 Cytocompatibility of SCM hybrid inks at days 1, 3, and 5. a) MTT assay, b) Live/Dead assay. Error bars represent ± SD, n = 3.

2.4 Conclusion

In this study, a series of novel silicone-based inks consisting of aminosilicone, CNC, and MA have been developed with tunable viscoelastic and mechanical features for ME 3D printing of human articular cartilage. The SCM inks were prepared via grafting MA to the side chain of the aminosilicone and incorporating the CNC into the polymer matrix simultaneously. The UV-curable and hydrophilic inks were characterized in terms of their shear-thinning and viscoelastic properties, confirming their capability of quick-recovery responses. Owing to the fast-curing feature of the developed inks, curing in less than 3 seconds, high aspect ratio, and overhanging structures can be directly created without using any sacrificial supports.

By altering the concentration of the CNC and MA, noncytotoxic inks with a broad range of compression moduli from 0.25 to 1.32 MPa were developed. To mimic the multizonal structure of the HAC, a multilayered structure with a gradual increase of the compression modulus from the top layer to the bottom one was printed using different inks, including SC3M3, SC3M5, and SC5M5. Normal and cyclic compression tests were performed to show not only the mechanical stability but the capability of our inks to withstand highly repeated compression loads, up to 400 cycles, making them as an ideal candidate for replacing damaged human articular cartilage. Overall, the results represent a new class of silicone-based materials with promising features such as hydrophilicity, rapid curing, shear-thinning, mechanical stability, and biocompatibility, for use in fabricating tissue mimetic structures that can be used for various biomedical applications.

Chapter 3 One-step Fabrication of Highly Flexible Microfluidic Devices via Microextrusion of Hydrophilic and UV-curable Silicone-based Ink

3.1 Introduction

MFDs have grabbed significant interest due to their unique features, such as low-cost fabrication, miniaturization, simplicity, and reduced reagent consumption.[307] However, there are several challenges regarding fabrication method and materials selection, limiting the wide clinical applications and the commercialization of the available PDMS-based chips.

Among different microprocessing techniques, such as laser cutting, soft lithography, injection molding, and milling, soft lithography, a multi-step fabrication method consisting of replica molding, curing, corning, and assembly, is a frequently used method to create MFDs.[308–310] This fabrication method possesses poor manufacturing efficiency, which makes it labor-intensive.[311] Additionally, this approach requires layer alignment and bonding during assembly, which makes it much more difficult to produce complex, multi-layered devices. That is to say, the problems associated with soft lithography, including time-consuming manufacturing stages, extensive prior knowledge, and the need for a cleanroom facility for prototype manufacturing, require that researchers find suitable alternative fabrication methods to pave the way for the wider applications of MFDs.[312]

3D printing has arisen with the potential to solve many of the issues associated with the fabrication of MFDs.[313] Indeed, 3D printing has brought several advantages over traditional fabrication methods, such as easy geometry customization, multi-material printing, one-step printing, and better device integrity. Therefore, 3D-printed MFDs can allow high flow rates of up to hundreds of $\mu L.\ min^{-1}$, provide more reliable structural alternatives to existing MFDs.[314] Despite the capability of various 3D printing methods, including digital light projection (DLP),[315] fused

deposition modelling (FDM),[316,317] direct ink writing (DIW),[221,318] and stereolithography (SLA),[319,320] in the fabrication of MFDs, each of these fabrication methods has its own drawbacks as well. For instance, DLP and SLA printers are renowned for their capability to produce complex structures with high precision; however, some deficiencies, such as limited materials selection, costly reagents, incapability of multi-material printing, and slow printing pace, make them an unsuitable candidate for MFDs fabrication.[223,319] Additionally, another significant limitation is the possibility of remaining uncured resin materials inside the channels, which may lead to channel blockage. This blockage can result in post/pre-processing of the fabricated MFDs, which can significantly prolong the manufacturing process.[219] It is true that DIW and FDM have a lower resolution compared to SLA and DLP, but the advantages, including ease of operation, wider materials choice, multi-material printing, and higher printing speed, make these printing methods more favorable for the manufacturing of MFDs.[220,321] The majority of FDM-made MFDs, however, are non-transparent and produced from hard polymers, which results in creating channels with high surface roughness, hindering their biomedical applications.[322,323] Among various 3D printing methods, DIW (particularly ME 3D printing) can not only address most of the above-mentioned drawbacks but also provide the widest material choice due to its capability of using soft polymers; However, manufacturing the MFDs by combining the use of soft polymers and ME printing method remains a challenge because of the lack of printable materials.

Among various soft polymers, silicone elastomers (particularly PDMS) have been extensively used for MFDs fabrication due to their unique features such as biocompatibility, suitable resistance to biodegradation, proper mechanical features, and chemical stability; however, there are several challenges in terms of their curing speed, viscosity, and wettability which limits their wide application for 3D printing purposes.[84,324,325] To address such issues, we employed our hydrophilic

and rapidly curing silicon-based ink (SC3M3), consisting of aminosilicone, CNC, and MA, to 3D print various silicone-based MFDs devices, using the ME printing method. In this study, besides the characterization of channels' printing accuracy, SC3M3 ink was used to fabricate T-junction and Y-channel chips as a proof-of-concept to demonstrate the wide range of applications of our recently developed ink. Lastly, the compatibility of the printed constructs against organic solvents was investigated.

3.2 Materials and Methods

3.2.1 Materials

Methacrylic anhydride (MA), and lithium phenyl-2, 4, 6,-trimethylbenzoyphosphinate (LAP) were purchased from Sigma Aldrich. Aminosilicone (Silamine D2 EDA) was purchased from Siltech Corporation. Isopropyl alcohol (IPA), xylenes, toluene, acetone, and n-hexane were purchased from Sigma Aldrich. Cellulose nanocrystal (CNC) was provided by Professor Michael K. C. Tam from the Department of Chemical Engineering at the University of Waterloo. All the aqueous solutions were prepared by using Milli-Q water (18.2 MΩ cm–1).

3.2.2 3D Printer and Printing Procedure

A FlashForge Creator Pro (FlashForge, China) was used to print the channels and MFDs (Figure 3.1). SC3M3 hybrid inks were loaded into 10 mL pneumatic syringes and centrifuged for 10 min at 3250 G to remove the bubbles. 3D structures were designed in SolidWorks and converted to the STL file. G-codes were generated by PrusaSlicer with the printer's moving speed of 100% and an extrusion pressure of 38 psi. A gooseneck UV light setup was used for in-situ crosslinking.

3.2.3 Microfluidic Operation

For evaluating the performance of the 3D-printed MFDs, we used a Harvard Apparatus syringe pump 33. Syringes (20 mL, Henke-ject Luer Lock syringes) were loaded with the blue and red dyes and connected to the inlets of the 3D-printed Y-channel and T-junction. The inlet holes were created by poking and sealing using glue to make sure of a tight leak-proof connection.

3.2.4 Characterization of Channel Printing Accuracy

The printing accuracy of the channels was analysed in terms of lateral dimensions. Printing parameters such as nozzle diameter, pressure, and speed were kept constant at 23 G (337 µm), 38 psi, and 1.5 mm. s^{-1}, respectively, during the printing process. Channels were printed with various widths, from 100 up to 1000 µm. The actual channels' width was measured using the microscope (Nikon Eclipse ti) and analysed with ImageJ. All the channels were printed without a cap for ease of image analysis.

3.2.5 Solvent Compatibility Measurement

SC3M3 hybrid ink was printed and cured in a rectangular shape with a dimension of 1 × 1 × 0.1 cm^3. The printed constructs were weighed and imaged to measure the initial mass (M_o) and initial volume (V_o) and then soaked in various solvents (5 mL) at room temperature. After 24 hr, the printed constructs were imaged and analyzed using ImageJ to measure the final volume (V_f).[91] The swelling ratio was calculated as follows:

$$Swelling\ ratio = \frac{V_f - V_0}{V_0} \qquad \text{Equation 3.1}$$

To measure the final mass of the constructs (M_f), the concentration of the solvent solutions was reduced by sequential dilution with IPA. Subsequently, the printed constructs were heated at 120

°C for 24 hr to evaporate the solvent. Then, the printed constructs were weighed, and the mass loss was calculated as follows:

$$Mass\ loss = \frac{M_f - M_0}{M_0} \qquad \text{Equation 3.2}$$

3.3 Results and Discussion

3.3.1 Characterization of Channel Printing Accuracy

Printing resolution is a crucial factor for fabricating MFDs. To investigate the printing resolution, a set of 10 lines with the same width and height, 400 µm and 1000 µm, respectively, and different gap distances, from 100 to 900 µm, was designed and printed using a 23 G nozzle (Figure 3.1). The printing speed and pressure were set to 1.5 mm. s^{-1} and 38 psi, respectively. As can be seen in Figure 3.1b, channels with 400 µm width and above were successfully printed; however, channels below 400 µm width could not be printed. The zoomed-in images of the printed channels are also depicted in Figure 3.1c. Although all the printed walls are exceedingly smooth, the actual printed widths of the channels were approximately half of the designed dimensions. This deviation increased by decreasing the gap between the channels; for instance, the lowest channel width was 96 µm attributing to the channel with the designed width of 400 µm. This deviation is mainly caused by the filament-spreading phenomenon. Indeed, two parameters affect the wall thickness deformation; first, the downward compression of the upper layers and the second is the tendency of the bottom layer's filament to integrate with the surface layer of the substrate.[326]

Taken all together, the results showed the capability of our developed ink and printing strategy in fabricating high aspect ratio microfluidic channels (with 100 and 1000 µm).

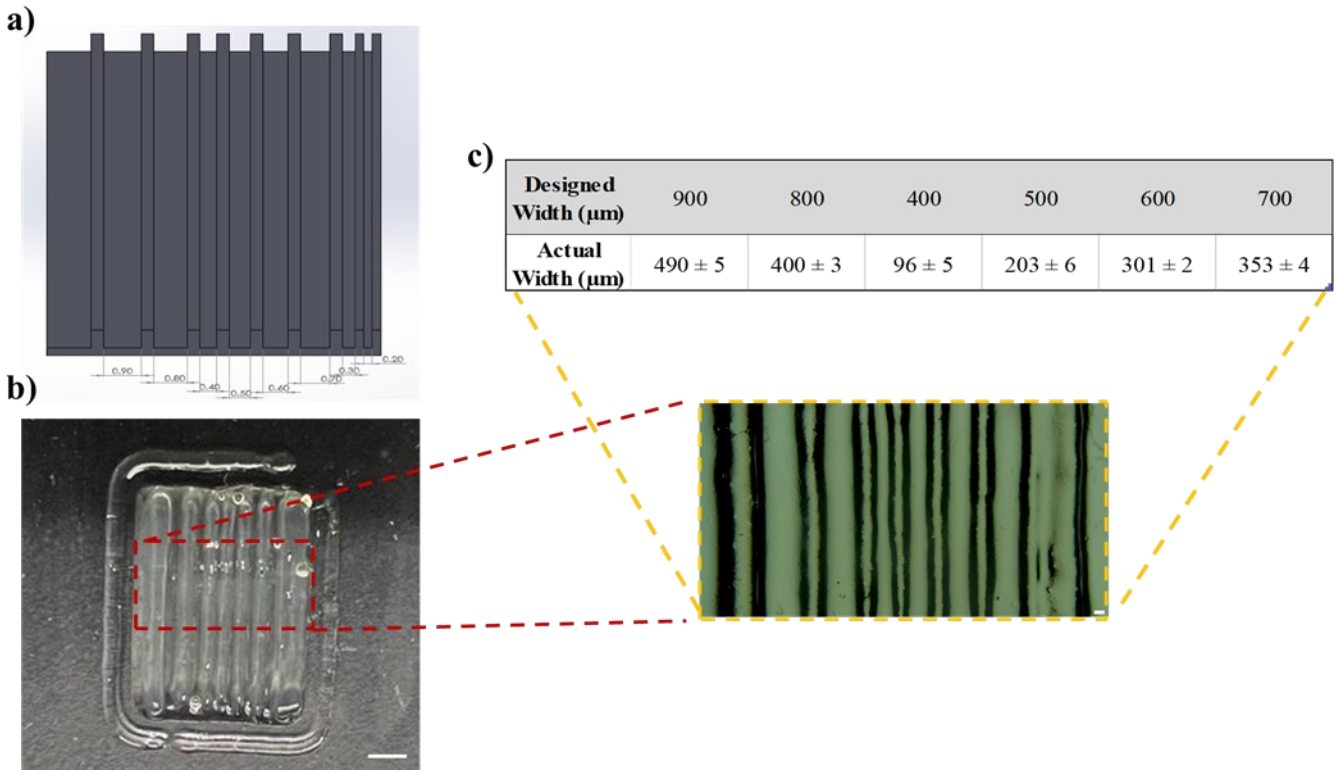

Figure 3.1 Characterization of channel printing accuracy. a) schematic design of channels, b) 3D printed channels. Scale bar 800 µm, c) Zoomed-in images of 3D printed channels with actual and designed dimensions. Scale bar 200 µm

3.3.2 3D-printed Microfluidic Devices (MFDs)

To illustrate the capability of our developed ink in the fabrication of MFDs, various examples of MFDs, including Y-channel and T-junction chips, were fabricated (Figure 3.2). There are several printing parameters, including printing speed, pressure, bridging angle, bridge flow ratio, and bridging speed, that need to be adjusted to create MFDs with suitable shape integrity. The printing speed and pressure were set to 1.5 mm. s^{-1} and 38 psi, respectively, for printing all the chips. However, when it comes to bridging the gaps and sealing the channels, bridging parameters, including bridging angle, bridge flow ratio, and bridging speed, are considered the main

challengeable parameters requiring to be adjusted to prevent sagging and channel's blockage.[219,326] The bridging speed was set to 0.8 mm. s^{-1} which is lower than that used for printing the whole substrate to give the extrudates more time to be crosslinked without sagging. In terms of bridging angle, 90^{o} was the best one since it can reduce the length of the bridging filament, to some extent, leading to less sagging. By decreasing the bridge flow ratio, a parameter that affects the amount of ink for bridging, extrudates can be slightly pulled to prevent sagging. After several trials and errors, 0.44% was chosen as the best. As can be seen in Figure 3.2, the Y-channel with a width of 0.7 mm and 1 mm height could be printed smoothly. A gooseneck UV light setup was used for in situ crosslinking.

To further demonstrate the applicability of our developed ink, a T-junction chip, one of the most popular MFDs, was also fabricated (Figure 3.2). All the printing parameters were similar to those used for printing the Y-channel, except the bridging angle. By setting the bridging angle to 90^{o}, one of the channels needs to be capped by depositing long filaments resulting in either sagging or forming a complete crosslinked filament, which the latter may deprive filaments of integrating with each other. Therefore, 45^{o} was the best value for the bridging angle to cap the T-junction's channels.

Although the printed microfluidic chips confirm the efficacy and capability of our developed ink and fabrication method for producing basic microfluidic modalities, there are some drawbacks that need to be taken into account as well. Figure 3.2 (middle panel) illustrates zoomed-in images of the printed chips showing some obstructions which can be caused by partial polymer sagging during the bridging process. The formation of the concaved walls is another challenge that might affect the flow profile and shear stress distribution of the injected fluid. [327]

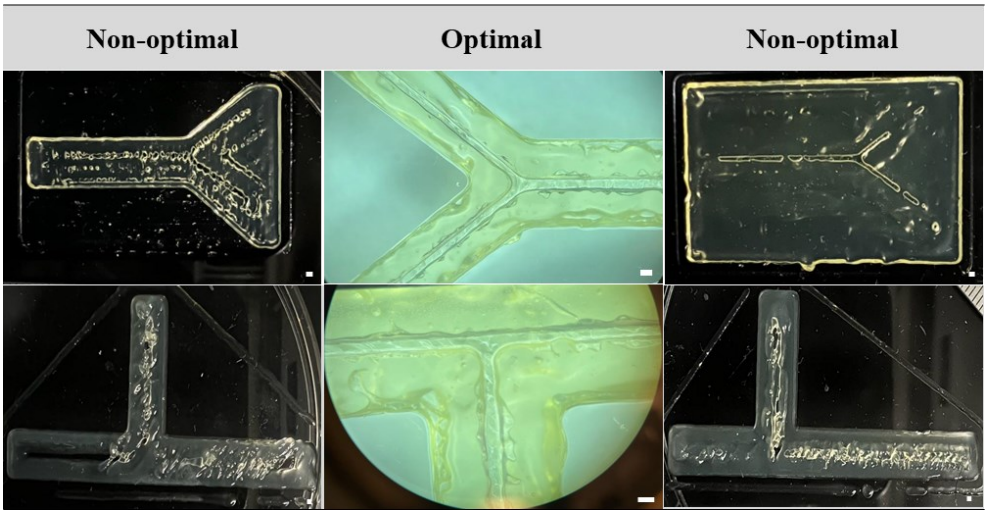

Figure 3.2 3D printed basic microfluidic modalities. Left panel: printed structures with the low bridging flow and high bridging speed; middle panel: zoomed-in images of printed structures with optimal parameters; right panel: printed structures with the low bridging flow and high bridging speed. Scale bar 200 μm.

To evaluate the performance of our printed chips, the red and blue dyes were injected into the Y- channel and T-junction chips (Figure 3.3). As can be seen in Figure 3.3, in the Y-channel chip, the boundary of the co-laminar flow of red and blue dyes (with an injection rate of 5 mL/hr) can be easily observed. This phenomenon enables the coexistence of two laminar streams with just cross-stream diffusion serving as the method of mixing.[91]

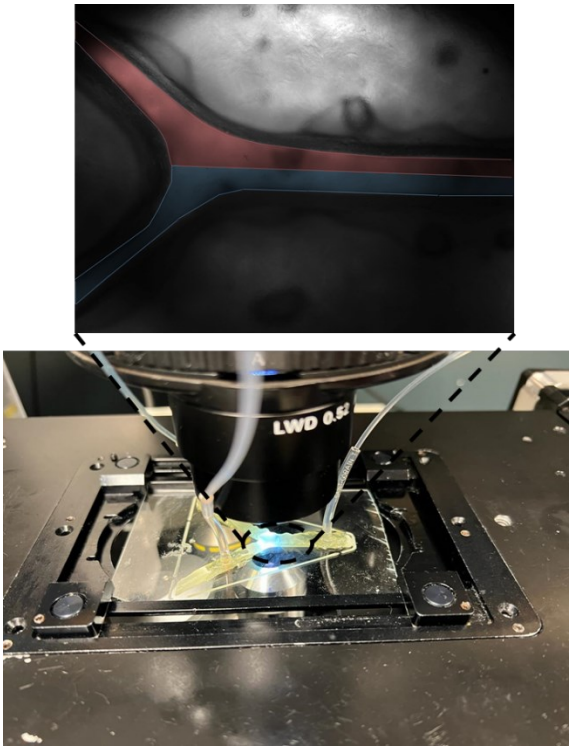

Figure 3.3 Visualization of the performance of the 3D-printed Y-channel chip. Two streams of blue and red dye (5mL/hr) produce a laminar flow in the 3D-printed chip (zoomed-in image).

In the T-junction chip, as shown in Figure 3.4, the two dyes were thoroughly mixed once they left the chip. It is worth noting that due to a few channel obstructions and surface roughness, the generation of the oil droplets in water was unsuccessful.

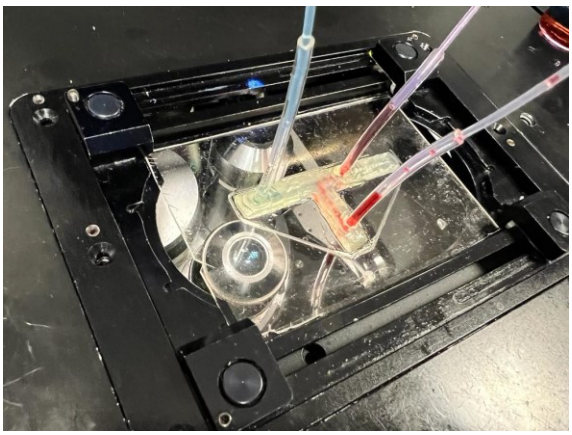

Figure 3.4 Visualization of the performance of the 3D-printed T-junction chip.

Overall, our results show that the developed ink has a promising potential for fabricating integrated MFDs in one step and within a short time (45 mins, without any post-curing process).

3.3.3 Solvent Compatibility

The solubility of our fabricated devices in organic solvents is an important consideration in deciding the solvent utilized in the post-processing of MFDs devices.[91] After printing, the solvent needs to effectively clean the channels from uncured ink through dissolving and extracting. Besides, the solvent must be able to penetrate the 3D-printed MFDs to remove the partially cured macromers and other possible by-products from the main body of the MFDs. However, if the solvent is excessively volatile, quick deswelling might lead to partial deformation in the printed MFDs once the solvent is extracted or swapped.[91] Hence, to evaluate the effect of various solvents on the swelling and dissolution of the uncured materials, rectangular slabs were printed and immersed in various solvents for 24 h (Figure 3.5). The results show that the 3D-printed slabs swelled noticeably more in IPA (36%) compared to other solvents (below 13%). Additionally, all the solvents, except IPA and chloroform, had relatively similar mass losses (between 20 and 25%), probably caused by the dissolution of unbonded by-products. Therefore, among various organic solvents, chloroform can provide significantly higher dissolution of unbounded and uncured materials with a lower swelling ratio.

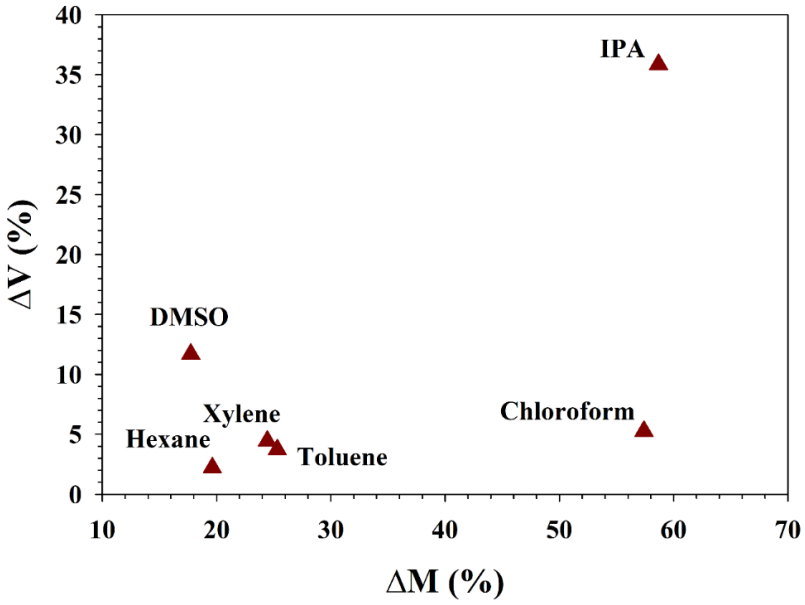

Figure 3.5 Solubility of 3D-printed slabs in Organic Solvents. Scatter plot of the change in mass (due to extraction) and the change in volume (due to swelling) of 3D-printed slabs cubes in different organic solvents.

It is worth noting that all the printed slabs not only preserved their structural integrity but also showed remarkable flexibility even after being immersed for 24 h in an organic solvent (Figure 3.6). As can be seen in Figure 3.6, for instance, the printed slab immersed in IPA, possessing the highest swelling ratio and mass loss, regained its original shape after being completely bent for 5 min.

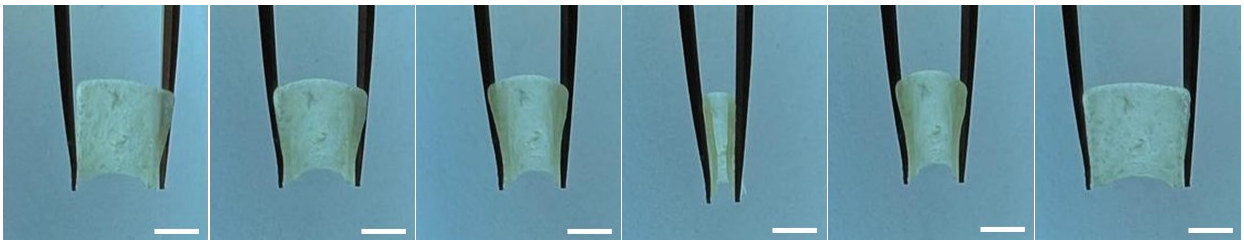

Figure 3.6 Flexibility of the 3D-printed slabs after being immersed for 24 h in IPA. Scale bar 4 mm.

3.4 Conclusion

In this study, the one-step and time-efficient fabrication of the various MFDs, including Y-channel and T-junction, using our developed ink (SC3M3), was illustrated. To evaluate the printing accuracy, a 3D ME printer was employed to fabricate the 3D printed channels, designed by SolidWorks, that subsequently were characterized in terms of channel width. The printing parameters, such as printing speed, pressure, bridging angle, bridge flow ratio, and bridging speed, were optimized. Additionally, the Y-channel and T-junction chips were 3D printed and tested to perform approximately as effectively as currently available PDMS-based MFDs. The swelling and dissolution characteristics of the 3D-printed constructs in various organic solvents were evaluated as well. Overall, the developed ink showed a promising potential to be employed by ME printers for MFDs fabrication, which can pave the way towards rapid and high-throughput manufacturing of biocompatible MFDs with advanced functionalities; however, further studies must be performed to address the problems associated with this fabrication method including the formation of concave walls and partial polymer sagging during the capping process.

Chapter 4 Conclusions and Future Work

4.1 Conclusions

Silicone elastomers have been widely utilized in various biomedical applications, such as fabricating tissue-mimetic substitutes and MFDs, due to their remarkable features, including flexibility, adaptability, and biocompatibility, but the slow curing speed, low viscosity, and hydrophobicity of the existing silicones are challenges that hinder silicone applications. A series of strategies has been pursued throughout this thesis to develop 3D-printable, UV-curable, and hydrophilic silicone-based inks. To this end, various novel silicone-based inks consisting of aminosilicone, CNC, and MA have been developed with tunable viscoelastic and mechanical features for ME 3D printing applications.

In chapter 2, I developed various SCM inks via grafting MA to the side chain of the aminosilicone and incorporating the CNC into the polymer matrix simultaneously. To confirm the capability of quick-recovery responses, the developed inks were characterized in terms of their shear-thinning and viscoelastic properties. Additionally, the printability of the SCM inks was thoroughly evaluated in terms of extrudability, accuracy, homogeneity, resolution, and shape fidelity. Thanks to the rapidly-curing property of the developed inks, curing in less than 3 seconds, high aspect ratio (18:1, height: diameter) and overhanging structures can be directly created without using any sacrificial supports. The wettability of the printed structures using our developed inks was also evaluated. By altering the concentration of the CNC and MA, noncytotoxic inks with a broad range of compression moduli from 0.25 to 1.32 MPa were developed. To mimic the multizonal structure of the HAC, a multilayered structure with a gradual increase of the compression modulus from the top layer to the bottom one was printed using different inks, including SC3M, SC3M5, and SC5M5. Normal and cyclic compression tests were

performed at different time points (immediately, 1 week, and 2 weeks after printing) to show not only the mechanical stability but the capability of our inks to withstand highly repeated compression loads, up to 400 cycles, which makes them as an ideal candidate for replacing damaged human articular cartilage.

In chapter 3, I presented the one-step and time-efficient fabrication of the various MFDs, including Y-channel and T-junction, using our developed ink (SC3M3). The printing accuracy of the printed channels, in terms of channel width, was characterized to find the highest achievable channel resolution (approximately 300 μm). Besides, various printing parameters, including printing speed, pressure, bridging angle, bridge flow ratio, and bridging speed, were optimized. The Y-channel and T-junction chips were fabricated and tested to perform approximately as effectively as currently available PDMS-based MFDs. Various organic solvents, including toluene, hexane, xylene, chloroform, DMSO, and IPA, were used to evaluate the swelling and dissolution characteristics of the 3D printed constructs.

Overall, our results represent a new class of silicone-based materials with promising features such as hydrophilicity, rapid curing, shear-thinning, mechanical stability, and biocompatibility, for use in fabricating not only personalized and biocompatible tissue-mimetic models but also various microfluidic modalities which offer new strategies to pave the way towards rapid and high-throughput manufacturing of complex 3D human-like constructs and biomedical devices.

4.2 Future Work

The research presented in this thesis was designed to develop a series of hydrophilic, rapidly curing, and 3D-printable silicone-based inks with tunable mechanical characteristics for various

biomedical applications. To this end, two different applications of the developed inks, including the fabrication of AC substitute and different microfluidic modalities, were introduced and investigated. However, further studies on material formulation, printing techniques, and applications should be carried out to accomplish our intended goal of developing an economically feasible system for additive manufacturing of a new class of silicone-based biomedical devices.

1- The viscoelastic features of the cartilage play a crucial role in providing superior mechanical support to diminish wear and relieve stress. In this study, we focused on the mechanical strength of the developed inks in terms of normal and cyclic compression behaviors rather than investigating their elastic properties. Hence, the elastic properties of the printed substitutes should be studied in the next step.

2- The mechanical feature tunability of our developed inks makes them a potential candidate for fabricating various human tissues. Besides AC, other tissue models, such as the meniscus, trachea, and heart aortic valve, may be fabricated in future studies. However, the ink formulation should be developed based on the characteristics of the targeted tissues. This development can be achieved by incorporating various additives such as nanoparticles, nanotubes, and fibers into the aminosilicone matrix.

3- Although the printing parameters were thoroughly investigated in this study, even a minor change in the ink formulation can affect the optimized parameters. Thus, there is a need to develop a numerical model for predicting printing parameters based on the ink properties, such as rheological features, or employing machine learning techniques, such as image processing, for analyzing the printed filaments in terms of their uniformity to correlate printing parameter optimization with ink characterization techniques, which in turn can significantly speed up the optimization process.

4- The 3D printability of our developed inks makes them a suitable candidate for various biomedical applications. In this study, we focused on fabricating human tissues and MFDs, while silicone elastomers also have a broad range of applications in soft electronics. Therefore, in future studies, electrical conductivity can be introduced to the aminosilicone matrix by incorporating electroconductive materials, including graphene oxide, CNTs, and conductive CNC fillers, to fabricate various flexible electronics, such as train sensors.

5- The developed silicone-based inks presented in this study showed similar mechanical strength to the human one and no significant toxicity against fibroblast cells. However, further In vivo experiments are required to investigate the performance of the 3D-printed substitutes and their possible cytotoxicity over a longer period under conditions that are more similar to the human body. Besides the mechanical functionality of the 3D printed substitutes, their interaction with the local environment of the ECM must also be thoroughly investigated by implanting the fabricated substitutes into an animal model, such as mice or pigs.

6- The MFDs printed with our developed ink (Chapter 3) demonstrated a suitable performance and potential applications in mixing and cross-stream diffusion; however, only basic microfluidic modalities were fabricated. Hence more complex devices need to be designed and fabricated, such as passive/active micro-mixer and 3D-fluid routers.

7- The fabricated MFDs presented in chapter 3 showed a few channel obstructions and surface roughness due to the partial polymer sagging during the bridging process, which can dramatically affect the flow control capability over the channels. This problem can be solved by implementing the following strategies: a) changing the printing direction by rotating the designed structure; b) changing the geometry of the channel to reduce the amount of required bridging across the channel; c) using a PMMA substrate or glass to seal the channels instead of bridging.

8- This study has successfully shown the potential of our developed ink in fabricating MFDs in one step using a single material; however, all the capabilities of the ME printing method, such as multi-material printing, have yet to be employed. Hence, the inner surface of MFD channels can be patterned with a selected material for different lab-on-chip applications. For instance, these patterns can be functionalized pillars with specific biomarkers to capture various biomolecules, such as circulating cancer tumor cells.

References

1. Zhou, L. Y., Fu, J. & He, Y. A Review of 3D Printing Technologies for Soft Polymer Materials. *Adv. Funct. Mater.* **30**, 1–38 (2020).
2. Oropallo, W. & Piegl, L. A. Ten challenges in 3D printing. *Eng. Comput.* **32**, 135–148 (2016).
3. Awad, R. H., Habash, S. A. & Hansen, C. J. 3D printing methods. *3D Printing Applications in Cardiovascular Medicine* 11–32 (Elsevier Inc., 2018). doi:10.1016/B978-0-12-803917-5.00002-X.
4. Berman, B. 3-D printing: The new industrial revolution. *Bus. Horiz.* **55**, 155–162 (2012).
5. Truby, R. L. & Lewis, J. A. Printing soft matter in three dimensions. *Nature* **540**, 371–378 (2016).
6. Kinstlinger, I. S. *et al.* Open-Source Selective Laser Sintering (OpenSLS) of Nylon and Biocompatible Polycaprolactone. *PLoS One* **11**, e0147399 (2016).
7. Brandt, M. *Laser Additive Manufacturing: Materials, Design, Technologies, and Applications*. (Elsevier Inc., 2016).
8. Caulfield, B., McHugh, P. E. & Lohfeld, S. Dependence of mechanical properties of polyamide components on build parameters in the SLS process. *J. Mater. Process. Technol.* **182**, 477–488 (2007).
9. Drummer, D., Rietzel, D. & Kühnlein, F. Development of a characterization approach for the sintering behavior of new thermoplastics for selective laser sintering. *Phys. Procedia* **5**, 533–542 (2010).
10. Novitsky, T. F., Mathias, L. J., Osborn, S., Ayotte, R. & Manning, S. Synthesis and Thermal Behavior of Polyamide 12,T Random and Block Copolymers. *Macromol. Symp.* **313**, 90–99 (2012).
11. Williams, J. M. *et al.* Bone tissue engineering using polycaprolactone scaffolds fabricated via selective laser sintering. *Biomaterials* **26**, 4817–4827 (2005).
12. Zhou, W. Y., Lee, S. H., Wang, M., Cheung, W. L. & Ip, W. Y. Selective laser sintering of porous tissue engineering scaffolds from poly(L-lactide)/carbonated hydroxyapatite nanocomposite microspheres. *J. Mater. Sci. Mater. Med.* **19**, 2535–2540 (2008).
13. Shirazi, S. F. S. *et al.* A review on powder-based additive manufacturing for tissue engineering: selective laser sintering and inkjet 3D printing. *Sci. Technol. Adv. Mater.* **16**, 33502–33522 (2015).
14. Duan, B. & Wang, M. Encapsulation and release of biomolecules from Ca–P/PHBV nanocomposite microspheres and three-dimensional scaffolds fabricated by selective laser

sintering. *Polym. Degrad. Stab.* **95**, 1655–1664 (2010).

15. Kodama, H. Automatic method for fabricating a three-dimensional plastic model with photo-hardening polymer. *Rev. Sci. Instrum.* **52**, 1770 (1998).

16. Tumbleston, J. R. *et al.* Continuous liquid interface production of 3D objects. *Science* **347**, 1349–1352 (2015).

17. Lu, Y., Mapili, G., Suhali, G., Chen, S. & Roy, K. A digital micro-mirror device-based system for the microfabrication of complex, spatially patterned tissue engineering scaffolds. *J. Biomed. Mater. Res. Part A* **77A**, 396–405 (2006).

18. Tianyue Yu, B. *et al.* Chemically Amplified Positive Resists for Two-Photon Three-Dimensional Microfabrication. *Adv. Mater.* **15**, 517–521 (2003).

19. Gong, H., Bickham, B. P., Woolley, A. T. & Nordin, G. P. Custom 3D printer and resin for 18 μm × 20 μm microfluidic flow channels. *Lab Chip* **17**, 2899–2909 (2017).

20. Raman, R. *et al.* Bioprinting: High-Resolution Projection Microstereolithography for Patterning of Neovasculature. *Adv. Healthc. Mater.* **5**, 622–622 (2016).

21. Guvendiren, M., Molde, J., Soares, R. M. D. & Kohn, J. Designing Biomaterials for 3D Printing. *ACS Biomater. Sci. Eng.* **2**, 1679–1693 (2016).

22. Jang, J., Yi, H. G. & Cho, D. W. 3D Printed Tissue Models: Present and Future. *ACS Biomater. Sci. Eng.* **2**, 1722–1731 (2016).

23. Guo, Y., Patanwala, H. S., Bognet, B. & Ma, A. W. K. Inkjet and inkjet-based 3D printing: Connecting fluid properties and printing performance. *Rapid Prototyp. J.* **23**, 562–576 (2017).

24. Derby, B. Inkjet printing of functional and structural materials: Fluid property requirements, feature stability, and resolution. *Annu. Rev. Mater. Res.* **40**, 395–414 (2010).

25. Gao, G., Kim, B. S., Jang, J. & Cho, D. W. Recent Strategies in Extrusion-Based Three-Dimensional Cell Printing toward Organ Biofabrication. *ACS Biomater. Sci. Eng.* **5**, 1150–1169 (2019).

26. McCoul, D., Rosset, S., Schlatter, S. & Shea, H. Inkjet 3D printing of UV and thermal cure silicone elastomers for dielectric elastomer actuators. *Smart Mater. Struct.* **26**, 125022 (2017).

27. Sirringhaus, H. *et al.* High-resolution inkjet printing of all-polymer transistor circuits. *Science* **290**, 2123–2126 (2000).

28. Turner, B. N., Strong, R. & Gold, S. A. A review of melt extrusion additive manufacturing processes: I. Process design and modeling. *Rapid Prototyp. J.* **20**, 192–204 (2014).

29. Lewis, J. A. Direct Ink Writing of 3D Functional Materials. *Adv. Funct. Mater.* **16**, 2193–2204 (2006).

30. Paxton, N. *et al.* Proposal to assess printability of bioinks for extrusion-based bioprinting and evaluation of rheological properties governing bioprintability. *Biofabrication* **9**, 044107 (2017).

31. Lei, D. *et al.* A general strategy of 3D printing thermosets for diverse applications. *Mater. Horizons* **6**, 394–404 (2019).

32. Jin, Y., Liu, C., Chai, W., Compaan, A. & Huang, Y. Self-Supporting Nanoclay as Internal Scaffold Material for Direct Printing of Soft Hydrogel Composite Structures in Air. *ACS Appl. Mater. Interfaces* **9**, 17456–17465 (2017).

33. Gao, Q. *et al.* 3D printing of complex GelMA-based scaffolds with nanoclay. *Biofabrication* **11**, 035006 (2019).

34. Kokkinis, D., Schaffner, M. & Studart, A. R. Multimaterial magnetically assisted 3D printing of composite materials. *Nat. Commun.* **6**, 1–10 (2015).

35. Hinton, T. J., Hudson, A., Pusch, K., Lee, A. & Feinberg, A. W. 3D Printing PDMS Elastomer in a Hydrophilic Support Bath via Freeform Reversible Embedding. *ACS Biomater. Sci. Eng.* **2**, 1781–1786 (2016).

36. Grosskopf, A. K. *et al.* Viscoplastic Matrix Materials for Embedded 3D Printing. *ACS Appl. Mater. Interfaces* **10**, 23353–23361 (2018).

37. O'Bryan, C. S. *et al.* Self-assembled micro-organogels for 3D printing silicone structures. *Sci. Adv.* **3**, (2017).

38. Noor, N. *et al.* 3D Printing of Personalized Thick and Perfusable Cardiac Patches and Hearts. *Adv. Sci.* **6**, (2019).

39. Liu, S. *et al.* Bioactive and Biocompatible Macroporous Scaffolds with Tunable Performances Prepared Based on 3D Printing of the Pre-Crosslinked Sodium Alginate/Hydroxyapatite Hydrogel Ink. *Macromol. Mater. Eng.* **304**, (2019).

40. Wüst, S., Godla, M. E., Müller, R. & Hofmann, S. Tunable hydrogel composite with two-step processing in combination with innovative hardware upgrade for cell-based three-dimensional bioprinting. *Acta Biomater.* **10**, 630–640 (2014).

41. Colosi, C. *et al.* Microfluidic Bioprinting of Heterogeneous 3D Tissue Constructs Using Low-Viscosity Bioink. *Adv. Mater.* **28**, 677–684 (2016).

42. Chen, Q. *et al.* Mechanically Robust, Ultraelastic Hierarchical Foam with Tunable Properties via 3D Printing. *Adv. Funct. Mater.* **28**, (2018).

43. Jiang, T., Munguia-Lopez, J. G., Flores-Torres, S., Kort-Mascort, J. & Kinsella, J. M. Extrusion bioprinting of soft materials: An emerging technique for biological model fabrication. *Appl. Phys. Rev.* **6**, (2019).

44. Tian, K. *et al.* 3D Printing of Transparent and Conductive Heterogeneous Hydrogel–

Elastomer Systems. *Adv. Mater.* **29**, 1604827 (2017).

45. Highley, C. B. *et al.* Direct 3D Printing of Shear-Thinning Hydrogels into Self-Healing Hydrogels. *Adv. Mater.* **27**, 5075–5079 (2015).

46. Gao, Q., He, Y., Fu, J. zhong, Liu, A. & Ma, L. Coaxial nozzle-assisted 3D bioprinting with built-in microchannels for nutrients delivery. *Biomaterials* **61**, 203–215 (2015).

47. Hun Park, J. *et al.* Processing parameters investigation for the fabrication of self-supported and freeform polymeric microstructures using ultraviolet-assisted three-dimensional printing. *J. Micromechanics Microengineering* **24**, (2014).

48. Kirchmajer, D. M., Gorkin, R. & In Het Panhuis, M. An overview of the suitability of hydrogel-forming polymers for extrusion-based 3D-printing. *J. Mater. Chem. B* **3**, 4105–4117 (2015).

49. Tian, K. *et al.* 3D Printing of Transparent and Conductive Heterogeneous Hydrogel–Elastomer Systems. *Adv. Mater.* **29**, (2017).

50. Kim, Y., Yuk, H., Zhao, R., Chester, S. A. & Zhao, X. Printing ferromagnetic domains for untethered fast-transforming soft materials. *Nature* **558**, 274–279 (2018).

51. Miri, A. K. *et al.* Effective bioprinting resolution in tissue model fabrication. *Lab Chip* **19**, 2019–2037 (2019).

52. Lee, A. *et al.* 3D bioprinting of collagen to rebuild components of the human heart. *Science* **365**, 482–487 (2019).

53. Mehrotra, S., Moses, J. C., Bandyopadhyay, A. & Mandal, B. B. 3D Printing/Bioprinting Based Tailoring of in Vitro Tissue Models: Recent Advances and Challenges. *ACS Appl. Bio Mater.* **2**, 1385–1405 (2019).

54. Jiang, Z. *et al.* Extrusion 3D Printing of Polymeric Materials with Advanced Properties. *Adv. Sci.* **7**, 1–32 (2020).

55. Pugliese, R., Beltrami, B., Regondi, S. & Lunetta, C. Polymeric biomaterials for 3D printing in medicine: An overview. *Ann. 3D Print. Med.* **2**, (2021).

56. Mobaraki, M., Ghaffari, M., Yazdanpanah, A., Luo, Y. & Mills, D. K. Bioinks and bioprinting: A focused review. *Bioprinting* **18**, e00080 (2020).

57. Skardal, A. Perspective: "Universal" bioink technology for advancing extrusion bioprinting-based biomanufacturing. *Bioprinting* **10**, (2018).

58. Du, X., Fu, S. & Zhu, Y. 3D printing of ceramic-based scaffolds for bone tissue engineering: an overview. *J. Mater. Chem. B* **6**, 4397–4412 (2018).

59. Denry, I. & Kelly, J. R. Emerging ceramic-based materials for dentistry. *J. Dent. Res.* **93**, 1235–1242 (2014).

60. Ghalayini, S., Susapto, H. H., Hall, S., Kahin, K. & Hauser, C. A. E. Preparation and printability of ultrashort self-assembling peptide nanoparticles. *Int. J. Bioprinting* **5**, 109–116 (2019).

61. Xia, Y. *et al.* Printable Fluorescent Hydrogels Based on Self-Assembling Peptides. *Sci. Rep.* **7**, (2017).

62. Ligon, S. C., Liska, R., Stampfl, J., Gurr, M. & Mülhaupt, R. Polymers for 3D Printing and Customized Additive Manufacturing. *Chem. Rev.* **117**, 10212–10290 (2017).

63. Guzzi, E. A., Tibbitt, M. W., Guzzi, E. A. & Tibbitt, M. W. Additive Manufacturing of Precision Biomaterials. *Adv. Mater.* **32**, (2020).

64. Shirazi, S. F. S. *et al.* A review on powder-based additive manufacturing for tissue engineering: selective laser sintering and inkjet 3D printing. *Sci. Technol. Adv. Mater.* **16**, 33502–33522 (2015).

65. Duan, B. *et al.* Three-dimensional nanocomposite scaffolds fabricated via selective laser sintering for bone tissue engineering. *Acta Biomater.* **6**, 4495–4505 (2010).

66. Ning, F., Cong, W., Qiu, J., Wei, J. & Wang, S. Additive manufacturing of carbon fiber reinforced thermoplastic composites using fused deposition modeling. *Compos. Part B Eng.* **80**, 369–378 (2015).

67. Dul, S., Pegoretti, A. & Fambri, L. Effects of the Nanofillers on Physical Properties of Acrylonitrile-Butadiene-Styrene Nanocomposites: Comparison of Graphene Nanoplatelets and Multiwall Carbon Nanotubes. *Nanomaterials* **8**, 674 (2018).

68. Wei, X. *et al.* 3D Printable Graphene Composite. *Sci. Rep.* **5**, 1–7 (2015).

69. Zhong, W., Li, F., Zhang, Z., Song, L. & Li, Z. Short fiber reinforced composites for fused deposition modeling. *Mater. Sci. Eng. A* **301**, 125–130 (2001).

70. Levenhagen, N. P. & Dadmun, M. D. Bimodal molecular weight samples improve the isotropy of 3D printed polymeric samples. *Polymer* **122**, 232–241 (2017).

71. Levenhagen, N. P. & Dadmun, M. D. Interlayer diffusion of surface segregating additives to improve the isotropy of fused deposition modeling products. *Polymer* **152**, 35–41 (2018).

72. Levenhagen, N. P. & Dadmun, M. D. Reactive Processing in Extrusion-Based 3D Printing to Improve Isotropy and Mechanical Properties. *Macromolecules* **52**, 6495–6501 (2019).

73. Chen, L. *et al.* 3D printable robust shape memory PET copolyesters with fire safety via π-stacking and synergistic crosslinking. *J. Mater. Chem. A* **7**, 17037–17045 (2019).

74. Shi, Q. *et al.* Recyclable 3D printing of vitrimer epoxy. *Mater. Horizons* **4**, 598–607 (2017).

75. Zou, W. *et al.* Dynamic Covalent Polymer Networks: from Old Chemistry to Modern Day Innovations. *Adv. Mater.* **29**, 1606100–1606118 (2017).

76. Yang, K. *et al.* Diels–Alder Reversible Thermoset 3D Printing: Isotropic Thermoset Polymers via Fused Filament Fabrication. *Adv. Funct. Mater.* **27**, 1700318–1700329 (2017).

77. Kaoutzanis, C., Winocour, J., Unger, J., Gabriel, A. & Maxwell, G. P. The Evolution of Breast Implants. *Semin. Plast. Surg.* **33**, 217–223 (2019).

78. Braley, S. The Chemistry and Properties of the Medical-Grade Silicones. *J. Macromol. Sci. Part A - Chem.* **4**, 529–544 (2006).

79. Noll, W. *Chemistry and Technology of Silicones.* (Elsevier Inc., 1968).

80. Zare, M., Ghomi, E. R., Venkatraman, P. D. & Ramakrishna, S. Silicone-based biomaterials for biomedical applications: Antimicrobial strategies and 3D printing technologies. *J. Appl. Polym. Sci.* 1–18 (2021) doi:10.1002/app.50969.

81. Sołoducho, J., Zając, D., Spychalska, K., Baluta, S. & Cabaj, J. Conducting silicone-based polymers and their application. *Molecules* **26**, (2021).

82. Jones, R. G., Ando, W. & Chojnowski, J. Silicon Containing Polymers: The Science and Technology of Their Synthesis and Applications. *Silicon Chem.* **1**, 309–311 (2002).

83. Wolf, M. P., Salieb-Beugelaar, G. B. & Hunziker, P. PDMS with designer functionalities—Properties, modifications strategies, and applications. *Prog. Polym. Sci.* **83**, 97–134 (2018).

84. Liravi, F. & Toyserkani, E. Additive manufacturing of silicone structures: A review and prospective. *Addit. Manuf.* **24**, 232–242 (2018).

85. Rodrigue, H., Bhandari, B., Wang, W. & Ahn, S. H. 3D soft lithography: A fabrication process for thermocurable polymers. *J. Mater. Process. Technol.* **217**, 302–309 (2015).

86. Ozbolat, V. *et al.* 3D Printing of PDMS Improves Its Mechanical and Cell Adhesion Properties. *ACS Biomater. Sci. Eng.* **4**, 682–693 (2018).

87. Plott, J. & Shih, A. The extrusion-based additive manufacturing of moisture-cured silicone elastomer with minimal void for pneumatic actuators. *Addit. Manuf.* **17**, 1–14 (2017).

88. Liravi, F., Salarian, M., Dal Castel, C., Simon, L. & Toyserkani, E. High-speed material jetting additive manufacturing of silicone structures: mechanical characterization. *Prog. Addit. Manuf.* **4**, 479–495 (2019).

89. Liravi, F. & Toyserkani, E. A hybrid additive manufacturing method for the fabrication of silicone bio-structures: 3D printing optimization and surface characterization. *Mater. Des.* **138**, 46–61 (2018).

90. Wallin, T. J. *et al.* 3D printable tough silicone double networks. *Nat. Commun.* **11**, 1–10 (2020).

91. Bhattacharjee, N., Parra-Cabrera, C., Kim, Y. T., Kuo, A. P. & Folch, A. Desktop-Stereolithography 3D-Printing of a Poly(dimethylsiloxane)-Based Material with Sylgard-

184 Properties. *Adv. Mater.* **30**, (2018).

92. Patel, D. K. *et al.* Highly Stretchable and UV Curable Elastomers for Digital Light Processing Based 3D Printing. *Adv. Mater.* **29**, 1–7 (2017).

93. Kim, D. S. (Danny), Kao, Y. T. & Tai, B. L. Hydrostatic 3D-printing for soft material structures using low one-photon polymerization. *Manuf. Lett.* **10**, 6–9 (2016).

94. Zheng, S., Zlatin, M., Selvaganapathy, P. R. & Brook, M. A. Multiple modulus silicone elastomers using 3D extrusion printing of low viscosity inks. *Addit. Manuf.* **24**, 86–92 (2018).

95. Duoss, E. B. *et al.* Three-Dimensional Printing of Elastomeric, Cellular Architectures with Negative Stiffness. *Adv. Funct. Mater.* **24**, 4905–4913 (2014).

96. Robinson, S. S. *et al.* Integrated soft sensors and elastomeric actuators for tactile machines with kinesthetic sense. *Extrem. Mech. Lett.* **5**, 47–53 (2015).

97. Lv, J. *et al.* 3D printing of a mechanically durable superhydrophobic porous membrane for oil–water separation. *J. Mater. Chem. A* **5**, 12435–12444 (2017).

98. Femmer, T., Kuehne, A. J. C. & Wessling, M. Print your own membrane: direct rapid prototyping of polydimethylsiloxane. *Lab Chip* **14**, 2610–2613 (2014).

99. Wallin, T. J. *et al.* Click chemistry stereolithography for soft robots that self-heal. *J. Mater. Chem. B* **5**, 6249–6255 (2017).

100. Rekštytė, S., Malinauskas, M. & Juodkazis, S. Three-dimensional laser micro-sculpturing of silicone: towards bio-compatible scaffolds. *Opt. Express* **21**, 17028 (2013).

101. Hardin, J. O. *et al.* Microfluidic Printheads for Multimaterial 3D Printing of Viscoelastic Inks. *Adv. Mater.* **27**, 3279–3284 (2015).

102. Liravi, F., Darleux, R. & Toyserkani, E. Nozzle dispensing additive manufacturing of polysiloxane: dimensional control. *Int. J. Rapid Manuf.* **5**, 20 (2015).

103. Mannoor, M. S. *et al.* 3D printed bionic ears. *Nano Lett.* **13**, 2634–2639 (2013).

104. Anderson, J. M., Rodriguez, A. & Chang, D. T. Foreign body reaction to biomaterials. *Semin. Immunol.* **20**, 86–100 (2008).

105. Au, A. K., Lee, W. & Folch, A. Mail-order microfluidics: evaluation of stereolithography for the production of microfluidic devices. *Lab Chip* **14**, 1294–1301 (2014).

106. Zheng, S., Zlatin, M., Selvaganapathy, P. R. & Brook, M. A. Multiple modulus silicone elastomers using 3D extrusion printing of low viscosity inks. *Addit. Manuf.* **24**, 86–92 (2018).

107. Roh, S. *et al.* 3D Printing by Multiphase Silicone/Water Capillary Inks. *Adv. Mater.* **29**, 1701554 (2017).

108. Han, D., Gu, H., Kim, J. wan & Yokota, S. A bio-inspired 3D-printed hybrid finger with integrated ECF (electro-conjugate fluid) micropumps. *Sensors Actuators A Phys.* **257**, 47–57 (2017).

109. Wu, M.-H. *et al.* Development of PDMS microbioreactor with well-defined and homogenous culture environment for chondrocyte 3-D culture. *Biomed. Microdevices* **8**, 331–340 (2006).

110. Belder, D. & Ludwig, M. Surface modification in microchip electrophoresis. *Electrophoresis* **24**, 3595–3606 (2003).

111. Hu, S. *et al.* Surface modification of poly(dimethylsiloxane) microfluidic devices by ultraviolet polymer grafting. *Anal. Chem.* **74**, 4117–4123 (2002).

112. Gokaltun, A., Yarmush, M. L., Asatekin, A. & Usta, O. B. Recent advances in nonbiofouling PDMS surface modification strategies applicable to microfluidic technology. *Technology* **5**, 1–12 (2017).

113. Gomez-Sjoberg, R., Leyrat, A. A., Houseman, B. T., Shokat, K. & Quake, S. R. Biocompatibility and reduced drug absorption of sol-gel-treated poly(dimethyl siloxane) for microfluidic cell culture applications. *Anal. Chem.* **82**, 8954–8960 (2010).

114. Tan, S. H., Nguyen, N. T., Chua, Y. C. & Kang, T. G. Oxygen plasma treatment for reducing hydrophobicity of a sealed polydimethylsiloxane microchannel. *Biomicrofluidics* **4**, 032204 (2010).

115. Bartalena, G., Loosli, Y., Zambelli, T. & Snedeker, J. G. Biomaterial surface modifications can dominate cell–substrate mechanics: the impact of PDMS plasma treatment on a quantitative assay of cell stiffness. *Soft Matter* **8**, 673–681 (2011).

116. Zhang, J., Chen, Y. & Brook, M. A. Facile functionalization of PDMS elastomer surfaces using thiol-ene click chemistry. *Langmuir* **29**, 12432–12442 (2013).

117. Hu, S. *et al.* Cross-linked coatings for electrophoretic separations in poly(dimethylsiloxane) microchannels. *Electrophoresis* **24**, 3679–3688 (2003).

118. Gökaltun, A., Kang, Y. B. (Abraham), Yarmush, M. L., Usta, O. B. & Asatekin, A. Simple Surface Modification of Poly(dimethylsiloxane) via Surface Segregating Smart Polymers for Biomicrofluidics. *Sci. Rep.* **9**, 1–14 (2019).

119. Schneider, F., Draheim, J., Kamberger, R. & Wallrabe, U. Process and material properties of polydimethylsiloxane (PDMS) for Optical MEMS. *Sensors Actuators A Phys.* **151**, 95–99 (2009).

120. Schneider, F., Fellner, T., Wilde, J. & Wallrabe, U. Mechanical properties of silicones for MEMS. *J. Micromechanics Microengineering* **18**, 065008 (2008).

121. Goiato, M. C., Pesqueira, A. A., dos Santos, D. M. & Dekon, S. F. de C. Evaluation of hardness and surface roughness of two maxillofacial silicones following disinfection. *Braz.*

Oral Res. **23**, 49–53 (2009).

122. Han, Y., Rogalsky, A. D., Zhao, B. & Kwon, H. J. The application of digital image techniques to determine the large stress–strain behaviors of soft materials. *Polym. Eng. Sci.* **52**, 826–834 (2012).

123. Aziz, T., Waters, M. & Jagger, R. Analysis of the properties of silicone rubber maxillofacial prosthetic materials. *J. Dent.* **31**, 67–74 (2003).

124. Zhang, Y. S. & Khademhosseini, A. Advances in engineering hydrogels. *Science* **356**, (2017).

125. Buwalda, S. J. *et al.* Hydrogels in a historical perspective: From simple networks to smart materials. *J. Control. Release* **190**, 254–273 (2014).

126. Guan, X. *et al.* Development of hydrogels for regenerative engineering. *Biotechnol. J.* **12**, 1600394–1600413 (2017).

127. Geckil, H., Xu, F., Zhang, X., Moon, S. & Demirci, U. Engineering hydrogels as extracellular matrix mimics. *Nanomedicine* **5**, 469–484 (2010).

128. Prince, E. & Kumacheva, E. Design and applications of man-made biomimetic fibrillar hydrogels. *Nat. Rev. Mater.* **4**, 99–115 (2019).

129. Zandi, N. *et al.* Nanoengineered shear-thinning and bioprintable hydrogel as a versatile platform for biomedical applications. *Biomaterials* **267**, 120476 (2021).

130. Mantha, S. *et al.* Smart Hydrogels in Tissue Engineering and Regenerative Medicine. *Materials (Basel).* **12**, 3323–3356 (2019).

131. Zimmerling, A. & Chen, X. Bioprinting for combating infectious diseases. *Bioprinting* **20**, e00104 (2020).

132. Nesic, D. *et al.* Could 3D printing be the future for oral soft tissue regeneration? *Bioprinting* **20**, e00100 (2020).

133. Kirchmajer, D. M., Gorkin, R. & In Het Panhuis, M. An overview of the suitability of hydrogel-forming polymers for extrusion-based 3D-printing. *J. Mater. Chem. B* **3**, 4105–4117 (2015).

134. Placone, J. K. & Engler, A. J. Recent Advances in Extrusion-Based 3D Printing for Biomedical Applications. *Adv. Healthc. Mater.* **7**, 1701161 (2018).

135. Stanton, M. M., Samitier, J. & Sánchez, S. Bioprinting of 3D hydrogels. *Lab Chip* **15**, 3111–3115 (2015).

136. Miranda-Nieves, D. & Chaikof, E. L. Collagen and Elastin Biomaterials for the Fabrication of Engineered Living Tissues. *ACS Biomater. Sci. Eng.* **3**, 694–711 (2016).

137. Pugliese, R. & Gelain, F. Peptidic Biomaterials: From Self-Assembling to Regenerative

Medicine. *Trends Biotechnol.* **35**, 145–158 (2017).

138. Freeman, F. E. & Kelly, D. J. Tuning Alginate Bioink Stiffness and Composition for Controlled Growth Factor Delivery and to Spatially Direct MSC Fate within Bioprinted Tissues. *Sci. Reports 2017 71* **7**, 1–12 (2017).

139. Lim, K. S. *et al.* Fundamentals and Applications of Photo-Cross-Linking in Bioprinting. *Chem. Rev.* **120**, 10662–10694 (2020).

140. Si, H. *et al.* 3D Bioprinting of the Sustained Drug Release Wound Dressing with Double-Crosslinked Hyaluronic-Acid-Based Hydrogels. *Polymers (Basel).* **11**, 1584 (2019).

141. Pereira, R. F., Sousa, A., Barrias, C. C., Bártolo, P. J. & Granja, P. L. A single-component hydrogel bioink for bioprinting of bioengineered 3D constructs for dermal tissue engineering. *Mater. Horizons* **5**, 1100–1111 (2018).

142. Li, J., Wu, C., Chu, P. K. & Gelinsky, M. 3D printing of hydrogels: Rational design strategies and emerging biomedical applications. *Mater. Sci. Eng. R Reports* **140**, 100543 (2020).

143. Moncal, K. K. *et al.* 3D printing of poly(ε-caprolactone)/poly(D,L-lactide-co-glycolide)/hydroxyapatite composite constructs for bone tissue engineering. *J. Mater. Res.* **33**, 1972–1986 (2018).

144. Ravanbakhsh, H., Bao, G., Luo, Z., Mongeau, L. G. & Zhang, Y. S. Composite Inks for Extrusion Printing of Biological and Biomedical Constructs. *ACS Biomater. Sci. Eng.* **7**, 4009–4026 (2021).

145. Cui, X. *et al.* Advances in Extrusion 3D Bioprinting: A Focus on Multicomponent Hydrogel-Based Bioinks. *Adv. Healthc. Mater.* **9**, 1901648 (2020).

146. Nerger, B. A., Brun, P. T. & Nelson, C. M. Microextrusion printing cell-laden networks of type I collagen with patterned fiber alignment and geometry. *Soft Matter* **15**, 5728–5738 (2019).

147. Schaefer, N. *et al.* 3D Electrophysiological Measurements on Cells Embedded within Fiber-Reinforced Matrigel. *Adv. Healthc. Mater.* **8**, 1801226 (2019).

148. Fan, R. *et al.* Bio-printing cell-laden Matrigel-agarose constructs. *J. Biomater. Appl.* **31**, 684–692 (2016).

149. Mulakkal, M. C., Trask, R. S., Ting, V. P. & Seddon, A. M. Responsive cellulose-hydrogel composite ink for 4D printing. *Mater. Des.* **160**, 108–118 (2018).

150. Wang, Z. *et al.* 3D printed graphene/polydimethylsiloxane composite for stretchable strain sensor with tunable sensitivity. *Nanotechnology* **30**, 345501 (2019).

151. Ravanbakhsh, H., Bao, G., Latifi, N. & Mongeau, L. G. Carbon nanotube composite hydrogels for vocal fold tissue engineering: Biocompatibility, rheology, and porosity.

Mater. Sci. Eng. C **103**, 109861 (2019).

152. Jin, Y., Shen, Y., Yin, J., Qian, J. & Huang, Y. Nanoclay-Based Self-Supporting Responsive Nanocomposite Hydrogels for Printing Applications. *ACS Appl. Mater. Interfaces* **10**, 10461–10470 (2018).

153. Guo, J., Zhang, R., Zhang, L. & Cao, X. 4D printing of robust hydrogels consisted of agarose nanofibers and polyacrylamide. *ACS Macro Lett.* **7**, 442–446 (2018).

154. Ravanbakhsh, H., Bao, G. & Mongeau, L. Carbon nanotubes promote cell migration in hydrogels. *Sci. Rep.* **10**, 1–10 (2020).

155. Marques, C. F. *et al.* Collagen-based bioinks for hard tissue engineering applications: a comprehensive review. *J. Mater. Sci. Mater. Med.* **30**, 1–12 (2019).

156. Balasubramanian, P., Prabhakaran, M. P., Sireesha, M. & Ramakrishna, S. Collagen in human tissues: Structure, function, and biomedical implications from a tissue engineering perspective. *Adv. Polym. Sci.* **251**, 173–206 (2013).

157. Ozcelikkale, A. & Han, B. Thermal Destabilization of Collagen Matrix Hierarchical Structure by Freeze/Thaw. *PLoS One* **11**, e0146660 (2016).

158. Moncal, K. K., Ozbolat, V., Datta, P., Heo, D. N. & Ozbolat, I. T. Thermally-controlled extrusion-based bioprinting of collagen. *J. Mater. Sci. Mater. Med.* **30**, 1–14 (2019).

159. Suo, H., Zhang, J., Xu, M. & Wang, L. Low-temperature 3D printing of collagen and chitosan composite for tissue engineering. *Mater. Sci. Eng. C* **123**, 111963 (2021).

160. Gupta, N., Gupta, S. M. & Sharma, S. K. Carbon nanotubes: synthesis, properties and engineering applications. *Carbon Lett.* **29**, 419–447 (2019).

161. Ho, C. M. B. *et al.* 3D Printed Polycaprolactone Carbon Nanotube Composite Scaffolds for Cardiac Tissue Engineering. *Macromol. Biosci.* **17**, 1600250 (2017).

162. Razzazan, A., Atyabi, F., Kazemi, B. & Dinarvand, R. In vivo drug delivery of gemcitabine with PEGylated single-walled carbon nanotubes. *Mater. Sci. Eng. C* **62**, 614–625 (2016).

163. Izadifar, M., Chapman, D., Babyn, P., Chen, X. & Kelly, M. E. UV-Assisted 3D Bioprinting of Nanoreinforced Hybrid Cardiac Patch for Myocardial Tissue Engineering. *Tissue Eng. - Part C Methods* **24**, 74–88 (2018).

164. Li, H. *et al.* Preparation and properties of carbon nanotube (Fe)/hydroxyapatite composite as magnetic targeted drug delivery carrier. *Mater. Sci. Eng. C* **97**, 222–229 (2019).

165. Zhang, Q., Zhang, L., Wu, W. & Xiao, H. Methods and applications of nanocellulose loaded with inorganic nanomaterials: A review. *Carbohydr. Polym.* **229**, 115454 (2020).

166. Du, X., Zhang, Z., Liu, W. & Deng, Y. Nanocellulose-based conductive materials and their emerging applications in energy devices - A review. *Nano Energy* **35**, 299–320 (2017).

167. Lee, Y., Zhang, H., Yu, H. Y. & Tam, K. C. Electroconductive cellulose nanocrystals — Synthesis, properties and applications: A review. *Carbohydr. Polym.* **289**, 119419 (2022).

168. Domingues, R. M. A., Gomes, M. E. & Reis, R. L. The potential of cellulose nanocrystals in tissue engineering strategies. *Biomacromolecules* **15**, 2327–2346 (2014).

169. Habibi, Y., Hoeger, I., Kelley, S. S. & Rojas, O. J. Development of Langmuir - Schaeffer cellulose nanocrystal monolayers and their interfacial behaviors. *Langmuir* **26**, 990–1001 (2010).

170. Kam, D. *et al.* 3D Printing of Cellulose Nanocrystal-Loaded Hydrogels through Rapid Fixation by Photopolymerization. *Langmuir* **37**, 6451–6458 (2021).

171. Zadpoor, A. A. Design for Additive Bio-Manufacturing: From Patient-Specific Medical Devices to Rationally Designed Meta-Biomaterials. *Int. J. Mol. Sci.* **18**, 1607 (2017).

172. Hu, Q. *et al.* Additive manufacture of complex 3D Au-containing nanocomposites by simultaneous two-photon polymerisation and photoreduction. *Sci. Rep.* **7**, 1–9 (2017).

173. Norman, J., Madurawe, R. D., Moore, C. M. V., Khan, M. A. & Khairuzzaman, A. A new chapter in pharmaceutical manufacturing: 3D-printed drug products. *Adv. Drug Deliv. Rev.* **108**, 39–50 (2017).

174. Coelho, G. *et al.* Multimaterial 3D printing preoperative planning for frontoethmoidal meningoencephalocele surgery. *Child's Nerv. Syst.* **34**, 749–756 (2018).

175. Yang, C. *et al.* 3D-Printed Bioactive Ca3SiO5 Bone Cement Scaffolds with Nano Surface Structure for Bone Regeneration. *ACS Appl. Mater. Interfaces* **9**, 5757–5767 (2017).

176. Arabnejad, S., Johnston, B., Tanzer, M. & Pasini, D. Fully porous 3D printed titanium femoral stem to reduce stress-shielding following total hip arthroplasty. *J. Orthop. Res.* **35**, 1774–1783 (2017).

177. Singh, A. V. *et al.* The Adoption of Three-Dimensional Additive Manufacturing from Biomedical Material Design to 3D Organ Printing. *Appl. Sci.* **9**, 811 (2019).

178. Vijayavenkataraman, S. *et al.* 3D bioprinting of functional human skin: production and in vivo analysis. *Biofabrication* **9**, 015006 (2016).

179. Grix, T. *et al.* Bioprinting Perfusion-Enabled Liver Equivalents for Advanced Organ-on-a-Chip Applications. *Genes (Basel).* **9**, 176 (2018).

180. Ahangar, P., Cooke, M. E., Weber, M. H. & Rosenzweig, D. H. Current biomedical applications of 3D printing and additive manufacturing. *Appl. Sci.* **9**, (2019).

181. Vignesh, U., Mehrotra, D., Dichen, Anand, V. & Howlader, D. Three dimensional reconstruction of late post traumatic orbital wall defects by customized implants using CAD-CAM, 3D stereolithographic models: A case report. *J. Oral Biol. Craniofacial Res.* **7**, 212–218 (2017).

182. Eggbeer, D., Bibb, R., Evans, P. & Ji, L. Evaluation of direct and indirect additive manufacture of maxillofacial prostheses. *Proc. Inst. Mech. Eng. Part H J. Eng. Med.* **226**, 718–728 (2012).

183. Gaharwar, A. K., Singh, I. & Khademhosseini, A. Engineered biomaterials for in situ tissue regeneration. *Nat. Rev. Mater.* **5**, 686–705 (2020).

184. Murphy, S. V. & Atala, A. 3D bioprinting of tissues and organs. *Nat. Biotechnol. 2014 328* **32**, 773–785 (2014).

185. Naba, A. *et al.* The extracellular matrix: Tools and insights for the "omics" era. *Matrix Biol.* **49**, 10–24 (2016).

186. Stockwell, R. A. The cell density of human articular and costal cartilage. *J. Anat.* **101**, 753 (1967).

187. Apostolakos, J. *et al.* The enthesis: a review of the tendon-to-bone insertion. *Muscles. Ligaments Tendons J.* **4**, 333 (2014).

188. BENJAMIN, M. & RALPHS, J. R. Fibrocartilage in tendons and ligaments — an adaptation to compressive load. *J. Anat.* **193**, 481–494 (1998).

189. Krishnan, Y. & Grodzinsky, A. J. Cartilage diseases. *Matrix Biol.* **71**–**72**, 51–69 (2018).

190. Xu, J., Jin, R., Ren, X. & Gao, G. Cartilage-inspired hydrogel strain sensors with ultrahigh toughness, good self-recovery and stable anti-swelling properties. *J. Mater. Chem. A* **7**, 25441–25448 (2019).

191. Armiento, A. R., Stoddart, M. J., Alini, M. & Eglin, D. Biomaterials for articular cartilage tissue engineering: Learning from biology. *Acta Biomater.* **65**, 1–20 (2018).

192. CHARNLEY, J. The Lubrication of Animal Joints in Relation to Surgical Reconstruction by Arthroplasty. *Ann. Rheum. Dis.* **19**, 10 (1960).

193. Gao, J. *et al.* Cell-Free Bilayered Porous Scaffolds for Osteochondral Regeneration Fabricated by Continuous 3D-Printing Using Nascent Physical Hydrogel as Ink. *Adv. Healthc. Mater.* **10**, 2001404 (2021).

194. Qu, D., Mosher, C. Z., Boushell, M. K. & Lu, H. H. Engineering Complex Orthopaedic Tissues Via Strategic Biomimicry. *Ann. Biomed. Eng.* **43**, 697–717 (2014).

195. Castro, N. J., Hacking, S. A. & Zhang, L. G. Recent Progress in Interfacial Tissue Engineering Approaches for Osteochondral Defects. *Ann. Biomed. Eng.* **40**, 1628–1640 (2012).

196. Di Luca, A., Van Blitterswijk, C. & Moroni, L. The osteochondral interface as a gradient tissue: From development to the fabrication of gradient scaffolds for regenerative medicine. *Birth Defects Res. Part C Embryo Today Rev.* **105**, 34–52 (2015).

197. Fu, L. *et al.* Advances and prospects in biomimetic multilayered scaffolds for articular

cartilage regeneration. *Regen. Biomater.* **7**, 527–542 (2020).

198. Apostu, D. *et al.* Systemic drugs with impact on osteoarthritis. *Drug Metab. Rev.* **51**, 498–523 (2019).

199. Buttgereit, F., Burmester, G. R. & Bijlsma, J. W. J. Non-surgical management of knee osteoarthritis: where are we now and where do we need to go? *RMD Open* **1**, e000027 (2015).

200. Mahmoudifar, N. & Doran, P. M. Chondrogenesis and cartilage tissue engineering: the longer road to technology development. *Trends Biotechnol.* **30**, 166–176 (2012).

201. Bhattacharjee, M. *et al.* Tissue engineering strategies to study cartilage development, degeneration and regeneration. *Adv. Drug Deliv. Rev.* **84**, 107–122 (2015).

202. Huey, D. J., Hu, J. C. & Athanasiou, K. A. Unlike bone, cartilage regeneration remains elusive. *Science* **338**, 917–921 (2012).

203. Arjmandi, M. & Ramezani, M. Mechanical and tribological assessment of silica nanoparticle-alginate-polyacrylamide nanocomposite hydrogels as a cartilage replacement. *J. Mech. Behav. Biomed. Mater.* **95**, 196–204 (2019).

204. Nakamura, A. *et al.* Bio-3D printing iPSC-derived human chondrocytes for articular cartilage regeneration. *Biofabrication* **13**, 044103 (2021).

205. Ansari, S., Khorshidi, S. & Karkhaneh, A. Engineering of gradient osteochondral tissue: From nature to lab. *Acta Biomater.* **87**, 41–54 (2019).

206. Pereira, D. R., Reis, R. L. & Oliveira, J. M. Layered Scaffolds for Osteochondral Tissue Engineering. *Adv. Exp. Med. Biol.* **1058**, 193–218 (2018).

207. Zhu, Y. *et al.* Designed composites for mimicking compressive mechanical properties of articular cartilage matrix. *J. Mech. Behav. Biomed. Mater.* **36**, 32–46 (2014).

208. Liu, J. *et al.* 3D printing of biomimetic multi-layered GelMA/nHA scaffold for osteochondral defect repair. *Mater. Des.* **171**, 107708 (2019).

209. Jeong, G. S. *et al.* Sprouting angiogenesis under a chemical gradient regulated by interactions with an endothelial monolayer in a microfluidic platform. *Anal. Chem.* **83**, 8454–8459 (2011).

210. Zhu, J. & Zhu, J. Application of Organ-on-Chip in Drug Discovery. *J. Biosci. Med.* **8**, 119–134 (2020).

211. Bein, A. *et al.* Microfluidic Organ-on-a-Chip Models of Human Intestine. *Cell. Mol. Gastroenterol. Hepatol.* **5**, 659–668 (2018).

212. Herland, A. *et al.* Quantitative prediction of human pharmacokinetic responses to drugs via fluidically coupled vascularized organ chips. *Nat. Biomed. Eng.* **4**, 421–436 (2020).

213. Dhiman, N. *et al.* Selective Cytotoxicity of a Novel Trp-Rich Peptide against Lung Tumor Spheroids Encapsulated inside a 3D Microfluidic Device. *Adv. Biosyst.* **4**, 1900285 (2020).

214. Sankar, S., Sharma, C. S. & Rath, S. N. Enhanced osteodifferentiation of MSC spheroids on patterned electrospun fiber mats - An advanced 3D double strategy for bone tissue regeneration. *Mater. Sci. Eng. C* **94**, 703–712 (2019).

215. Sankar, S., Kakunuri, M., D. Eswaramoorthy, S., Sharma, C. S. & Rath, S. N. Effect of patterned electrospun hierarchical structures on alignment and differentiation of mesenchymal stem cells: Biomimicking bone. *J. Tissue Eng. Regen. Med.* **12**, e2073–e2084 (2018).

216. Chan, H. N. *et al.* Direct, one-step molding of 3D-printed structures for convenient fabrication of truly 3D PDMS microfluidic chips. *Microfluid. Nanofluidics* **19**, 9–18 (2015).

217. Bhattacharjee, N., Urrios, A., Kang, S. & Folch, A. The upcoming 3D-printing revolution in microfluidics. *Lab Chip* **16**, 1720–1742 (2016).

218. Mehta, V. & Rath, S. N. 3D printed microfluidic devices: a review focused on four fundamental manufacturing approaches and implications on the field of healthcare. *Bio-Design Manuf.* **4**, 311–343 (2021).

219. Nelson, M. D., Ramkumar, N. & Gale, B. K. Flexible, transparent, sub-100 µm microfluidic channels with fused deposition modeling 3D-printed thermoplastic polyurethane. *J. Micromechanics Microengineering* **29**, 095010 (2019).

220. Salentijn, G. I. J., Oomen, P. E., Grajewski, M. & Verpoorte, E. Fused Deposition Modeling 3D Printing for (Bio)analytical Device Fabrication: Procedures, Materials, and Applications. *Anal. Chem.* **89**, 7053–7061 (2017).

221. Ching, T. *et al.* Fabrication of integrated microfluidic devices by direct ink writing (DIW) 3D printing. *Sensors Actuators B Chem.* **297**, 126609 (2019).

222. Kuo, A. P. *et al.* High-Precision Stereolithography of Biomicrofluidic Devices. *Adv. Mater. Technol.* **4**, 1800395 (2019).

223. Gong, H., Bickham, B. P., Woolley, A. T. & Nordin, G. P. Custom 3D printer and resin for 18 µm × 20 µm microfluidic flow channels. *Lab Chip* **17**, 2899–2909 (2017).

224. Shankles, P. G., Millet, L. J., Aufrecht, J. A. & Retterer, S. T. Accessing microfluidics through feature-based design software for 3D printing. *PLoS One* **13**, e0192752 (2018).

225. Huang Goh, W., Hashimoto, M., Goh, W. H. & Hashimoto, M. Fabrication of 3D Microfluidic Channels and In-Channel Features Using 3D Printed, Water-Soluble Sacrificial Mold. *Macromol. Mater. Eng.* **303**, 1700484 (2018).

226. Tang, W. *et al.* Elasto-inertial particle focusing in 3D-printed microchannels with unconventional cross sections. *Microfluid. Nanofluidics* **23**, 1–10 (2019).

227. Saggiomo, V., Velders, A. H., Saggiomo, V. & Velders, A. H. Simple 3D Printed Scaffold-Removal Method for the Fabrication of Intricate Microfluidic Devices. *Adv. Sci.* **2**, 1500125 (2015).

228. Wu, W., Deconinck, A. & Lewis, J. A. Omnidirectional Printing of 3D Microvascular Networks. *Adv. Mater.* **23**, 178–183 (2011).

229. He, Y. *et al.* Printing 3D microfluidic chips with a 3D sugar printer. *Microfluid. Nanofluidics* **19**, 447–456 (2015).

230. Brossard, R., Brouchet, T. & Malloggi, F. Replication of a Printed Volatile Mold: a novel microfabrication method for advanced microfluidic systems. *Sci. Rep.* **9**, 1–10 (2019).

231. Langelier, S. M. *et al.* Flexible casting of modular self-aligning microfluidic assembly blocks. *Lab Chip* **11**, 1679–1687 (2011).

232. Bhargava, K. C., Thompson, B. & Malmstadt, N. Discrete elements for 3D microfluidics. *Proc. Natl. Acad. Sci. U. S. A.* **111**, 15013–15018 (2014).

233. Ching, T., Toh, Y. C. & Hashimoto, M. Fabrication of Complex 3D Fluidic Networks via Modularized Stereolithography. *Adv. Eng. Mater.* **22**, 1901109 (2020).

234. Lee, H. & Cho, D. W. One-step fabrication of an organ-on-a-chip with spatial heterogeneity using a 3D bioprinting technology. *Lab Chip* **16**, 2618–2625 (2016).

235. Mehta, G. *et al.* Hard top soft bottom microfluidic devices for cell culture and chemical analysis. *Anal. Chem.* **81**, 3714–3722 (2009).

236. Lynh, H. D. & Pin-Chuan, C. Novel solvent bonding method for creation of a three-dimensional, non-planar, hybrid PLA/PMMA microfluidic chip. *Sensors Actuators A Phys.* **280**, 350–358 (2018).

237. Lynh, H. D. & Pin-Chuan, C. Novel solvent bonding method for creation of a three-dimensional, non-planar, hybrid PLA/PMMA microfluidic chip. *Sensors Actuators, A Phys.* **280**, 350–358 (2018).

238. Carrell, C. S., McCord, C. P., Wydallis, R. M. & Henry, C. S. Sealing 3D-printed parts to poly(dimethylsiloxane) for simple fabrication of Microfluidic devices. *Anal. Chim. Acta* **1124**, 78–84 (2020).

239. Meng, Y., Cao, J., Chen, Y., Yu, Y. & Ye, L. 3D printing of a poly(vinyl alcohol)-based nano-composite hydrogel as an artificial cartilage replacement and the improvement mechanism of printing accuracy. *J. Mater. Chem. B* **8**, 677–690 (2020).

240. Xiao, H. *et al.* Friction pair evaluation of cartilage-diamond for partial joint repair. *Carbon N. Y.* **80**, 551–559 (2014).

241. Camarero-Espinosa, S., Weder, C., Rothen-Rutishauser, B. & Foster, E. J. Articular cartilage: from formation to tissue engineering. *Biomater. Sci.* **4**, 727–882 (2016).

242. Bas, O. *et al.* Biofabricated soft network composites for cartilage tissue engineering. *Biofabrication* **9**, 025014 (2017).

243. Kienle, S. *et al.* Comparison of friction and wear of articular cartilage on different length scales. *J. Biomech.* **48**, 3052–3058 (2015).

244. Martín, A. R., Patel, J. M., Zlotnick, H. M., Carey, J. L. & Mauck, R. L. Emerging therapies for cartilage regeneration in currently excluded 'red knee' populations. *npj Regen. Med.* **4**, 1–11 (2019).

245. Sophia Fox, A. J., Bedi, A. & Rodeo, S. A. The basic science of articular cartilage: Structure, composition, and function. *Sports Health* **1**, 461–468 (2009).

246. Vikingsson, L., Claessens, B., Gómez-Tejedor, J. A., Gallego Ferrer, G. & Gómez Ribelles, J. L. Relationship between micro-porosity, water permeability and mechanical behavior in scaffolds for cartilage engineering. *J. Mech. Behav. Biomed. Mater.* **48**, 60–69 (2015).

247. Theodoridis, K. *et al.* Hyaline cartilage next generation implants from adipose-tissue–derived mesenchymal stem cells: Comparative study on 3D-printed polycaprolactone scaffold patterns. *J. Tissue Eng. Regen. Med.* **13**, 342–355 (2019).

248. Wu, Y., Wenger, A., Golzar, H. & Tang, X. (Shirley). 3D bioprinting of bicellular liver lobule-mimetic structures via microextrusion of cellulose nanocrystal-incorporated shear-thinning bioink. *Sci. Rep.* **10**, 1–12 (2020).

249. Kim, M. & Nam, S. Assessment of coaxial printability for extrusion-based bioprinting of alginate-based tubular constructs. *Bioprinting* **20**, e00092 (2020).

250. He, C. & Li, Z. *Silicon containing hybrid copolymers*. (Wiley Online Library, 2020). doi:10.1002/9783527823499.

251. Liravi, F. & Toyserkani, E. Additive manufacturing of silicone structures: A review and prospective. *Addit. Manuf.* **24**, 232–242 (2018).

252. Zare, M., Ghomi, E. R., Venkatraman, P. D. & Ramakrishna, S. Silicone-based biomaterials for biomedical applications: Antimicrobial strategies and 3D printing technologies. *J. Appl. Polym. Sci.* **138**, 1–18 (2021).

253. Gaebel, R. *et al.* Patterning human stem cells and endothelial cells with laser printing for cardiac regeneration. *Biomaterials* **32**, 9218–9230 (2011).

254. Zhang, Y. S. *et al.* 3D Bioprinting for Tissue and Organ Fabrication. *Ann. Biomed. Eng.* **45**, 148–163 (2016).

255. Zhou, L. Y. *et al.* Multimaterial 3D Printing of Highly Stretchable Silicone Elastomers. *ACS Appl. Mater. Interfaces* **11**, 23573–23583 (2019).

256. Lin, N. & Dufresne, A. Nanocellulose in biomedicine: Current status and future prospect. *Eur. Polym. J.* **59**, 302–325 (2014).

257. Ureña-Benavides, E. E., Ao, G., Davis, V. A. & Kitchens, C. L. Rheology and phase behavior of lyotropic cellulose nanocrystal suspensions. *Macromolecules* **44**, 8990–8998 (2011).

258. Moon, R. J., Martini, A., Nairn, J., Simonsen, J. & Youngblood, J. Cellulose nanomaterials review: structure, properties and nanocomposites. *Chem. Soc. Rev.* **40**, 3941–3994 (2011).

259. Ma, Y., Yang, R. & Zhao, W. Innovative water-insoluble edible film based on biocatalytic crosslink of gelatin rich in glutamine. *Foods* **9**, 503–513 (2020).

260. Kolesky, D. B. *et al.* 3D Bioprinting of Vascularized, Heterogeneous Cell-Laden Tissue Constructs. *Adv. Mater.* **26**, 3124–3130 (2014).

261. Markstedt, K. *et al.* 3D Bioprinting Human Chondrocytes with Nanocellulose–Alginate Bioink for Cartilage Tissue Engineering Applications. *Biomacromolecules* **16**, 1489–1496 (2015).

262. Malda, J. *et al.* 25th Anniversary Article: Engineering Hydrogels for Biofabrication. *Adv. Mater.* **25**, 5011–5028 (2013).

263. Compton, B. G. & Lewis, J. A. 3D-Printing of Lightweight Cellular Composites. *Adv. Mater.* **26**, 5930–5935 (2014).

264. Durban, M. M. *et al.* Custom 3D Printable Silicones with Tunable Stiffness. *Macromol. Rapid Commun.* **39**, 1700563 (2018).

265. Liu, C., Ortega, Z. & Ajami, S. Polycaprolactone – carboxymethyl cellulose composites for manufacturing porous scaffolds by material extrusion. *Bio-Design Manuf.* **1**, 245–253 (2018).

266. Huq, T. *et al.* Nanocrystalline cellulose (NCC) reinforced alginate based biodegradable nanocomposite film. *Carbohydr. Polym.* **90**, 1757–1763 (2012).

267. Habibi, Y., Lucia, L. A. & Rojas, O. J. Cellulose Nanocrystals: Chemistry, Self-Assembly, and Applications. *Chem. Rev.* **110**, 3479–3500 (2010).

268. Domingues, R. M. A., Gomes, M. E. & Reis, R. L. The potential of cellulose nanocrystals in tissue engineering strategies. *Biomacromolecules* **15**, 2327–2346 (2014).

269. Burkholder-Wenger, A. C., Golzar, H., Wu, Y. & Tang, X. S. Development of a Hybrid Nanoink for 3D Bioprinting of Heterogeneous Tumor Models. *ACS Biomater. Sci. Eng.* **8**, 777–785 (2022).

270. Shirahama, H., Lee, B. H., Tan, L. P. & Cho, N.-J. Precise Tuning of Facile One-Pot Gelatin Methacryloyl (GelMA) Synthesis. *Sci. Rep.* **6**, 31036–31047 (2016).

271. Yin, Y., Tian, X., Jiang, X., Wang, H. & Gao, W. Modification of cellulose nanocrystal via SI-ATRP of styrene and the mechanism of its reinforcement of polymethylmethacrylate. *Carbohydr. Polym.* **142**, 206–212 (2016).

272. Zandi, N. *et al.* Nanoengineered shear-thinning and bioprintable hydrogel as a versatile platform for biomedical applications. *Biomaterials* **267**, 120476 (2021).

273. Peak, C. W., Stein, J., Gold, K. A. & Gaharwar, A. K. Nanoengineered Colloidal Inks for 3D Bioprinting. *Langmuir* **34**, 917–925 (2018).

274. Wang, X. & Soucek, M. D. Investigation of non-isocyanate urethane dimethacrylate reactive diluents for UV-curable polyurethane coatings. *Prog. Org. Coatings* **76**, 1057–1067 (2013).

275. Wu, Y., Wenger, A., Golzar, H. & Tang, X. (Shirley). 3D bioprinting of bicellular liver lobule-mimetic structures via microextrusion of cellulose nanocrystal-incorporated shear-thinning bioink. *Sci. Rep.* **10**, 1–12 (2020).

276. Wu, Y., Lin, Z. Y. (William), Wenger, A. C., Tam, K. C. & Tang, X. (Shirley). 3D bioprinting of liver-mimetic construct with alginate/cellulose nanocrystal hybrid bioink. *Bioprinting* **9**, 1–6 (2018).

277. Cai, L. *et al.* Injectable Hydrogels with In Situ Double Network Formation Enhance Retention of Transplanted Stem Cells. *Adv. Funct. Mater.* **25**, 1344–1351 (2015).

278. Kunc, F. *et al.* Quantification and Stability Determination of Surface Amine Groups on Silica Nanoparticles Using Solution NMR. *Anal. Chem.* **90**, 13322–13330 (2018).

279. Brinkman, W. T., Nagapudi, K., Thomas, B. S. & Chaikof, E. L. Photo-cross-linking of type I collagen gels in the presence of smooth muscle cells: Mechanical properties, cell viability, and function. *Biomacromolecules* **4**, 890–895 (2003).

280. Soderberg, T. *Organic Chemistry with a Biological Emphasis*. vol. I (Chemistry Publications, 2016).

281. Nabi, R. *et al.* A biochemical & biophysical study on in-vitro anti-glycating potential of iridin against D-Ribose modified BSA. *Arch. Biochem. Biophys.* **686**, (2020).

282. Cayot, P. & Tainturier, G. The Quantification of Protein Amino Groups by the Trinitrobenzenesulfonic Acid Method: A Reexamination. *Anal. Biochem.* **249**, 184–200 (1997).

283. Gillispie, G. *et al.* Assessment methodologies for extrusion-based bioink printability. *Biofabrication* **12**, 022003 (2020).

284. Hölzl, K. *et al.* Bioink properties before, during and after 3D bioprinting. *Biofabrication* **8**, 032002 (2016).

285. Liang, J. Z. Effects of extrusion conditions on die-swell behavior of polypropylene/diatomite composite melts. *Polym. Test.* **27**, 936–940 (2008).

286. Wang, K. Die Swell of Complex Polymeric Systems. in *Viscoelasticity - From Theory to Biological Applications* 372 (IntechOpen, 2012). doi:10.5772/50137.

287. Habib, A., Sathish, V., Mallik, S. & Khoda, B. 3D printability of alginate-carboxymethyl cellulose hydrogel. *Materials (Basel).* **11**, (2018).

288. Su, W.-F. Radical Chain Polymerization. in *Principles of Polymer Design and Synthesis* 137–183 (Springer, 2013). doi:10.1007/978-3-642-38730-2_7.

289. Bai, H., Li, Z., Zhang, S., Wang, W. & Dong, W. Interpenetrating polymer networks in polyvinyl alcohol/cellulose nanocrystals hydrogels to develop absorbent materials. *Carbohydr. Polym.* **200**, 468–476 (2018).

290. Zhou, X., Wang, J., Nie, J. & Du, B. Poly(N-isopropylacrylamide)-based ionic hydrogels: synthesis, swelling properties, interfacial adsorption and release of dyes. *Polym. J.* **48**, 431–438 (2016).

291. Wang, X., Hu, H., Chen, B., Dang, L. & Gao, G. Efficient synthesis of dimethyl carbonate via transesterification of ethylene carbonate catalyzed by swelling poly(ionic liquid)s. *Green Chem. Eng.* **2**, 423–430 (2021).

292. Salimi-Kenari, H., Mollaie, F., Dashtimoghadam, E., Imani, M. & Nyström, B. Effects of chain length of the cross-linking agent on rheological and swelling characteristics of dextran hydrogels. *Carbohydr. Polym.* **181**, 141–149 (2018).

293. Anderson, J. M., Rodriguez, A. & Chang, D. T. Foreign body reaction to biomaterials. *Semin. Immunol.* **20**, 86–100 (2008).

294. Vishwakarma, A. *et al.* Engineering Immunomodulatory Biomaterials To Tune the Inflammatory Response. *Trends Biotechnol.* **34**, 470–482 (2016).

295. Rowley, A. T., Nagalla, R. R., Wang, S. W. & Liu, W. F. Extracellular matrix-based strategies for immunomodulatory biomaterials engineering. *Adv. Healthc. Mater.* **8**, e1801578 (2019).

296. Wilson, C. J., Clegg, R. E., Leavesley, D. I. & Pearcy, M. J. Mediation of biomaterial-cell interactions by adsorbed proteins: A review. *Tissue Eng.* **11**, 1–18 (2005).

297. Jung, H. S. *et al.* Surface modification of multipass caliber-rolled ti alloy with dexamethasone-loaded graphene for dental applications. *ACS Appl. Mater. Interfaces* **7**, 9598–9607 (2015).

298. Barthes, J. *et al.* Biofunctionalization of 3D-printed silicone implants with immunomodulatory hydrogels for controlling the innate immune response: An in vivo model of tracheal defect repair. *Biomaterials* **268**, 120549 (2021).

299. Yang, J., Han, C. R., Zhang, X. M., Xu, F. & Sun, R. C. Cellulose nanocrystals mechanical reinforcement in composite hydrogels with multiple cross-links: Correlations between dissipation properties and deformation mechanisms. *Macromolecules* **47**, 4077–4086 (2014).

300. Huang, S., Zhao, Z., Feng, C., Mayes, E. & Yang, J. Nanocellulose reinforced P(AAm-co-

AAc) hydrogels with improved mechanical properties and biocompatibility. *Compos. Part A Appl. Sci. Manuf.* **112**, 395–404 (2018).

301. Eschweiler, J. *et al.* The Biomechanics of Cartilage — An Overview. *Life* **11**, 302–316 (2021).

302. Li, H., Li, J., Yu, S., Wu, C. & Zhang, W. The mechanical properties of tibiofemoral and patellofemoral articular cartilage in compression depend on anatomical regions. *Sci. Rep.* **11**, 1–11 (2021).

303. Sanchez-Adams, J., Leddy, H. A., McNulty, A. L., O'Conor, C. J. & Guilak, F. The Mechanobiology of Articular Cartilage: Bearing the Burden of Osteoarthritis. *Curr. Rheumatol. Rep.* **16**, 1–9 (2014).

304. Nguyen, Q. T., Tinard, V. & Fond, C. The modelling of nonlinear rheological behaviour and Mullins effect in High Damping Rubber. *Int. J. Solids Struct.* **75**–**76**, 235–246 (2015).

305. Cantournet, S., Desmorat, R. & Besson, J. Mullins effect and cyclic stress softening of filled elastomers by internal sliding and friction thermodynamics model. *Int. J. Solids Struct.* **46**, 2255–2264 (2009).

306. Weizel, A. *et al.* Complex mechanical behavior of human articular cartilage and hydrogels for cartilage repair. *Acta Biomater.* **118**, 113–128 (2020).

307. Fujii, T. PDMS-based microfluidic devices for biomedical applications. *Microelectron. Eng.* **61**–**62**, 907–914 (2002).

308. Konstantinou, D., Shirazi, A., Sadri, A. & Young, E. W. K. Combined hot embossing and milling for medium volume production of thermoplastic microfluidic devices. *Sensors Actuators B Chem.* **234**, 209–221 (2016).

309. Zhou, Z., Chen, D., Wang, X. & Jiang, J. Milling Positive Master for Polydimethylsiloxane Microfluidic Devices: The Microfabrication and Roughness Issues. *Micromachines* **8**, 287 (2017).

310. Mukherjee, P., Nebuloni, F., Gao, H., Zhou, J. & Papautsky, I. Rapid Prototyping of Soft Lithography Masters for Microfluidic Devices Using Dry Film Photoresist in a Non-Cleanroom Setting. *Micromachines* **10**, 192 (2019).

311. McDonald, J. C., Metallo, S. J. & Whitesides, G. M. Fabrication of a configurable, single-use microfluidic device. *Anal. Chem.* **73**, 5645–5650 (2001).

312. Chen, C. *et al.* 3D-printed microfluidic devices: fabrication, advantages and limitations - a mini review. *Anal. Methods* **8**, 6005–6012 (2016).

313. Gross, B. C., Erkal, J. L., Lockwood, S. Y., Chen, C. & Spence, D. M. Evaluation of 3D printing and its potential impact on biotechnology and the chemical sciences. *Anal. Chem.* **86**, 3240–3253 (2014).

314. Kitson, P. J., Rosnes, M. H., Sans, V., Dragone, V. & Cronin, L. Configurable 3D-Printed millifluidic and microfluidic 'lab on a chip' reactionware devices. *Lab Chip* **12**, 3267–3271 (2012).

315. Gong, H., Bickham, B. P., Woolley, A. T. & Nordin, G. P. Custom 3D printer and resin for 18 μm × 20 μm microfluidic flow channels. *Lab Chip* **17**, 2899–2909 (2017).

316. Gyimah, N., Scheler, O., Rang, T. & Pardy, T. Can 3D Printing Bring Droplet Microfluidics to Every Lab?—A Systematic Review. *Micromachines* **12**, 339 (2021).

317. Rehmani, M. A. A., Jaywant, S. A. & Arif, K. M. Study of Microchannels Fabricated Using Desktop Fused Deposition Modeling Systems. *Micromachines* **12**, 14 (2020).

318. Peng, Y. *et al.* Direct ink writing combined with metal-assisted chemical etching of microchannels for the microfluidic system applications. *Sensors Actuators A Phys.* **315**, 112320 (2020).

319. Kim, Y. T., Castro, K., Bhattacharjee, N. & Folch, A. Digital Manufacturing of Selective Porous Barriers in Microchannels Using Multi-Material Stereolithography. *Micromachines 2018, Vol. 9, Page 125* **9**, 125 (2018).

320. Kotz, F., Risch, P., Helmer, D. & Rapp, B. E. Highly Fluorinated Methacrylates for Optical 3D Printing of Microfluidic Devices. *Micromachines 2018, Vol. 9, Page 115* **9**, 115 (2018).

321. Balakrishnan, H. K. *et al.* 3D Printing: An Alternative Microfabrication Approach with Unprecedented Opportunities in Design. *Anal. Chem.* **93**, 350–366 (2021).

322. Kim, H. J., Huh, D., Hamilton, G. & Ingber, D. E. Human gut-on-a-chip inhabited by microbial flora that experiences intestinal peristalsis-like motions and flow. *Lab Chip* **12**, 2165–2174 (2012).

323. Huh, D. *et al.* Reconstituting organ-level lung functions on a chip. *Science* **328**, 1662–1668 (2010).

324. Cheng, W., Kai, D., Loh, X. J., He, C. & Li, Z. Silicone Copolymers for Healthcare and Personal Care Applications. *Silicon Containing Hybrid Copolymers* 145–166 (John Wiley & Sons, Ltd, 2020). doi:10.1002/9783527823499.CH6.

325. Miranda, I. *et al.* Properties and applications of PDMS for biomedical engineering: A review. *J. Funct. Biomater.* **13**, (2022).

326. Jin, Y., Xiong, P., Xu, T. & Wang, J. Time-efficient fabrication method for 3D-printed microfluidic devices. *Sci. Rep.* **12**, 1–9 (2022).

327. Ching, T. *et al.* Fabrication of integrated microfluidic devices by direct ink writing (DIW) 3D printing. *Sensors Actuators, B Chem.* **297**, 126609 (2019).